Aus dem Fachbereich Medizin
der Johann Wolfgang Goethe-Universität
Frankfurt am Main

betreut am
Zentrum der Physiologie
Institut für Physiologie I (Kardiovaskuläre Physiologie)
Direktor: Prof. Dr. Ralf Brandes

Loss of endothelial cytochrome P450 reductase induces vascular dysfunction in mice

Thesis
zur Erlangung des Grades Doctor of Philosophy (PhD)
des Fachbereichs Medizin
der Johann Wolfgang Goethe-Universität
Frankfurt am Main

vorgelegt von
Pedro Felipe Malacarne

aus Vila Velha-ES, Brasilien

Frankfurt am Main, 2023

Aus dem Fachbereich Medizin
der Johann Wolfgang Goethe-Universität
Frankfurt am Main

betreut am
Zentrum der Physiologie
Institut für Physiologie I (Kardiovaskuläre Physiologie)
Direktor: Prof. Dr. Ralf Brandes

Loss of endothelial cytochrome P450 reductase induces vascular dysfunction in mice

Thesis
zur Erlangung des Grades Doctor of Philosophy (PhD)
des Fachbereichs Medizin
der Johann Wolfgang Goethe-Universität
Frankfurt am Main

vorgelegt von
Pedro Felipe Malacarne

aus Vila Velha-ES, Brasilien

Frankfurt am Main, 2023

Dekan: Prof. Dr. Stefan Zeuzem

Referent: Prof. Dr. Ralf Brandes

1. Korreferent: Herr Prof. Dr. Jaya Krishnan

Tag der mündlichen Prüfung: 09.10.2023

Contents

Abstract

Aim

The cytochrome P450 reductase (POR) along with the cytochrome P450 enzymes (CYP) are responsible for the metabolism of a multitude of metabolites important for the maintenance of tissue function. Defects in this system have been associated with cardiovascular diseases. These enzymes are known to produce vasoactive lipids that modulate vascular tone. The aim of this study was to identify the consequence of a loss in endothelial POR for vascular function.

Methods and Results

To identify the endothelial contribution of the POR/CYP450 system to vascular function, we generated an endothelial-specific, tamoxifen-inducible POR knockout mouse (ecPOR$^{-/-}$). Under basal condition ecPOR$^{-/-}$ already exhibited endothelial dysfunction in aorta and mesenteric vessels (acetylcholine-dependent relaxation, LogEC50 -7.6M for CTR vs. -7.2M for ecPOR$^{-/-}$ in aorta) and lower nitric oxide levels in the plasma (CTR: 236.8 ±77.4; ecPOR$^{-/-}$ 182.8 ±34.1 nmol/L). This dysfunction was coupled to attenuated eNOS function detected by the heavy arginine assay and decreased eNOS phosphorylation on S1177. Furthermore, insulin-induced phosphorylation of the eNOS activator, AKT, was also attenuated in the aorta from ecPOR$^{-/-}$ mice as compared to control mice. CYP450-dependent EET production was lower in plasma, lung and aorta of ecPOR$^{-/-}$ mice and this was accompanied with increased levels of vasoconstriction prostanoids (lipidomics of aorta, plasma and lung freshly isolated from CTR and ecPOR$^{-/-}$ mice). MACE-RNAseq from these aortas also showed a significant increase in genes annotated to eicosanoid production. In an in vivo angiotensin II model, acute deletion of POR increased the blood pressure as measured by telemetry and tail cuff (137.4 ± 15.9 mmHg in WT; 152.1 ± 7.154 mmHg in ecPOR$^{-/-}$). In a rescue experiment using the NSAID naproxen, the increase in blood pressure induced by deletion of endothelial POR was abolished.

Conclusion

Collectively, in endothelial cells POR regulates eNOS activity and orchestrates the metabolic fate of arachidonic acid towards the vessel dilating EETs and away

from deleterious prostanoids. In the absence of POR this endothelial regulation is compromised leading to vascular dysfunction.

Zusammenfassung

Ziel

Die Cytochrom-P450-Reduktase (POR) ist zusammen mit den Cytochrom-P450-Enzymen (CYP) für den Stoffwechsel einer Vielzahl von Metaboliten verantwortlich, die für die Aufrechterhaltung der Gewebefunktion wichtig sind. Defekte in diesem System werden mit Herz-Kreislauf-Erkrankungen in Verbindung gebracht. Von diesen Enzymen ist bekannt, dass sie vasoaktive Lipide produzieren, die den Gefäßtonus modulieren. Ziel dieser Studie war es, herauszufinden, inwieweit POR die Funktion des Endothels aufrechterhält und welche Mechanismen dem zugrunde liegen.

Methoden und Ergebnisse

Um die vaskuläre Funktion von POR zu ermitteln, haben wir eine endothelspezifische, Tamoxifen-induzierbare POR-Knockout-Maus (ecPOR$^{-/-}$) erzeugt. Am auffälligsten ist, dass ecPOR$^{-/-}$ bereits unter basalen Bedingungen eine endotheliale Dysfunktion in der Aorta und den Mesenterialgefäßen [Acetylcholin-abhängige Relaxation (LogEC50 -7,6M für CTR vs. -7,2M für ecPOR$^{-/-}$ in der Aorta)] und niedrigere Stickstoffoxidwerte im Plasma (CTR: 236,8 ±77,4; ecPOR$^{-/-}$ 182,8 ±34,1 nmol/L) aufweist. Diese Funktionsstörung war mit einer abgeschwächten eNOS-Funktion gekoppelt, die durch den Assay mit schwerem Arginin und durch eine Abnahme der eNOS-Phosphorylierung von S1177 nachgewiesen wurde, begleitet von einer unveränderten eNOS-Expression. Darüber hinaus wies der eNOS-Aktivator AKT in der Aorta von ecPOR$^{-/-}$ Mäusen im Vergleich zur Kontrollgruppe ebenfalls eine geringere Phosphorylierung auf. Bemerkenswerterweise war die CYP450-abhängige EET-Produktion im Plasma, in der Lunge und in der Aorta der ecPOR$^{-/-}$- Mäuse geringer, während gleichzeitig die Menge der vasokonstriktorischen Prostanoide anstieg (Lipidomik der Aorta, des Plasmas und der Lunge, die frisch aus CTR- und ecPOR$^{-/-}$- Mäusen isoliert wurden). MACE-RNAseq aus diesen Aorten zeigte auch einen signifikanten Anstieg von Genen, die für die Eicosanoidproduktion verantwortlich sind. In einem in vivo Angiotensin-II-Modell führte die akute Deletion von POR zu einem Anstieg des Blutdrucks, der mittels Telemetrie und Schwanzmanschette gemessen wurde (137,4 ± 15,9 mmHg bei WT; 152,1 ± 7,154 mmHg bei ecPOR$^{-/-}$).In einem

Rettungsversuch mit dem NSAID Naproxen wurde die durch Prostanoide ausgelöste Funktionsstörung der ecPOR$^{-/-}$- Mäuse durch Normalisierung des Angiotensin-II-induzierten Blutdruckanstiegs (Telemetrie) aufgehoben.

Schlussfolgerung

Insgesamt deutet dies darauf hin, dass POR in Endothelzellen die eNOS-Aktivität reguliert und das metabolische Schicksal der Arachidonsäure in Richtung der gefäßerweiternden EETs und weg von den schädlichen Prostanoiden lenken. Fehlt POR, ist diese endotheliale Regulierung beeinträchtigt, was zu vaskulärer Dysfunktion führt.

List of abbreviations

Symbol	Name
AA	Arachidonic acid
AngII	Angiotensin II
BKCa	Large-conductance Ca^{2+}-activated K^+ channel
BP	Blood pressure
BPM	Beats per minute
cGMP	cyclic guanosine monophosphate
COX	Cyclooxigenase
CTR	Control
CVD	Cardiovascular diseases
CYP450	Cytochrome P450
DBP	Diastolic blood pressure
DHET	Dihydroxieicosatrienoic acid
DP1	Prostaglandin D2 receptor 1
DP2	Prostaglandin D2 receptor 2
EBM	Endothelial Basal Medium
EC	Endothelial cells
ecPOR-/-	Endothelial cell-specific cytochrome P450 reductase knockout mouse
EDCF	Endothelium-derived contracting factor
EDRF	Endothelium-derived relaxing factor
5, 6 EET	5, 6 Epoxyeicosatrienoic acid
8, 9 EET	8, 9 Epoxyeicosatrienoic acid
11, 12 EET	11, 12 Epoxyeicosatrienoic acid
14, 15 EET	14, 15 Epoxyeicosatrienoic acid
EGM	Endothelial Growth Medium
eNOS	Endothelial nitric oxide synthase
EP1	Prostaglandin E2 receptor 1
EP2	Prostaglandin E2 receptor 2
EP3	Prostaglandin E2 receptor 3
EP4	Prostaglandin E2 receptor 4
ET-1	Endothelin-1
FAD	Flavin Adenine Nucleotide
FMN	Flavin mononucleotide
FP	Prostaglandin F receptor
HAEC	Human Aortic Endothelial Cells
HETE	hydroxyeicosatetranoic acids
HMEC	Human Mammary Epithelial Cells
HR	Heart rate
HUVEC	Human Umbelical Vein Endothelial Cells
IP	Prostacyclin receptor

Symbol	Name
L-NAME	N (gamma)-nitro-L-arginine methyl ester
NADPH	Nicotinamide adenine dinucleotide phosphate
NF-KB	nuclear factor kappa-light-chain-enhancer of activated B-cells
NO	Nitric oxide synthase
NOS	Nitric oxide synthase
NOX	NADPH oxidase
NSAID	Nonsteroidal anti-inflammatory drug
PGD2	Prostaglandin D2
PGE2	Prostaglandin E2
PGH2	Prostaglandin H2
PGI2	Prostaglandin I2
PKC	Protein kinase C
POR	Cytochorme P450 reductase
SBP	Systolic blood pressure
sEH	Soluble epoxide hydrolase
TBXA2	Thromboxane A2
TBXB2	Thromboxane B2
TP	Thromboxane receptor
VEGF	Vascular endothelil growth factor

Overview of publications

First authorship publications:

Malacarne, Pedro Felipe; Ratiu, Corina; Gajos-Draus, Anna; Müller, Niklas; Lopez, Melina; Pflüger-Müller, Beatrice et al. (2022): Loss of Endothelial Cytochrome P450 Reductase Induces Vascular Dysfunction in Mice. In Hypertension (Dallas, Tex.: 1979) 79 (6), pp. 1216–1226. DOI: 10.1161/HYPERTENSIONAHA.121.18752.

Malacarne, Pedro Felipe; Bezzenberger, Justus; Lopez, Melina; Warwick, Timothy; Müller, Niklas; Brandes, Ralf P.; Rezende, Flávia (2022): Epoxyeicosatrienoic Acid and Prostanoid Crosstalk at the Receptor and Intracellular Signaling Levels to Maintain Vascular Tone. In International journal of molecular sciences 23 (11). DOI: 10.3390/ijms23115939.

Co-authorship publications:

Müller, Niklas; Warwick, Timothy; Noack, Kurt; Malacarne, Pedro Felipe; Cooper, Arthur J. L.; Weissmann, Norbert et al. (2022): Reactive Oxygen Species Differentially Modulate the Metabolic and Transcriptomic Response of Endothelial Cells. In Antioxidants (Basel, Switzerland) 11 (2). DOI: 10.3390/antiox11020434.

Lopez, Melina; Malacarne, Pedro F.; Gajos-Draus, Anna; Ding, Xinxin; Daiber, Andreas; Lundberg, Jon O. et al. (2021): Vascular biotransformation of organic nitrates is independent of cytochrome P450 monooxygenases. In British journal of pharmacology 178 (7), pp. 1495–1506. DOI: 10.1111/bph.15362.

Rezende, Flávia; Malacarne, Pedro Felipe; Müller, Niklas; Rathkolb, Birgit; Hrabě de Angelis, Martin; Schröder, Katrin; P Brandes, Ralf (2021): Nox4 Maintains Blood Pressure during Low Sodium Diet. In Antioxidants (Basel, Switzerland) 10 (7). DOI: 10.3390/antiox10071103.

Wittig, Ilka; Malacarne, Pedro Felipe (2021): Complexome Profiling: Assembly and Remodeling of Protein Complexes. In International journal of molecular sciences 22 (15). DOI: 10.3390/ijms22157809.

Stenton, Sarah L.; Sheremet, Natalia L.; Catarino, Claudia B.; Malacarne, P.; Andreeva, Natalia A.; Assouline, Zahra; Barboni, Piero et al. (2021): Impaired complex I repair causes recessive Leber's hereditary optic neuropathy. In The Journal of clinical investigation 131 (6). DOI: 10.1172/JCI138267.

Siragusa, Mauro; Oliveira Justo, Alberto Fernando; Malacarne, Pedro Felipe; Strano, Anna; Buch, Akshay; Withers, Barbara et al. (2021): VE-PTP inhibition elicits eNOS phosphorylation to blunt endothelial dysfunction and hypertension in diabetes. In Cardiovasc Res 117 (6), pp. 1546–1556. DOI: 10.1093/cvr/cvaa213.

Schader, Tim; Löwe, Oliver; Reschke, Christina; Malacarne, Pedro; Hahner, Fabian; Müller, Niklas et al. (2020): Oxidation of HDAC4 by Nox4-derived H2O2 maintains tube formation by endothelial cells. In Redox Biology 36, p. 101669. DOI: 10.1016/j.redox.2020.101669.

Epah, Jeremy; Pálfi, Katalin; Dienst, Franziska Luise; Malacarne, Pedro Felipe; Bremer, Rolf; Salamon, Michael et al. (2018): 3D Imaging and Quantitative Analysis of Vascular Networks: A Comparison of Ultramicroscopy and Micro-Computed Tomography. In Theranostics 8 (8), pp. 2117–2133. DOI: 10.7150/thno.22610.

Introduction

The endothelium and regulation of vascular function

The endothelium is a single-cell tissue made up of endothelial cells (EC) that cover the inner surface of blood vessels, cardiac valves, and several other body cavities. Contrary to the other vessel components - connective tissue and smooth muscle – whose content varies according to the vessel's function or diameter, the endothelial lining of the vessels is always present [1].

A critical balance between endothelium-derived relaxing and contracting factors defines what is called vascular homeostasis. Further essential endothelium-associated vessel functions include its roles in: angiogenesis, leucocyte adhesion, transport processes and metabolism [2]. The molecular intricacies of the function of this tissue, particularly regarding to the spectrum of vasoactive substances it produces, has been a highlight in cardiovascular research. This is mainly because cardiovascular diseases (CVDs) still represent the major cause of death globally (statistics for 2020) and early detection of associated pathologies are needed to outline management procedures and medicinal interventions that are able to restore endothelial function [3].

The importance of the endothelium goes beyond its own sustenance. This tissue acts as a bridge between nutrients found in the blood and the nutrient dependent organs controlling the passage of materials [4]. How the endothelial cells handle the processing of these nutrients before being transported to other tissues is a matter of great interest, albeit the process is still poorly understood. Furthermore, ECs display a remarkable behavioural plasticity [5]. While they may stay quiescent for long periods of time, they can promptly switch to an activated, highly proliferative, and migratory state in response to growth factor stimuli, primarily through vascular endothelial growth factor (VEGF) signalling or other external factors [6].

Stimulation of endothelial cells by external factors such as hormones, platelet derived substances, mechanical sheer stress and neurotransmitters promote the release of substances that change endothelial function. These comprise molecules that are generally termed as endothelium-derived relaxing and contracting factors (respectively EDRF and EDCF) (**Figure 1)**. Each of them,

through unique pathways, result in vasomotion by stimulating or inhibiting smooth cell contraction. Currently, the term EDRF (endothelium-derived relaxing factors) expands beyond the notion that nitric oxide (NO) and Prostacyclin (PGI2) are the sole vessel relaxing factors [7]. A study using female double knockout mice for the endothelium nitric oxide synthase (eNOS) and cyclooxygenase-1 (COX-1), generators of NO and PGI2, respectively, showed no overall differences in arterial blood pressure when compared to the control littermate [8]. This highlights the notion that other molecules, designated as endothelium derived hyperpolarizing factors (EDHF), contribute to vessel tone. The identity of these EDHFs is not completely elucidated, but reported factors include the epoxyeicosatrienoic acids (EET), potassium and hydrogen peroxide which are products of enzymatic reactions of the cytochrome P450 enzymatic system and superoxide dismutase, respectively [7]. The contracting factors, termed as EDCFs counterbalances the effects of the EDRF in keeping the normal vessel tone. Some examples include: Endothelin-1, Angiotensin II, reactive oxygen species (ROS) and several cyclooxygenase (COX)-dependent prostanoid products such as Thromboxane A2 and Prostaglandin H2 [9].

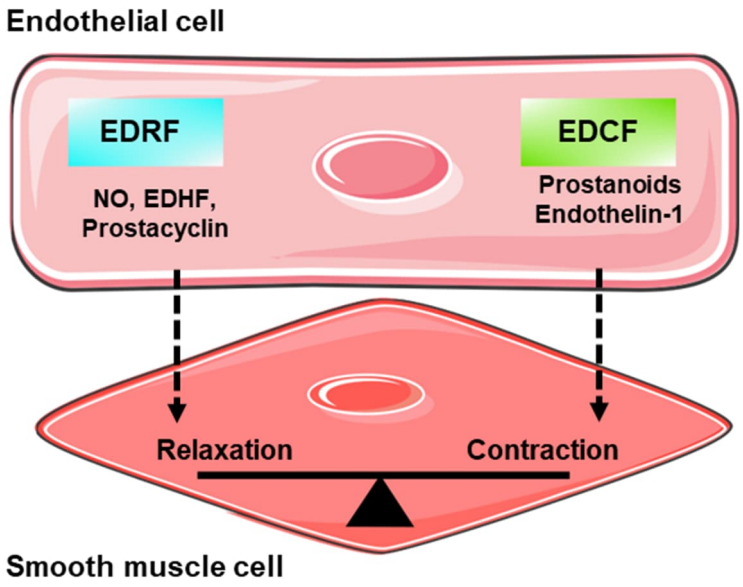

Figure 1: Control of vessel tone
Under steady-state conditions there is a balance in the production of EDRF and EDCF to maintain a healthy vessel tone. Under disease conditions such as hypertension this balance is shifted, with increased production of EDCF that increases vessel contraction.

The overall balance between EDRF and EDCF dictates the contraction of smooth muscle cells in the *tunica media* layer of the vessels. This, in turn, determines the diameter and tone of the blood vessels, and ultimately regulates blood flow and arterial blood pressure (BP). An unbalanced production of these factors along with endothelial inflammatory activation leads to endothelial dysfunction and to various cardiovascular diseases such as hypertension [10]. Generally, endothelial dysfunction of conduit vessels is caused by low NO availability due to reduced endothelial nitric oxide synthase (eNOS) activity [11] or NO scavenging by superoxide anions produced under inflammatory conditions. In smaller resistance vessels (<400 µm diameter) other endothelial mediators such hydrogen peroxide, potassium ions and EETs devise the effects of NO [12] (**Figure 2**). An unbalance in these mediators appear early in the course of cardiovascular disease, before the clinical manifestation of vascular disease and thus can serve as clinical parameters in prevention of cardiovascular events.

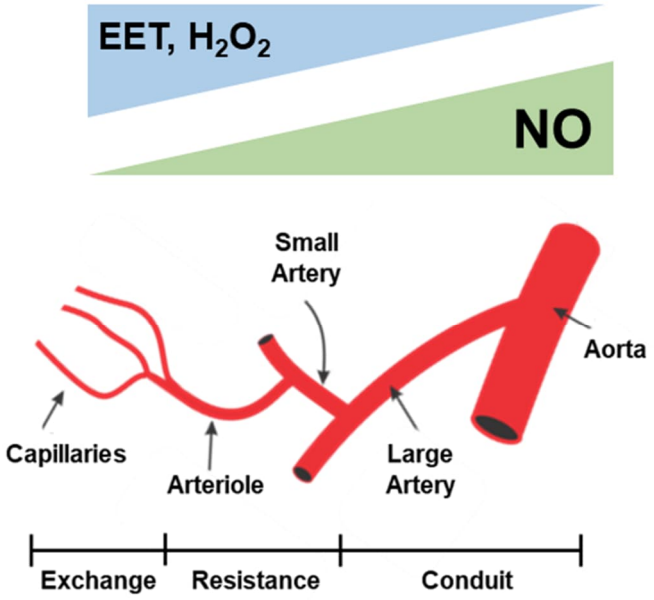

Figure 2: Arterial vessels
Conduit (aorta and large arteries) and resistance vessels (small arteries and arteriole) carry arterial blood to capillaries for tissue distribution of nutrients and gases. Adapted image from [13].

The cytochrome P450 system

Cytochrome P450 enzymes are a large family of heme-containing monooxygenases present in prokaryote and eukaryote organisms ranging from virtually every mammalian tissue as well as in plants, bacteria, yeast and insects

[14,15]. The CYP450 superfamily has a common overall structure and topology, however, the individual CYP450 isoenzymes share only between 16% to 26% of sequence identity [16]. CYP450 enzymes have central roles in the oxidative metabolism of endogenous (fatty acids, steroids, prostaglandins) and exogenous substrates such as drugs. This is due to their ability to efficiently catalyse a diversity of biotransformation, such as hydroxylation, epoxidation and isomerization among others represented in **Figure 3.** Functionally, all CYP450 share in common the transfer of molecular oxygen to X-H bonds of the substrate, with its consequential oxidation, alongside a reduction of molecular oxygen to water in their catalytic cycle [17].

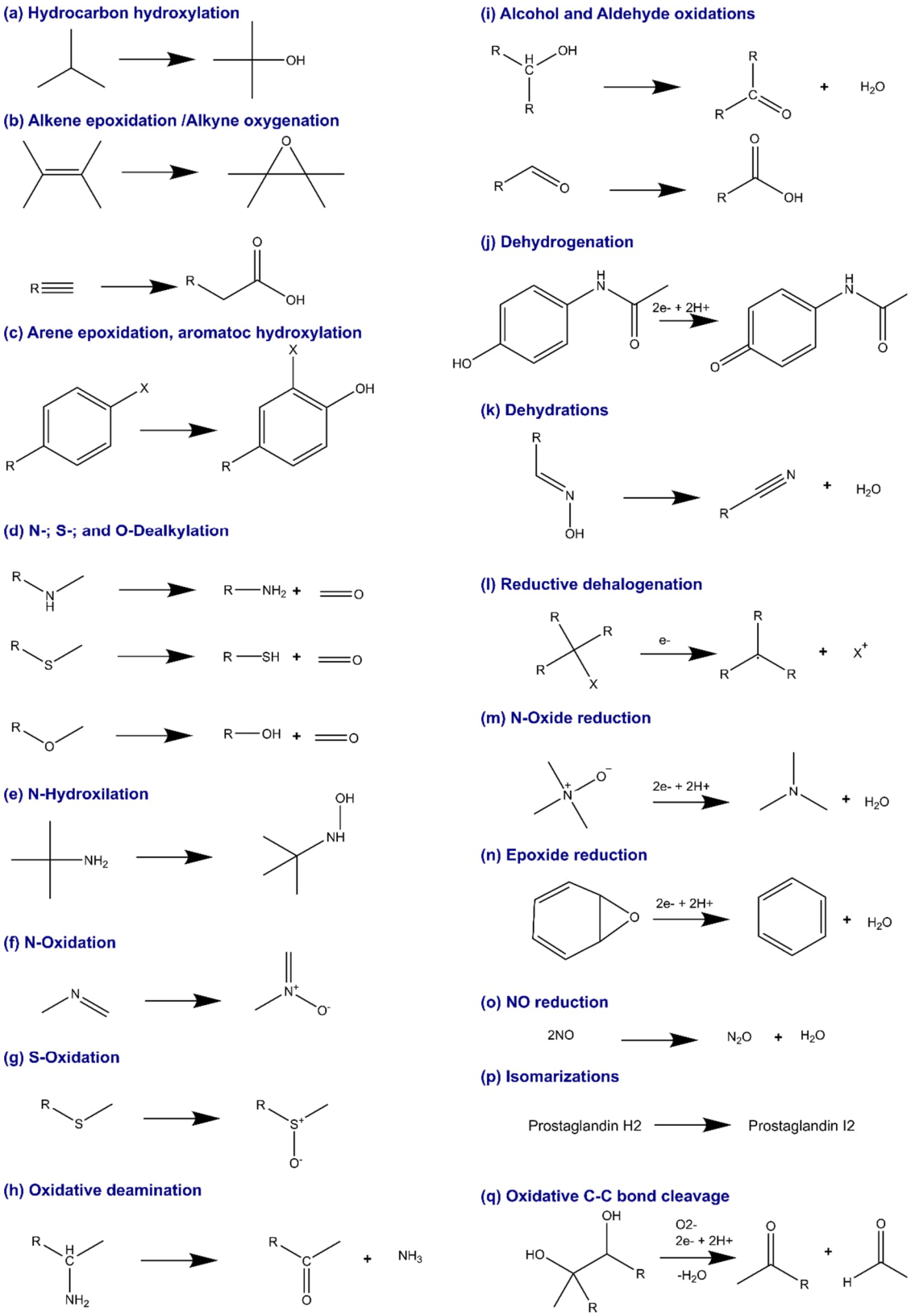

Figure 3 Schematic summary of the diverse P450-catalyzed reactions
Image adapted from review that describes the mechanism of action of CYP450s [15].

Regarding the CYP450 nomenclature, both the genes and the enzymes are abbreviated with the symbol “CYP” followed by a number representing the gene family, a capital letter which indicates the subfamily and an end number which depicts a specific member of that subfamily [18].

Genetic polymorphisms, xenobiotic, hormones, cytokine, different diseases and biological factors such as age and sex can all influence the expression of individual CYP [19]. Their expression level and isoform availability are also tissue dependent. Several studies focus on the pharmacological aspect of these enzymes, along with how their genetic variability or polymorphism may influence a patient's response to different drugs [20]. CYPs are largely expressed in the liver and thus important metabolic enzymes. Thirty different isoenzymes have been identified in human liver tissue [21], with the numbers continuing to grow as more genomes are sequenced. They are also expressed across across the vascular system in both endothelial and smooth muscle cells. The CYP4A, CYP2C, and CYP2J families are described to have a cardiovascular function [22]. The different CYP450 isoenzymes overlap functionally. Therefore, targeting individual CYP450 for inhibition can be problematic as isoenzymes can compensate at expression and functional levels [23,24]. Specific CYP450 inhibitors have been described and sulfaphenazole, a selective CYP2C9 inhibitor for example, is relevant for the the vascular system [25]. Its mode of action in the cardiovascular system is, however, unclear but suggested to mitigate reactive oxygen species [26] or supress the formation of arachidonic acid-derived endothelial contracting and relaxing factors [27].

The cytochrome P450 reductase is a master regulator of cytochrome P450 activity

All microsomal CYP450 isoenzymes depend on a single enzyme called the cytochrome P450 reductase (POR) for their function. POR is a membrane bound protein and the only enzyme so far known capable of oxidizing NADPH molecules that can supply electrons for the CYP450 system [28,29]. Albeit the cytochrome b5 enzymes can also deliver electrons to CYP450 enzymes, they act as bridges for incoming electrons generated by POR [29]. Thus, POR is essential for all microsomal CYP450-catalysed oxidative metabolic reactions such as fatty acid anabolism, drug metabolism, heme degradation and sterol biosynthesis.

POR is a membrane-bound flavoprotein with a MW of 78 kDa. It is located on the cytoplasmic leaflet of the endoplasmic reticulum and can be found associated with its interaction partners: the microsomal CYP450s, cytochrome b5, and hemeoxygenases (HO-1/2) (**Figure 4**). Studies report a ratio of CYP:POR of about 5:1 and that these enzymes form complexes in a way that a central POR enzyme is surrounded by multiple CYP molecules [30,31].

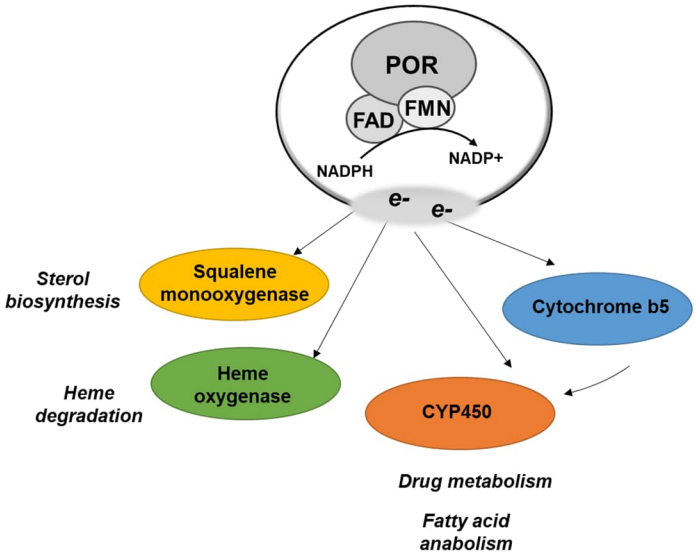

Figure 4: POR and its interaction partners.

Structurally, POR contains three main domains: (i) a hydrophobic N-terminal domain that anchors the enzyme to the membrane, (ii) a flavin mononucleotide (FMN)-binding domain, (iii) and a shared flavin adenine nucleotide (FAD) and reduced nicotinamide adenine dinucleotide phosphate (NADPH) binding domain which is homologous to ferredoxin-NADP+ reductases and which share significant sequence identity with nitric oxide synthase [32,33].

The catalic cycle performed by POR initiates with a transfers of two electrons from NADPH to the redox cofactor FAD. Then, these electrons flow through the FMN domain, which is acidic and able to interact with the basic binding site of its redox partners: CYP450s, CYPb5 or hemeoxygenase-1 and -2. From there on the electrons are transferred from POR to the heme iron of the later enzymes, powering their catalytic reaction [34] (**Figure 5**).

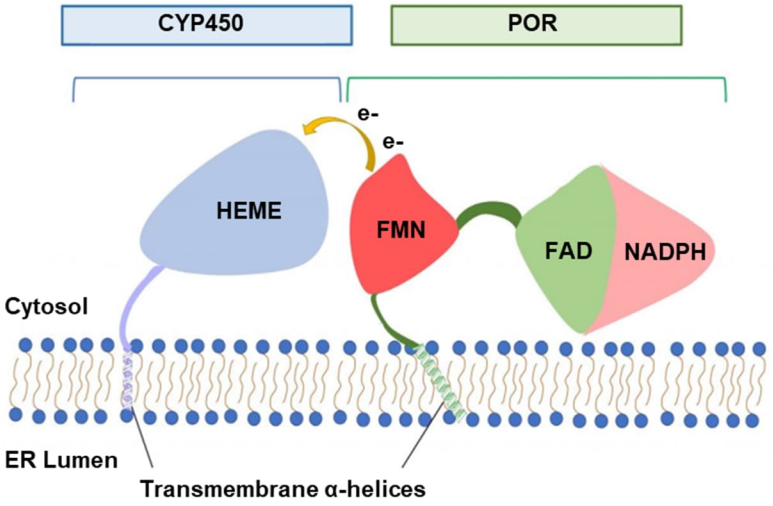

Figure 5 POR/CYP450 complex in the ER membrane
The formation of the CYP450-POR complex is required for the transfer of the electrons from NADPH to the CYP450 catalytic site. Transfers of electrons happen one at a time with a full cycle consisting of two electrons. Adapted figure [35].

POR is broadly expressed in the vascular system

The cytochrome P450 reductase is expressed in all tissues with distinct expression levels across the different cell types and organs as shown by *Tabula Muris*, a compendium of single cell transcriptome data from mice (*Mus musculus*) accessed on "https://tabula-muris.ds.czbiohub.org/" **(**Error! Reference source not found.**)**.

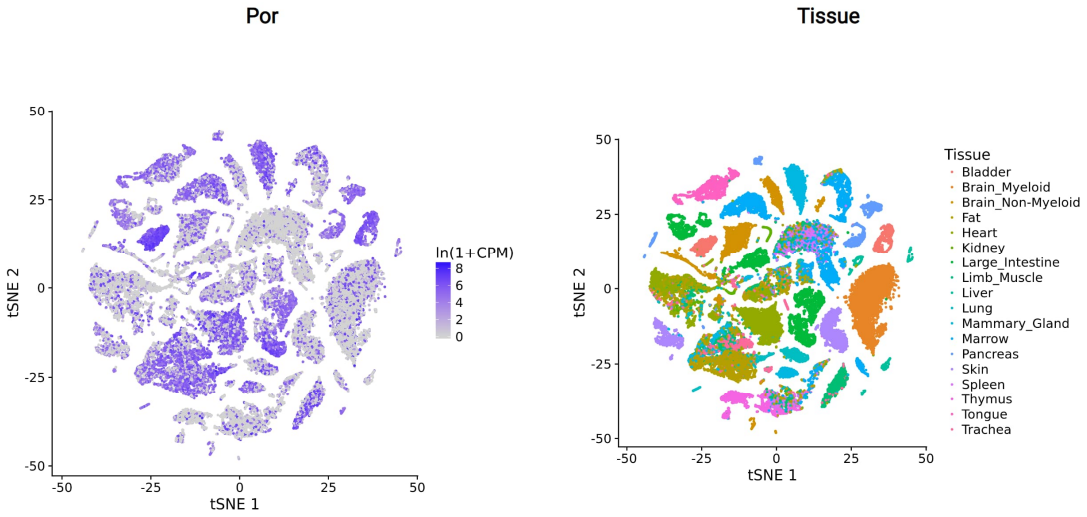

Figure 6: Expression of POR across murine tissue
Plots generated from the *Tabula muris* website: https://tabula-muris.ds.czbiohub.org/

Publicly available data from single cell sequencing of mouse aorta also shows that POR is expressed in vascular cells [36] **(Figure 6)**. POR expression is known to be controlled by transcription factors of the Kruppel family members (Klfs) [37].

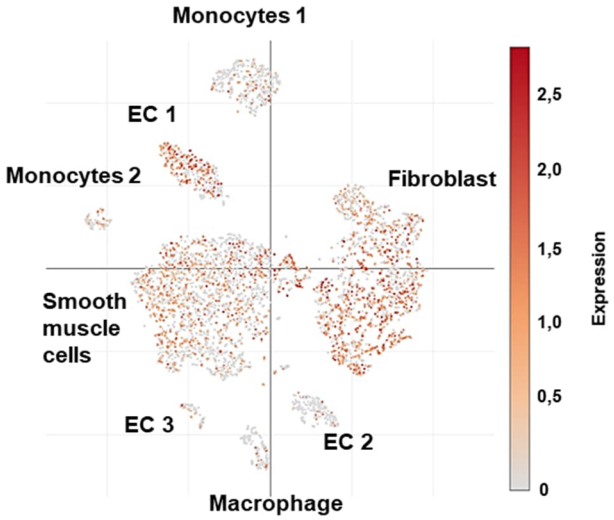

Figure 6: POR in the vascular tissue
Analysis of publicly available data [36] from single cell sequencing of mouse aorta. Distribution plot shows POR expression in murine aortic tissue.

POR deficiency has been linked to patients with steroidogenic disorders associated with Antley-Bixler syndrome (ABS, which leads to skeletal malformation) [38]. Of the single nucleotide polymorphism (SNPs) for POR listed on PubMed, 60% are yet of undefined clinical relevance. Genetic studies of POR in a population of 842 healthy individuals revealed 140 SNPs, of which 43 were found in ≥1% of alleles [39]. The correlation between SNPs and POR activity is experimentally limited. Usually POR activity is assayed in vitro by testing the capacity of the mutated purified POR (recombinantly expressed) to reduce cytochrome *c*, reflecting its initial identification as a cytochrome *c* reductase [39]. This method is taken as a poor readout, but to assay native CYP substrates individually is impracticable. For this reason, clinical demonstration of disease relevance of POR usually comes from individual clinical cases with steroidogenic disorder. An example is a case that relates congenital adrenal hyperplasia that shows a single amino acid mutation localized at the cofactor-binding sites of POR [40]. Furthermore, a genotype-phenotype association search performed with the online tool PhenoScanner [41] revealed a significant association of single

nucleotide position (SNPs) in the POR gene with congestive heart failure and peripheral vascular diseases.

So far only a few studies have worked with animal knockout models of POR [42,43]. This is partly due to the fact that constitutive knockout mice of POR are embryonically lethal [44]. Examination of the morphology of global POR-/- mouse embryos showed a spectrum of abnormalities, one of which included histological evidence of defective heart development [44].

Arachidonic acid is a key precursor for vasoactive lipids

Arachidonic acid (AA) is an essential polyunsaturated 20 carbons-ω6-fatty acid and a precursor of numerous bioactive PUFAs that regulates numerous cellular functions [45]. It is a substrate for various lipid oxidizing pathways that involve enzymatic systems such as POR/CYP450, lipoxygenase (LO) and cyclooxygenase (COX).

AA is an integral constituent of biological cell membranes, occupying the hydrophobic tail ends of phospholipids. It plays an important role in maintaining membrane structure and its fluidity [46,47]. Virtually all intracellular AA is found in lipid membranes where it is mainly esterified in the sn-2 position. Its dynamics is tightly regulated through multiple pathways which include activation of Toll-like receptor 4 (TLR4), purinergic receptors and inflammation [48]. It can be hydrolysed and released from membranes through the action of phospholipases; A2 and C [49]. Its metabolism by the aforementioned enzymatic systems leads to a variety of AA-derived oxylipins with distinct biological actions (**Figure 7**), many of which are still not completely characterized [50].

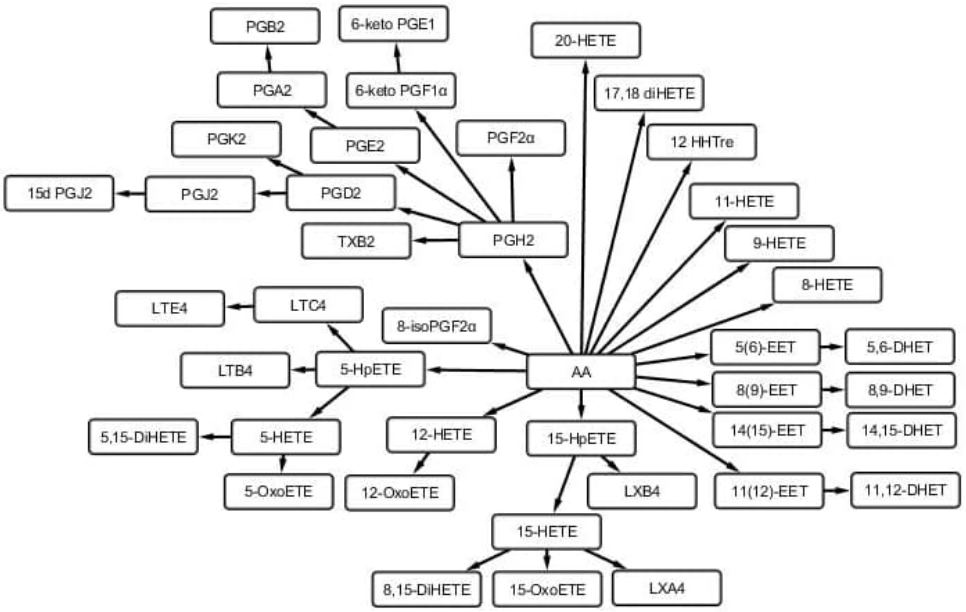

Figure 7: Overview on metabolites derived from arachidonic acid
Network map of oxylipins that derive from arachidonic acid metabolism made using the Cytoscape mapping tool [51].

In the vascular system, smooth muscle cells are often linked with the CYP4A-mediated metabolism of arachidonic acid to hydroxyeicosatetraenoic acids (HETEs)—which have vasoconstrictor properties [52]. Endothelial cells, on the other hand, are reported to generate mostly epoxyeicosatrienoic acids (EETs) which are associated to vasodilatation and lower blood pressure [53]. However, CYP450 enzymes can also demonstrate mixed functions generating both EETs and HETE with ratios varying between the specific CYP isoforms [54].

EETs and Vascular Function

EETs are epoxide eicosatrienoic acid metabolites of AA. They result from a CYP coordinated epoxygenase attack of one of the olefin bonds of AA, located between carbons 5-6, 8-9, 11-12 and 14-15, yielding their correspondent eicosatrienoic acid: 5,6-EET; 8,9-EET; 11,12-EET and 14,15-EET [54] (**Figure 8**). CYP have been shown to be relatively selective in which EET they produce, with different enzymes often producing significant amounts of only one or two of the isomers [55].

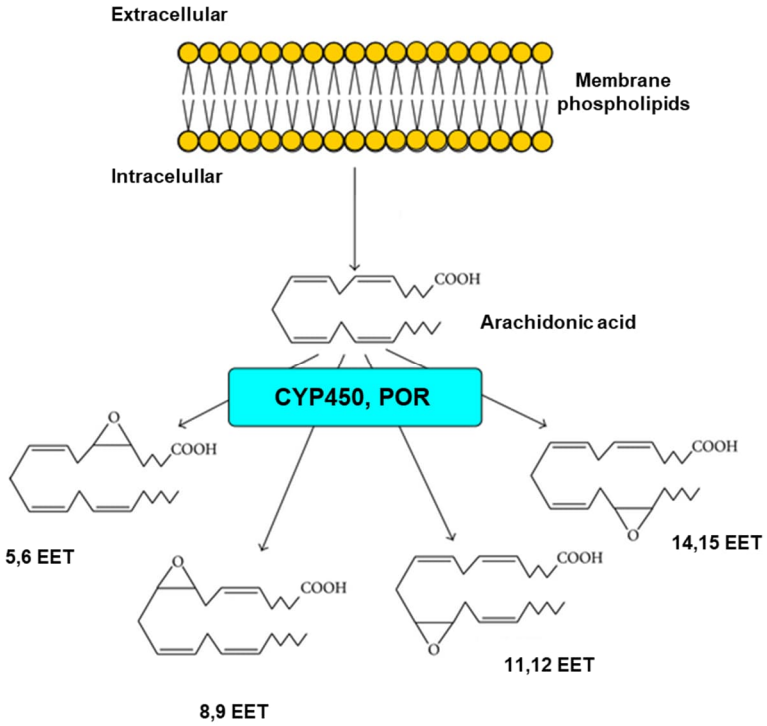

Figure 8: Production of EETs from arachidonic acid
Membrane-released arachidonic acid is catabolized by the POR/CYP450 system into one of the four region-isomers of EETs. Adapted figure [56].

Following production, EETs can be esterified into phospholipids through a coenzyme-A-dependent reaction, providing a temporary storage site for excess amounts of EET [55]. They can also be readily hydrolysed free from the membrane to initiate a cellular response. Several biological actions have been attributed to EETs: Control of hormone release from endocrine cells, increase of axon growth in neurons, regulation of platelet aggregation responses, cardio-protectiveness after an ischemic heart attack and the ability to control vascular tone and, consequently, blood pressure [57,58]. The mechanisms underlying the vascular effects of EET have not been fully elucidated yet. Several studies associate EETs released from the endothelium as transferable factors that interact with G protein–coupled receptors of the smooth muscle cell layer [59]. High affinity binding sites for EET have been described [60,61]. These activate large conductance, calcium-sensitive potassium channels that lead to K^+ influx and hyperpolarization of the smooth muscle cell membrane. This culminates with closure of calcium channels and reduction of cytosolic calcium levels. In parallel, another potential mechanism is that EETs from the endothelium act in an autocrine manner, leading to either a hyperpolarizing current that is spread from

endothelial cells to smooth muscle cells through gap junctions or an efflux of K+ from endothelial cells to the interstitial space leads to increased influx of K+ in SMCs [62]. Moreover, EETs, have been linked to NO release [63,64] thus yielding autocrine and paracrine effects [65].

Irrespective to the ambiguity of their molecular mechanism, EETs are linked to vessel relaxation. The identification of EETs as EDHF dates back to a study by Campbell and collaborators that showed an equivalent vasodilation with all four EET regioisomers on bovine coronary [63]. This effect was abolished by tetraethylammonium (TEA), an inhibitor of Ca^{2+}-activated K^+ channels, a hallmark mechanism for EDHF dependent relaxation. EETs have been identified in several vascular beds including human mammary arteries [66], porcine coronary arteries [67] and mouse skeletal muscle arteries [68]. In human arteries and arterioles, the main CYPs associated with EET production is CYP2C8, CYP2C9 and CYP2J2 [69]. Similarly, murine tissue also shows Cyp2C isoforms as the ones accounting for EET generation [70]. To date, information on the levels of CYP450 expression in different blood vessels and how the epoxygenase activity is regulated in pathophysiological states is still limited. Conversely, the regulation of intracellular levels of EETs is well understood. These epoxides are tightly controlled through their catabolism by the epoxide hydrolase 2 (sEH) enzyme. This is the most studied of the EETs catabolizing enzymes, oxidizing them to their corresponding diols (DHETs). Similarly to CYP450s, sEH is highly expressed in liver, but can also be found in the vascular endothelium, smooth muscle cells, neurons, leukocytes and in red blood cells [71]. Up-regulation of sEH is linked to the hypertensive phenotype found in spontaneous hypertensive rats (SHR), a result of the reduction in their EET levels and consequential blunt of endothelium-dependent vasodilatation [72]. sEH inhibitors have also been proposed as pharmaceutical tools in the treatment of hypertension [73,74]. Apart from the sEH dependent catabolism, these lipids can also be utilized in β-oxidation or fatty chain elongation reactions.

Prostanoids with a vascular function

Alongside EETs, prostanoids are the other major branch of AA-derived vasoactive lipids. They are a subclass of eicosanoids, oxidized polyunsaturated fatty acid (PUFA) which consists of the prostaglandins, the thromboxanes and prostacyclin which are collectivelly named oxylipins. The formation of prostanoids

mainly occurs through the action of the cyclooxygenase isoenzymes 1 and 2 (COX-1 which is constitutive and COX-2 is inducible) [62]. First, AA is converted to PGG_2 by COX through its cyclooxygenase activity. This reaction is followed by a COX-assisted peroxidase reduction of PGG_2 with formation of PGH_2. PGH_2, in turn, serves as substrate for various enzymes such as thromboxane synthase, prostacyclin synthase, prostaglandin D synthase, prostaglandin F synthase and prostaglandin E synthase, leading to the formation of Thromboxane A_2 (TXA_2), Prostacyclin (PGI_2), Prostaglandin D_2 (PGD_2), Prostaglandin F_2 (PGF_2) and Prostaglandin E_2 (PGE_2), respectively [49].

Studies have linked the metabolic fate of AA to the individual COX isoforms. By using COX-1 knockout mice (COX-$1^{-/-}$) it was shown that in brain tissue TXB2 production is preferentially coupled to COX-1, whereas PGE2 production is more associated to COX-2 [75]. COX-1 is the constitutive form, playing a housekeeping role, whereas the inducible COX-2 can be up-regulated due to sheer stress, cytokines and tumours [76]. Structurally, both isozymes are nearly identical, differing only by the presence of a side pocket extension to the hydrophobic channel in COX-2. This structural difference has led to the generation of specific inhibitors for COX-2, called COX-2 selective non-steroidal anti-inflammatory drugs (NSAIDs), which are used in clinical practice [77]. It is important to note that while COX-2 selective drugs show reduced side effects associated with non-selective cox inhibitors such as gastrointestinal events, they have been linked with increased cardiovascular events [78,79].

In vessels, prostanoids act by either contracting or relaxing the smooth muscle layer through activation of their different receptors. These receptors are termed based on their preferential ligand, seen as they show degrees of promiscuity among the different prostanoids [80]. They are G protein-coupled receptors of the rhodopsin-like receptor family (subfamily A14) [80] and are as follow: Prostaglandin DP1 receptor (DP_1), Prostaglandin DP2 receptor (DP_2), Prostaglandin EP1 receptor (EP_1), Prostaglandin EP2 receptor (EP_2), Prostaglandin EP3 receptor (EP_3), Prostaglandin EP4 receptor (EP_4), Prostaglandin F2α receptor (FP), Prostacyclin I2 receptor (IP) and Thromboxane A2 receptor (TP) [80].

The TP receptor is the preferential receptor for TXA2. Its function has been widely associated with platelet aggregation and smooth muscle contraction [81]. U46619

is a TP selective agonist that induces contraction in both aorta and mesenteric vessels, and it is commonly used to study the vessel relaxing properties of EETs. Different to the TP-mediated vessel contraction, prostacyclin and prostaglandin D_2 act on the IP and DP1 receptor, inducing vessel dilation. PGE_2's vessel effects, on the other hand, depend on which subset of receptor it binds to. Through the EP2 and EP4 receptors, PGE2 leads to vessel dilation, and through the EP1 and EP3 receptors it leads to constriction. The role of EP1 receptor signalling has been further explored in the context of Angiotensin II-dependent hypertension, and it frontlines as a possible novel target for new antihypertensive therapy [82,83]. A schematic representation of the prostanoids, its receptors, along with the different EETs is shown in **Figure 9**.

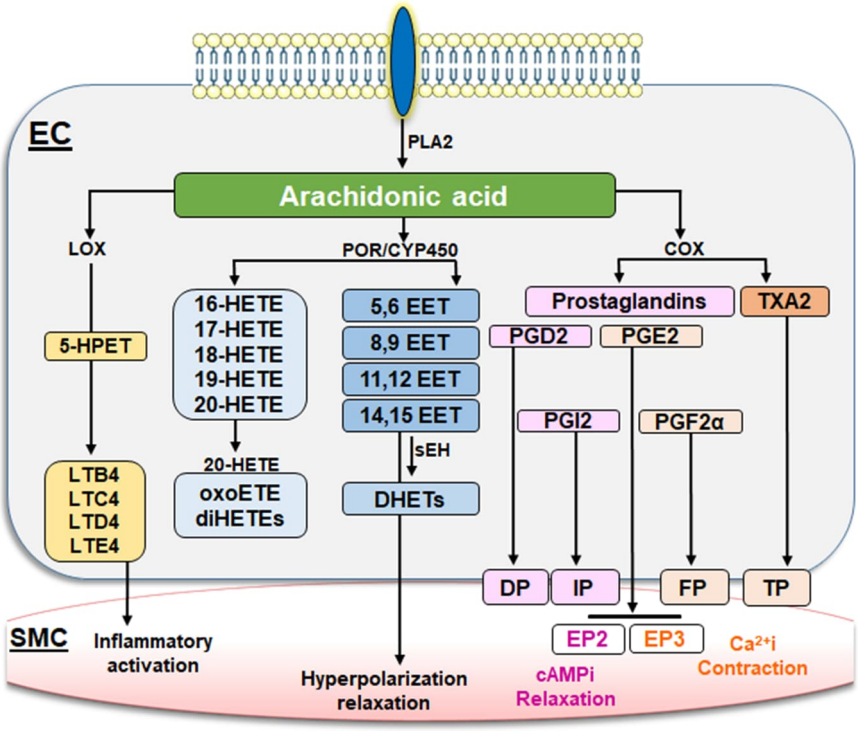

Figure 9: Arachidonic acid and its contracting and relaxing lipid metabolites
Figure adapted from [84].

The endothelial nitric oxide synthase

In mammals, one of the primary functions of NO is to relax smooth muscle cells. NO rapidly diffuses from its producing cells into the neighbouring ones. As its half-life is relatively short, about 5-10 seconds. It mainly acts locally before it is converted to nitrates and nitrites. The Nitric Oxide Synthase 3 (NOS3), also

termed endothelial NOS (eNOS), is one of the three isoforms of the nitric oxide (NO) generating enzymes. Interestingly, the reductase domain of eNOS is highly homologous to POR, sharing NADPH binding sites, along with two flavin domains, an FMN and an FAD domain [85]. Moreover, the N-terminal oxygenase domain of the enzyme contains binding sites for a heme group, zinc, (6R-)5,6,7,8-tetrahydro-L-biopterin (BH4) and the substrate L-arginine [86].

Nitric oxide results from the reaction of L-arginine and oxygen catalyzed by eNOS using reducing equivalents from NADPH. Similarly to the reaction cycle of POR, electron equivalents are first transferred from NADPH that sequentially flow through the FAD and FMN. These electrons then move to the heme system where they reduce O_2 to oxidize L-arginine to L-citruline and NO [87].

The activity of eNOS is determined by intracellular Ca^{2+} concentrations [87]. It can also be regulated at the post-translational level through lipidation by myristoylation or palmitoylation of the enzyme, or through fine tuning of its phosphorylation state. Kinases such as AKT [88], protein kinase (PK) [89] and adenosine monophosphate-activated kinase (AMPK) [90] phosphorylate eNOS the serine 1177 (Ser1177) of eNOS, facilitating its activity. Conversely, eNOS phosphorylation at threonine residue 495 (Thr495), through Protein Kinase C (PKC) blocks the Calmodulin binding site of the enzyme, decreasing its overall activity [86,91]. Similarly, phosphorylation of the tyrosine residue Tyr657 also leads to inhibition of the enzyme. Dysregulation of these controlling mechanics can lead to a reduction in nitric oxide (NO) and consequentially vascular dysfunction (**Figure 10**).

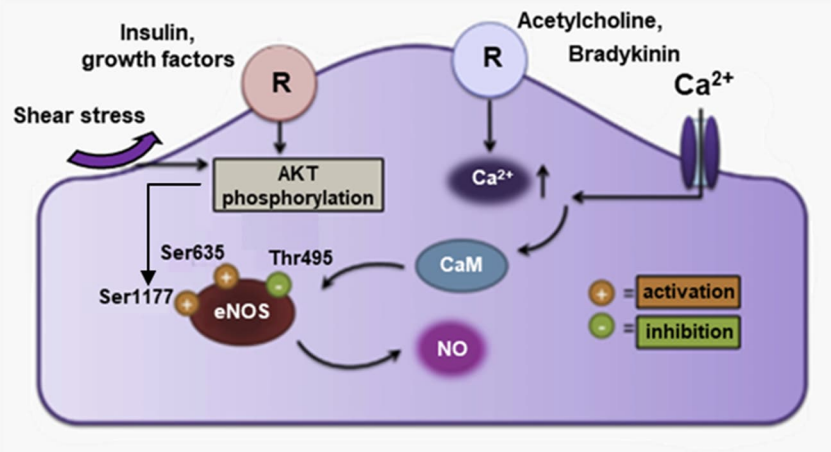

Figure 10: Activation of endothelial nitric oxide synthase
eNOS can be can be activated through calcium-dependent and independent mechanisms. Substances such as acetylcholine and bradykinin act on their specific receptors (R) which culminate with increased intracellular Ca^{2+} that binds to calmodulin (CaM) leading to the activation of calmodulin-binding domain of eNOS. On the other hand, shear stress, insulin and other growth factors can modulate phosphorylation of eNOS in a pathway independent of intracellular Ca^{2+}. Thr495 is an inhibitory site, while Ser635 and Ser1179 are activation sites. Adapted figure [77].

The physiological functions attributed to eNOS go beyond the aforementioned control of vessel tone and these include: inhibition of platelet aggregation, leucocyte adhesion and vascular inflammation, control of smooth muscle cell proliferation and regulation of myocardial contractility [87]. Endothelial dysfunction is often associated with eNOS dysregulation with lower eNOS activity or eNOS uncoupling which is characterized by a reduction in the synthesis of NO and increased generation of superoxide and hydrogen peroxide. This shift is considered a hallmark of many cardiovascular diseases [86].

Interactions between eNOS and EDHF producing systems

Experimental evidence shows that in the disease state there is an overall shift from the classical NO-mediated endothelium-dependent relaxation towards an EDHF dependent one [92]. Moreover, lower NO levels lead to an increase in superoxide anions ($O_2^{\bullet-}$) in cells. $O_2^{\bullet-}$ has been shown to increase the expression of endothelin-1 (ET-1) in endothelial and smooth muscle cells and this enhances the activation of its receptor, the endothelin A receptor, which culminates with activation of COX-2 and the subsequent increased formation of TXA2 and PGE2 [93]. Thus, a balance between NO and EDHF is detrimental to maintain vascular homeostasis.

Aim of Study

The aim here was to understand the physiological consequences of deleting POR specifically from endothelial cells. This was explored in the context of both a tamoxifen inducible knockout model and in cells using the CRISPR/Cas method. In terms of techniques used some examples include classical, yet insightful, physiology methods such as organ bath, nitric oxide measurements, alongside cutting edge molecular biology tools such as RNAseq and lipidomics.

Materials

Chemicals

Chemical	Source
A23187, Calcium ionophore	Sigma Aldrich
Acetic acid	Sigma Aldrich
Acetylcholine	Sigma Aldrich
Acrylamid-Biacrylamid Rotiphorese Gel 30	Roth
Angiotensin II	Bachem
Bepanthen	Bayer
Betadine (Braunol)	B.Braun
Bovine Serum Albumin (BSA) 7.5%	Gibco
Bromphenol Blue	Applichem
Buprenorphine	Phyzer
Calcium chloride dihydrate	Sigma Aldrich
Calcium Titriplex-dihydrate	Merck
CASYton	OLS
Clorgyline	Sigma
DETA NONOate	Enzo
Dithiothreitol DTT (qPCR)	ThermoFisher
dNTPs	Bioline
Dulbecco`s Phosphate Buffered Saline (DPBS)	Gibco
11,12 - EET	Cayman Chemicals
14,15 - EET	Cayman Chemicals
Ethanol absolut and ethanol 70%	Sigma Aldrich
Fetal Calf Serum (FCS)	Sigma Aldrich
Gelatine	Sigma Aldrich
Hank`s	Sigma Aldrich
Hank`s HBSS	Applichem
12- HETE	Cayman Chemicals
Hepes	Sigma Aldrich
Hydrochloric acid (HCl)	Roth
Insulin	Sigma Aldrich
Isoflurane	Abbvie
iTaq Universal SYBR Green Supermix	BioRad
Isoflurane (Forene)	Abbvie
L-Arginine:HCl (13C6)	Cambridge Isotope Lab
L-Glutamin (100x)	Gibco
L-NAME (Nω-Nitro-L-arginine methyl ester hydrochloride)	Sigma Aldrich
Loading Dye	Fermentas
Magnesium sulfate heptahydrate	Sigma Aldrich
Methanol	J.T.Baker
NaI	Sigma Aldrich
NADPH	Applichem
Naproxen	Sigma Aldrich
Nω-Nitro-L-arginine (L-NA)	Sigma Aldrich

Okadaic acid (OA)	Applichem
Orthovanadate (OV)	Applichem
(2x) PCR Master Mix	Thermo Fisher
Penicilin/Streptomycin	Gibco
Phenylephrine hydrochloride	Sigma Aldrich
Phenylmethanesulfonylfluoride (PMSF)	Sigma Aldrich
Polybrene	Sigma Aldrich
Potassium chloride (KCl)	Roche
Potassium dihydrogen phosphate	Roth
Puromycin	Sigma Aldrich
R-(-)-Deprenyl hydrochloride	Sigma Aldrich
Random Primers	Promega
Reverse Transcriptase Superscript III	Life Technologies
Roti-Block	Roth
Roti GelStain	Roth
Rotiphorese Gel 30	Roth
Roti-Quant	Roth
Sodium bicarbonate	Sigma Aldrich
Sodium chloride (NaCl)	Sigma Aldrich
Sodium dodecyl sulfate (SDS)	Roth
Sodium Nitrite	Merck
Tetramethylethylenediamine (TEMED)	Applichem
Trichloroacetic acid	Sigma Aldrich
TRIS	Roth
Triton X-100	Roth
Trypsin-EDTA	Sigma Aldrich
Tween 20	Sigma Aldrich
Tyrode's salt	Sigma Aldrich
U46619	Sigma Aldrich

Buffers and solutions

Buffer	**Content**
Hanks' buffer	Na_2CO_3 (4 mM) In Hanks' salt
Krebs-Henseleit solution (Stock solution I) (Organ bath)	$CaCl_2$ dihydrate(40 mM); NaCl (2.97 M); $MgSO_4$ heptahydrate(30 mM); KCl (120 mM)
Hepes Tyrode buffer (HT buffer)	19g Tyrodes' salt 4,77g Hepes to 2L ddH_2O, pH 7.4 at 37 °C
Potassium-enriched Krebs-Henseleit Solution (Stock solution I-KCl) (Organ bath)	NaCl (112 mM); KCl (1.97 M); $CaCl_2$ dihydrate(40 mM); $MgSO_4*7H_2O$ (30 mM)

Stock solution II (Organ bath)	$NaHCO_3$ (0.63 M); KH_2PO_4 (30 mM)
Ca-EDTA solution (4.1%) (Organ bath)	4.1g Ca-Titriplex; to 100 mL ddH_2O
Krebs-Henseleit Wash Buffer (Organ bath)	Glucose (12 mM); 80 mL Stock solution I; 80 mL Stock solution II; 520 µL Ca-EDTA; to 2L ddH_2O
Potassium-enriched buffer (Organ bath)	Glucose (12 mM); 40 mL Stock solution I-KCl; 40 mL Stock solution II; 260 µL Ca-EDTA; to 1L ddH_2O
Solution for NOA analyser	9 mL glacial acetic acid 1 mL NaI (50mg/mL)
Triton Lysis Buffer (Western blot)	Tris/HCl pH 7,5 (20 mM); NaCl (150 mM); NaF (20 mM); 1% Triton X-100; Sodium orthovanadate (OV) (2 mM); okadaic acid (OA) (10 nM); protein inhibitor mix (PIM) containing Antipain, Aprotinin, Chymostatin, Leupeptin, Pepstatin and Trypsin-Inhibitor (10 nM); phenylmethylsulfonyl fluoride (PMSF) (40 µg/mL)
10x Wash Buffer (Western blot)	0.3% Tween-20; Tris/HCl pH 7.5 (50 mM); NaCl (150 mM)
10x Running Buffer (Western blot)	Tris (25 mM); Glycine (190 mM); 0.1% SDS
10x Transfer Buffer (Western Blot)	Tris (25 mM); glycin (190 mM); 20% methanol
Genomic DNA Lysis Buffer	Tris/HCl pH=8.5 (0.5 M) NaCl (1 M) 20% SDS EDTA (0.5 M) Proteinase K (22.2 mg/mL)
50x modified TAE Buffer	Tris (242 g) 57.1 mL acetic acid EDTA pH=8.0 (10 mM) to 1L ddH_2O
6x DNA Loading Buffer	30% Glycerol 0.25% Bromphenol Blue 0.25% Xylene Cyanol to 10 mL ddH_2O

Cell culture media

Product	Source
Endothelial basal medium (EBM) supplemented with glutamine	Pelo Biotech
Enhanced Endothelial Cell Growth Medium (EGM) supplemented with glutamine, bFGF, hEGF, VEGF, 8% fetal calf serum, 0.5% penicillin/streptomycin	Pelo Biotech
Trypsin solution (10x)	Sigma Aldrich

Consumables

Material	**Source**
High profile strip PCR Tubes	Starlab
35mm cell culture plate	BD
60mm cell culture plate	Sarstedt
100mm cell culture plate	Sarstedt
24-well cell culture plate	Sarstedt
Ibidi µ-Slide 8 well	Ibidi
Test and centrifugal tubes (15 mL, 50 mL)	Sarstedt
Nitrocellulose Transfer Membrane PROTRan BA 85	NeoLab
Whatman Paper / Gel-Blotting-Paper	A. Hartenstein

Primary human and murine cells

Cell line	**Source**
Human Umbilical Vein Endothelial Cells -HUVEC	Lonza
Human Aortic Endothelial Cells - HAEC	Lonza
Human Mammary Epithelial Cells -HMEC	ThermoFisher
THP-1	ATCC

gRNAs for CRISPR/cas9

Gene	**Forward Primer (5`-3`)**	**Reverse Primer (3`-5`)**
NTC (non-	CACCGTTCCGGGCTAACAAGT CCT	AAACAGGACTTGTTAGCCCG GAAC

targeted control)		
POR	CACCGGTGTTCTACGGCTCCCAGA	AACTCTGGGAGCCGTAGAACACC

Genetically Modified Animals

Mouse Line	Official name	Background Strain
$Por^{flox/flox}$ mice	$Por^{tm1Ding}$	C57/Bl6J
Cdh5-CreERT2	$Tg(Cdh5\text{-}creERT2)^{1Rha}$	C57/Bl6J
Por(flox/flox)-Cdh5-CreERT2 0/0 (no cre expression)	$Por^{tm1Ding}$ x $Tg(Cdh5\text{-}creERT2)^{1Rha}$	C57/Bl6J
Por(flox/flox)-Cdh5-CreERT2 0/+ (heterozygous for cre)	$Por^{tm1Ding}$ x $Tg(Cdh5\text{-}creERT2)^{1Rha}$	C57/Bl6J

Reaction systems

Product	Source
cGMP RIA KIT	Biotrend
RNA Mini Kit (RNA isolation)	Bio&Sell

Synthetic oligonucleotides

Gene	Primer	Sequence
Murine MCP-1	forward	CCACTCACCTGCTGCTACTCATTC
	reverse	GTCACTCCTACAGAAGTGCTTGAGG
Murine IL-1β	forward	GACCTTCCAGGATGAGGACATGAG
	reverse	GGTGGGTGTGCCGTCTTTCATTAC
Murine IL-6	forward	CCAGTTGCCTTCTTGGGACTGATG
	reverse	CCTCCGACTTGTGAAGTGGTATAG
Murine CXCL1	forward	CTGCAGACCATGGCTGGGATTCAC
	reverse	TCAAGGCAAGCCTCGCGACCATTC

Murine VCAM	forward	ACTACGGGCTGCGAGTCACCA
	reverse	GACCGTGACCGGCTTCCCAA
Murine ICAM	forward	TGGCCTGGGGGATGCACACT
	reverse	GGCTGTAGGTGGGTCCGGGT
Murine E-Selectin	forward	ATGAAGCCAGTGCATACTGTC
	reverse	CGGTGAATGTTTCAGATTGGAGT
Murine HMOX1	forward	AAGCCGAGAATGCTGAGTTCA
	reverse	GCCGTGTAGATATGGTACAAGGA
Murine TNF-α	forward	TTCTCATTCCTGCTTGTGGCA
	reverse	GGGTCTGGGCCATAGAACTGA
Murine GAPDH	forward	GTGTGAACGGATTTGGCCGTATTG
	reverse	ACCAGTAGACTCCACGACATACTC
Murine ENOS	forward	CTCACCATAGCTGTGCTGGCTTAC
	reverse	GATGCAGGGCAAGTTAGGATCAGG

Antibodies

Target antigen	Vendor or Source	Catalog #	Working concentration
POR	Santa Cruz	sc25270	1:500
Anti-Mouse IgG 680nm	Li-COR	926-68072	1:10000
Anti-Mouse IgG 800nm	Li-COR	926-68070	1:10000
Anti-Rabbit IgG 680nm	Li-COR	926-68071	1:10000
Anti-Rabbit IgG 800nm	Li-COR	926-68073	1:10000
eNOS	BD Biosciences	610296	1:1000

p-eNOS (Ser1177)	BD Biosciences	612393	1:500
α-smc actin	ThermoFischer	701457	1:1000
β-actin	Sigma Aldrich	A1978	1:10000
pAKT	Cell Signalling	4058S	1:1000
AKT	Cell Signalling	2920S	1:1000
ERK	Cell Signalling	4696S	1:2000

General Equipment

Equipment	Source
Aria Mx Real-Time PCR	Agilent Technologies
Autoclave	Tuttnauer
Automatic Pipettes (Multistep)	Eppendorf
Axiovert 135 Microscope	Tuttnauer
Binocular surgical microscope	Zeiss
Cell counter CASY	Schärfe System
Electrophoresis chamber	BioRad
Electrophoresis device	BioRad
Freezer HERAfreeze basic (-80^{0}C)	Heraeus Instruments
Freezer -150^{0}C	Ewald
Gel documentation system INTAS Gel-Stick Imager	Royal Biotech
Heating Block Thermomixer	Eppendorf
Heraeus Megafuge 16	ThermoFisher
Incubator Hera Cell 150-CO_2 Incubator	ThermoFisher
Infrared Scanner Odyssey	LI-COR
Magnetic Rack	Invitrogen
Microcentrifuge	VWR
Microplate reader	Tecan
PCR Eppendorf Mastercycler Gradient	Eppendorf
pH Meter PP-50	Sartorius
Pipette stander	Eppendorf
Plate Reader Infinite 200 Pro	Tecan
Power Supply CS-300V	Roth
PowerPac HC	BioRad
PVDF Membrane	Merck Milipore
Rotor Stuart SB3	Stuart

Sievers NO Analyzer	Sievers
Shaker GFL-3013	ThermoFisher
Spectrophotometer NanoDrop ND-100	Nanodrop
Steril bench HeraSafe HS 12	Heraeus Instruments
Scale Analytical Balance	Sartorius
Vevo 3100	Fujifilm
Visitech BP-2000	Visitech
Volume Adjustable Pipettes	Eppendorf
Vortex Genie	Scientific Industries
Water Purification System MiliQ	Q-POD Milipore
Western Blot Chambers and Accessories	BioRad

Software

Software	**Source**
Agilent Aria MX 1.3	Agilent Technologies
Entrez (PubMed/GenBank)	http://www.ncbi.nlm.nih.gov/
GeneCards:The Human Gene Database	Weizmann Institute of Science
GraphPad Prism 8.3.0	GraphPad Software
Image Studio Lite 5.0	Li-COR Biosciences
LabChart 8	AdInstruments
Primer Bank	http://pga.mgh.harvard.edu/primerbank/
Ponemah 6.5	Data Science International
R Studio	RStudio Inc.
R package: DEseq2	Bioconductor
R package: ggplot2	CRAN
Visitech BP2000	Visitech

Methods

Generation of an endothelial cell-specific, tamoxifen inducible knockout mouse of POR and animal procedure

Endothelial cell-specific, tamoxifen inducible knockout mice of POR (ecPOR$^{-/-}$) were generated by crossing Por$^{flox/flox}$ mice (Cytochrome P450 reductase, Por^{tm1Ding}) provided by Prof. Xinxin Ding (SUNY Polytechnic Institute, Albany, NY) with Cdh5-CreERT2 (Tg(Cdh5-creERT2)^{1Rha})[94] mice, provided by Ralf Adams (MPI Münster, Germany). The knockout was induced either by tamoxifen feeding (400 mg/kg, 10 days) or intraperitoneal injections of tamoxifen (333 mg/kg, for three consecutive days). Animals were subjected to a wash out time of 14 days after tamoxifen feeding and had free access to chow and water in a specified pathogen-free facility with a 12h-day/12h-night cycle. Control animals (CTR) are defined as Por(flox/flox)-Cdh5-CreERT2 0/0 (no cre expression), treated with tamoxifen. All animal experiments were performed in accordance with the German animal protection law and were carried out after approval by the local authorities (FU1188).

Isolation of Murine Samples

To isolate vessels, mice were sacrificed and an incision of the skin was made from the abdominal region moving upwards to the thorax. The diaphragm was ruptured opening access to the thoracic cavity. Blood was directly sampled from the heart using a 23-gauge syringe. The inferior vena cava was cut and the left ventricle of the heart was infused with Hank`s solution in order to wash out all the leftover blood from the vascular bed. The mesenteric artery and the aorta were harvested and placed in Hank`s solution on ice. Lungs were also harvested for lipid measurements. The vessels were carefully cleaned, trimming away the surrounding fat tissue and were subsequently cut into 1 mm rings (**Figure 11**).

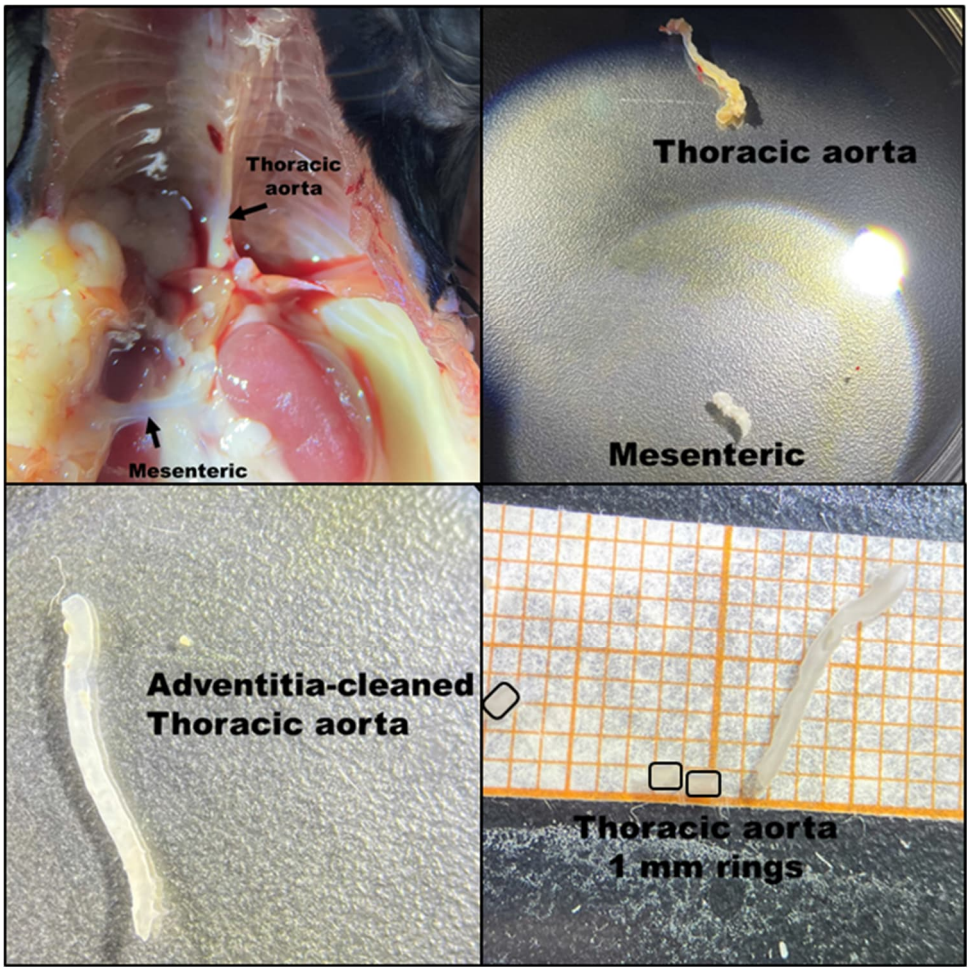

Figure 11: Isolation of aortic and mesenteric vessels from mice
Aorta and mesenteric vessels were isolated from control and ecPOR$^{-/-}$ mice. The perivascular fat was trimmed out and vessels were subsequently cut into 1 mm rings (the rings were outlined in a black box to facilitate visualization). The rings were then used for organ chamber, western blot, lipid measurements or eNOS activity assays.

Organ chamber experiments

Aortic and mesenteric rings (1 mm) were carefully mounted on two triangular metals as depicted in (**Figure 13**). This triangular setup was then attached to a F30 force transducer (Hugo Sachs Elektronik Harvard Apparatus) and before each experiment the organ bath setup was calibrated using standardized 1 g weights. The rings were submerged in the organ chamber bathed by a carbogen-aerated Krebs-Henseleit buffer (37°C, pH 7.4). The vessels were pre-conditioned to a starting force (0.6 gram for mesenteric and 1 gram for aorta) by consecutively increasing the force by 0.2 gram with three minutes rest between increases. Next, the buffer was exchanged to a KCl-enriched buffer (80 mM) in order to induce a maximum vascular contraction. After the contraction reached a steady plateau

the vessels were relaxed by using the Krebs-Henseleit buffer. Then, maximum contraction was once again induced by using the KCl-enriched buffer (80 mM) and this value was taken as the maximum contractile response for each ring.

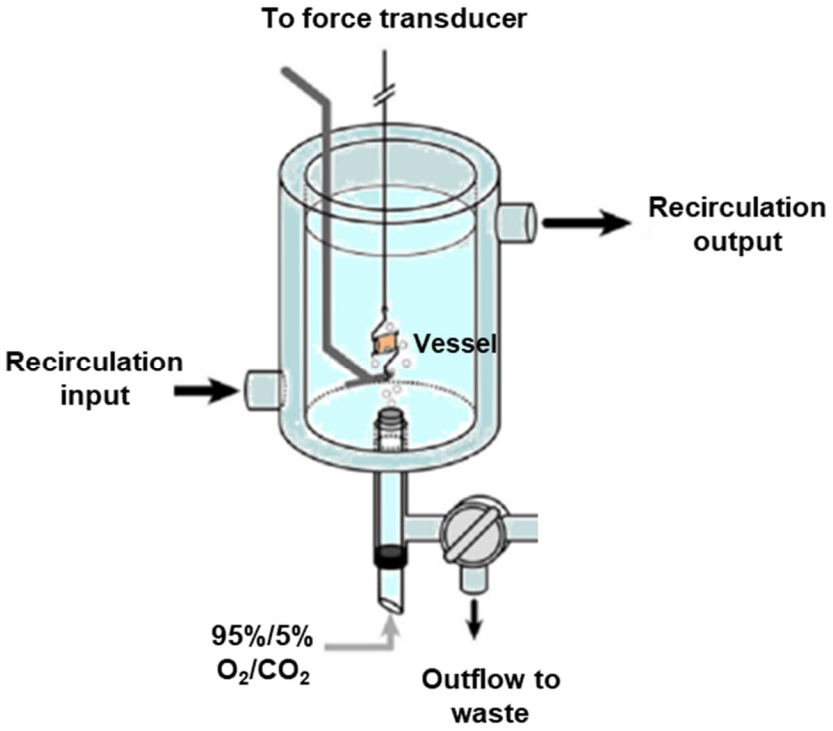

Figure 12: Schematic representation of the organ bath chamber with mounted vessel ring. Adapted figure [95]
The vessel is hung on a two-end triangular setup. One of the ends is fixed to a non-movable metal wire while the other is connected to a force transducer. The vessel is submerged in Krebs-Henseleit buffer, where different pharmacological agents can be applied. The buffer is always aerated with a carbogen mixture (95% O_2/5% CO_2). The buffer can be exchanged through an outflow valve and temperature is kept at 37°C though circulation of water in the inner of the doubled-wall glass.

Before the pharmacological interventions, the rings were washed three times with 10 mL of potassium free Krebs-Henseleit buffer. Phenylephrine was added in cumulative doses (range of 10^{-10} M to 10^{-6} M) up to a level of 80% of the initial KCl constriction. Subsequently, acetylcholine (ACh, 10^{-10} M to 10^{-5} M) was cumulatively added and dilation dose–response curves were generated and represented relative to the constrictor response. Alternatively, vessel relaxation was induced by the NO donor DETA NONOate (10^{-8} M to 10^{-5} M). Additionally, in order to completely block eNOS activity, mesenteric vessels were incubated with

L-NAME (100 µM, 30 min) in the organ bath chamber prior to addition of phenylephrine and acetylcholine.

Protein quantification

Protein concentration of the various tissue and cell lysate samples was determined by the Bradford method. Solutions of BSA at different concentrations were used to construct a standard curve: 2.5 µg/mL, 5 µg/mL, 10 µg/mL, 20 µg/mL, 30 µg/mL, 40 µg/mL, 50 µg/mL. The samples to be analysed were first diluted at 1:100, and both BSA standards and the diluted samples were mixed with the Bradford Reagent (Roti-Quant). The Tecan 2000 multiplate reader at wavelength of 540 nm was used to estimate the protein concentration.

Protein Isolation using Triton-lysis buffer

Isolation of protein from cells: cells were first washed twice with PBS. All remaining PBS was removed and the cells were snap frozen with liquid nitrogen for 5 min. The cells were then left at -20°C for 30 min. Following this, triton-lysis buffer containing: Tris-HCl (50 mmol/L), NaCl (150 mmol/L), sodium pyrophosphate (10 mmol/L), sodiumfluoride (20 mmol/L), Triton X-100 (1 %), sodiumdesoxycholate (0.5 %), proteinase inhibitor mix, phenylmethylsulfonyl fluoride (1), orthovanadate (2), okadaic acid (0.00001 mmol/L) (pH 7.4) was added to the dish and the cells were scraped with a cell scraper. The lysate was collected and this homogenate was vortexed and centrifuged (13.000 rpm, 10 min, 4 °C). The protein concentration of the supernatant was estimated by Bradford.

Isolation of proteins from the endothelium of murine aorta: the aorta was cut into 1 mm rings. For the p-eNOS experiments rings were directly placed in triton-lysis buffer containing calyculin (50 nM). For the p-AKT experiments, were first incubated in EBM (containing 0,1 % BSA and 0,1 % gentamycin, 4 h) and stimulated with insulin (0,1 µM, 15 min) before addition of the triton-lysis buffer. The endothelium was separated by gentle spinning of aortic rings on a wheel at 4 °C for 15 min in 60 µL triton lysis buffer. The endothelium-denuded rings were further processed with a tissue disruptor for two minutes with 100 µL lysis buffer to obtain the smooth muscle fraction. These lysates were centrifuged (13.000 rpm, 10 min, 4 °C) and protein concentration of the supernatant was estimated by Bradford.

Immunoblotting

Western blotting was performed in order to confirm the knockout efficiency of both ecPOR$^{-/-}$ mice and the POR$^{-/-}$ HUVEC cells, as well as to check the phosphorylation state of AKT and eNOS of the aorta of the CTR and ecPOR$^{-/-}$ mice. Proteins (30 µg) in 3x Laemmli buffer were separated by SDS/PAGE on 10 % polyacrylamide gels. Initial voltage was set at 60 V for the running through the upper stacking gel and 120 V for the separation portion of the gel. Proteins were transferred by western blotting (250 mA, 100 min) to a nitrocelulose membrane which was probed with the following antibodies: anti-POR (F-10, #sc-25270, mouse, dilution 1:500) antibody, anti-eNOS (BD #610296, mouse, dilution 1:1000), anti-p-eNOS S1177 (BD #612393, mouse, dilution 1:500), anti-β-actin (Sigma Aldrich, #A1978, mouse, dilution 1:10000), anti-p-AKT (Cell Signalling, #4058S, 1:1000), anti-AKT (Cell Signalling, 2920S, 1:1000), and anti-ERK (Cell Signalling, #4696S, 1:2000). Western blot analyses were performed with an infrared-based detection system (Odyssey, Licor, BadHomburg, Germany).

eNOS activity assay

eNOS activity was determined by the conversion of L-(^{13}C)-Arginine to L-(^{13}C)-Citrulline as detected by UHPLC/MS/MS. Freshly isolated aortic rings (1 mm) were equilibrated in HEPES-buffered Tyrode's solution (20 min, 37 °C) followed by the addition of L-(^{13}C) arginine (84 µg/mL). After incubation (20 min), rings were treated with or without calcium ionophore A23187 (1 µM, 5 min), acetylcholine (10^{-7} M, 5 min) or N$^{\omega}$nitro-L-arginine (LNA, 300 µM, 10 min). The reaction was stopped by addition of methanol (85% V/V, 100 µl). The UHPLC/MS/MS system consisted of a Kinetex 2.6u HILIC 100x2.1 mm column, an Agilent 1290 Infinity Binary Pump, a 1290 Infinity Sampler, a 1290 Infinity Thermostat, and a 1290 Infinity Thermostatted Column Compartment (Agilent, Mississauga, Ontario, Canada) connected to an AB SCIEX QTRAP® 5500 hybrid linear ion trap triple quadrupole mass spectrometer equipped with a Turbo Spray source (AB SCIEX, Concord, Ontario, Canada). The mass spectrometer was operated in positive ionization mode, and data were acquired using the Analyst 1.5.2 software. Data analysis was performed using MultiQuant 3.0 software.

AKT phosphorylation in the aortic endothelium

Aortic rings were cut into 1 mm segments and incubated in endothelial basal medium (EBM) (4h, 37°C). These rings were then incubated in the presence or absence of insulin (100 nmol/L, 15 min, 37°C). Immediately after incubation, the rings were first washed in a cold lysis buffer lacking triton. This step was followed by incubation of the rings with triton-containing triton lysis buffer. Isolation of endothelium proteins was performed as previously described in the protein isolation section and western blotting was performed as described in the immunoblotting section.

cGMP measurements

Aortic rings (1 mm) from control and ecPOR$^{-/-}$ mice were incubated in HEPES-buffered Tyrode solution in the presence or absence of the calcium ionophore A23187 (1 µM, 5 min) at 37°C in a 24-well plate. After this incubation, reaction was stopped by the gently addition of a solution of ice-cold trichloroacetic acid (6%). The concentration of cGMP from these rings was determined by a using a specific radioimmunoassay (RIA) and following the instructions provided by the kit (GMP [125 I] RIA KIT; Bio Trend, Germany).

Plasma Nitrite determination

Nitrite was measured as a footprint for NO by using the Sievert NO analyser (NoA) with the ozone-chemiluminescence technique. Measurements were performed in a 9 ml acetic acid/1 mL NaI (50 mg/mL) solution. A standard curve with sodium nitrite at concentrations of 100 nM, 250 nM, 500 nM, 1 µM, 5 µM and 10 µM was used as reference.

Blood sampled from the heart of control and ecPOR$^{-/-}$ knockout mice was immediately added to tubes containing heparin and centrifuged (10 min, 2000 x g, 4°C) in order to obtain the plasma. The plasma was deproteinated by using centrifugal filter units (Microcon®-10, Merck #MRCPRT010, 70 min, 14,000g, 4°C). The flow through was loaded onto the NoA (100 µl). Animals received bottled water that contained low nitrite for 5 days before the measurements.

Cell Culture

HUVECs, HAECs and HMECs were cultured in Endothelial Growth Medium (EGM) which contained 8 % fetal bovine serum (FBS) and 0.5 % penicillin-

streptomycin (Pen-Strep) as antibiotic. The culture dishes were coated with gelatin. Cultures were incubated in a cell culture incubator at 37 °C with 5 % carbon dioxide (CO_2) and 95 % humidity. The growth medium was renewed every 2 to 3 days for optimum growth conditions. Cells were not sub-cultured over passage 6. Cells were split when at least 80% confluent. The medium was aspirated and the cells were washed with 10 ml of sterile phosphate buffered saline (dPBS) in order to inactivate the FBS. Pre-warmed trypsin was added to the dishes in order for the cells to detach. After cell detachment, pre-warmed growth medium was added to the dish in order to inactivate the trypsin. The cells were centrifuged at 1200 g for 4 minutes, the supernatant was removed and the cells resuspended in EGM. When necessary, cells were counted using the CASY counter.

CRISPR/Cas9 for Cytochrome P450 reductase (POR)

CRISPR/Cas9 knockout HUVECs (Human umbilical vein endothelial cells) for POR or the control guide RNAs were generated according to the technology described previously using a lentiviral transduction system [96]. Briefly, guides were designed using the publicly available CRISPR algorithm (www.benchling.com). Oligonucleotides were cloned into the vector via the BsmBI restriction site. After cloning, the gRNA-containing vectors were purified and sequenced. Pseudotyped lentivirus were produced by transfection using PEI (polyethyleneimine, Sigma Aldrich) of LentiX cells (Takara, Japan) with LCV2 plasmid together with lentiviral packaging plasmid (Addgene #12260) and VSV-G (Addgene #12259). Viral supernatants were collected, filtrated and snap-frozen at the third day after transfection. HUVEC (at passage 1) were transduced with viral particles for 24 hours using polybrene (Sigma Aldrich, 8µg/ml) and then selected with puromycin (2 µg/mL) for 4 days. Knockout efficiency was controlled by western blot.

Oxylipid measurements

Arachidonic-acid enhanced lipid production in HUVEC

For oxylipid measurements in cells, NTC (non-targeted control) and $POR^{-/-}$ HUVEC were cultured in 10 cm^2 plates in EGM (endothelial growth media) with 0.2 % gelatine pre-coating of the plates. At 90 % confluence, arachidonic acid was added (30 min, 100 µM). One group of cells was treated with the CYP450

inhibitor SKF525 (10 µM, 60 min) 30 min prior to the addition of arachidonic acid). Another group received the calcium ionophore A23187 (1 µM, 5 min), 25 min after the addition of arachidonic acid. Cells were harvested after the incubation with arachidonic acid by scraping in ice cold methanol (700 µL, 85%). A two steps liquid-liquid extraction was performed, first with ethyl acetate (1 mL) and then with ethyl acetate/ 0.1 % of formic acid (1 mL). The organic phases were dried in vacuum and samples were reconstituted in 50 µL 1:1 (MeCN: H_2O). The UHPLC system consisted of an Agilent 1290 Infinity Binary Pump, a 1290 Infinity Sampler, a 1290 Infinity Thermostat, and a 1290 Infinity Thermostatted Column Compartment (Agilent, Mississauga, Ontario, Canada).

Oxylipin measurements from tissue and plasma

For the oxylipid measurements in tissues, freshly isolated lungs and aortas were frozen in liquid nitrogen. Blood was collected in heparin tube and processed into plasma by centrifugation (10 minutes at 2000 x g at 4 °C).

As free EET levels in vessels are typically below the detection level of mass spectrometry, esterified EETs stored in phospholipids were prepared for the analysis. For this, the aortic phospholipids were first desterified by alkaline hydrolysis: The vessel was mortared in liquid nitrogen and 9 mg of tissue were incubated in methanol-potassium hydroxide solution (50%, 0.2 M, 30 min, 37°C, 250 µl). The reaction was stopped by the addition of ice-cold methanol (150 µl) and lipids were subsequently extracted by liquid–liquid extraction, twice with 600 µl of ethyl acetate. The combined organic phases were removed at a temperature of 45 °C under a gentle stream of nitrogen. The residues were reconstituted in 50 µL of methanol:water:BHT.

Lipid measurements were performed in the Institut für Klinische Pharmakologie of Universitätsklinikum in Frankfurt am Main. Standard compounds and their corresponding deuterated derivatives were obtained from Cayman Chemicals (Ann Arbor, MI, USA): 5,6-EpETrE, 8,9-EpETrE 11,12- EpETrE, 14,15-EpETrE, 5,6-EpETrE -d11, 8,9-EpETrE -d11, 11,12-EpETrE -d11; 14,15- EpETrE,-d11, 5,6-DiHETrE, 8,9-DiHETrE, 11,12-DiHETrE, 14,15-DiHETrE, 8,9-DiHETrE -d11, 11,12-DiHETrE-d11 and 14,15-DiHETrE-d11. Stock solutions containing 25000 ng/mL of all analytes were prepared in methanol. The calibration curve ranged from 0.5 to 3000 ng/mL for EpETrE and from 0.25 to 1500 ng/mL for DiHETrE.

The LC system consisted of a Gemini NX C18 column attached to a precolumn (150 x 2 mm ID, 5 µm particle size, and 110 Å pore size; Phenomenex, Aschaffenburg, Germany). A linear gradient was used at a flow rate of 0.5 mL/min with a total run time of 17.5 min. Mobile phase A was water:ammonia (100:0.05, v/v), and mobile phase B was acetonitrile:ammonia (100:0.05, v/v). The gradient started at 85 % A and changed to 10 % A within 12 min. This setup was held for 1 min. Within 0.5 min, the gradient shifted back to 85 % A and was held for 4 min to re-equilibrate the column.

For the MS/MS, the chromatographic setups were connected to an AB SCIEX QTRAP® 5500 hybrid linear ion trap triple quadrupole mass spectrometer equipped with a Turbo Spray source (AB SCIEX, Concord, Ontario, Canada). The mass spectrometer was operated in negative ionization mode. Data was acquired using the Analyst 1.5.2 software and the analysis was performed using MultiQuant 3.0 software (both Sciex, Darmstadt, Germany) using the internal standard method (isotope-dilution mass spectrometry).

Measurement of sterol metabolites

A 10 mm segment of the thoracic aorta from CTR and ecPOR$^{-/-}$ mice was isolated and the adventitial fat was trimmed off. The aortic segments were then weighed and immediately snap frozen in nitrogen. Sterol measurements from these aorta was carried out by gas chromatography at the Institut für Klinische Chemie und Klinische Pharmakologie Universitätsklinikum Bonn. Cholesterol was measured by gas chromatography-flame ionisation detection (GC-FID) using 5α-cholestane as internal standard. The cholesterol precursors, plant-derived sterols and non-cholesterol sterols were measured by GC-mass spectrometry-selected ion-monitoring (GC-MS-SIM) using epicoprostanol as internal standard together with the oxysterols by isotope dilution GC-MS-SIM as described previously [97]. The following sterols were measured: cholesterol, cholestanol, lathosterol, campesterol, campestanol, stigmasterol, sitosterol, sitostanol, avenastrol, brassicasterol, lanosterol, dihydrolanosterol, desmosterol, 7-OH cholesterol, 24-OH cholesterol and 27-OH cholesterol.

RNA isolation

RNA was isolated and purified from human cells using an RNA mini kit (Bio&SELL). The cells were washed with Hanks buffer before being lysed with

RNA lysis buffer (200 µL). The isolation was done according to the manufacturer's protocol (Bio&SELL). The cell lysate was centrifuged in filtration columns at 10,000 g at RT for 2 minutes. The eluate was dilute with 70 % ethanol (1:1) and centrifuged (10,000 g) for 1 minute. The column was centrifuged (10,000 g at RT for 1 minute) consecutively with IT buffer (500 µL) and then MT buffer (700 µL). RNA was eluted from the column with 30 µL RNase-free water and centrifugation at 6,000 g at RT for 1 minute. The concentration of the purified RNA was estimated using a NanoDrop 1000.

Reverse transcription

The eluted RNA was reverse transcribed to complimentary DNA (cDNA) in order to perform quantitative real-time PCR experiments. 500 ng RNA was combined with 0.7 µL oligo (dT), 1 µL random primers and 1 µL dNTPs **Table 1** for the initial annealing step of 65°C for 10 minutes. After annealing, first strand buffer, DTT and the reverse transcriptase (SuperscriptIII) were added to the reaction mixture. The synthesis of cDNA was performed according to the cycles outlined in **Table 2**.

Table 1 Reverse transcription mastermixes used in this study

Component (concentration)	**Volume (final concentration)**
Step 1: annealing	
ssRNA + ddH2O	29.5 µL (1 µg)
random primer (0.5 µg/ µL)	4 µL (0.04 µg/ µL)
oligo(dT)23 anchored (70 µM)	1 µL (1.4 µM)
dNTPs (100 mM)	2.5 µL (5 mM)
Step 2: cDNA synthesis	
first strand buffer (5x)	10 µL (1x)
DTT (100 mM)	2.5 µL (5 mM)
reverse transcriptase (SuperScript® III) (200 U/ µL)	0.5 µL (2 U/ µL)

Table 2 Reverse transcription mastermixes used in this study

Temperature (°C)	**Time (minutes)**
Step 1: annealing	
65	10
4	∞
Step 2: cDNA synthesis	
25	5
50	60
70	15
4	∞

Quantitative real-time PCR (RT-qPCR)

The previously synthesized cDNA (10 ng) was combined with a PCR mastermix containing SYBR® Green Master Mix (polymerase), “forward” primers and “reverse” primers against a gene of interest or the housekeeping gene GAPDH **Table 3**. The AriaMX thermocycler was used in order to perform the reactions. The cycles and specifications are outlined in **Table 4**. The results were analysed using the delta-delta ct method ($2^{-\Delta\Delta CT}$).

Table 3 Quantitative real-time PCR (RT-qPCR) mastermix

Component	**Volume (µL)**
2x SYBR Green	10
Forward Primer (10µM)	0.25
Reverse Primer (10µM)	0.25
DNase-free H2O	4.5
cDNA	5

Table 4 Quantitative real-time PCR (RT-qPCR) Thermal Profile

Reaction	**Temperature (°C)**	**Time (s)**	**Cycles**
Initial Denaturation	95	195	1
Denaturation	95	15	45
Annealing	60	20	
Extension	72	20	

Melt	95	30	1
	65	30	
	95	30	

MACE seq

For the Massive analysis of cDNA ends (MACE), 150 ng RNA from aortic tissue from 3 different animals were pooled to make n = 1. Three different pooled aliquots comprising different animals were analysed for each group (control and ecPOR$^{-/-}$). The sequencing procedure was was performed at GenXPro, Frankfurt am Main. The “Rapid MACE-Seq Kit” was used to prepare the 3’mRNA libraries for low-input mRNA. The RNA was first fragmented to sizes of 350 bpsn in average. This was followed by poly-A specific cDNA synthesis, pooling and amplification by PCR using (number of cycles as described in the manual). The PCR product was purified by SPRI purification. The final product of 200-400 bps was quality controlled on a Perkin Elmer LabChip GXII. Concentration was estimated using the Qbit. Sequencing was performed on an Illumina NextSeq500 machine with 1x 75 bps. The MACE-reads were demultiplexed according to the sample IDs, PCR duplicates were removed with the help of the “TrueQuant” UMI barcodes. Low-quality and adapter-containing reads were cropped. The reads were mapped to the mouse genome (GRCm38.p6) and genes were quantified for the individual libraries for gene expression. Differential gene expression of the was analyzed using DESeq2. In order to simplify the analysis and facilitate readout, enrichment analysis was performed (GSEA) (functional enrichment analysis or pathway enrichment analysis) in order to identify classes of genes from the sequenced data. Enrichr was used as the tool for the annotation analysis. This is a freely available tool (Ma'ayan laboratory at Mount Sinai) which is available through the address: https://maayanlab.cloud/Enrichr/.

RNA seq

Total RNA was isolated with the RNA Mini Kit from Bio& SELL (Nuremberg, Germany) combined with on-column DNase digestion (DNase-Free DNase Set, Qiagen) to avoid contamination by genomic DNA. RNA, library preparation and sequencing were performed at the Institute for Lung and Heart Research, Max Planck, Bad Nauheim. RNA and library preparation integrity were verified with

LabChip Gx Touch 24 (Perkin Elmer, Massachusetts, EUA). 2 µg of total RNA was used as input VAHTS Stranded mRNA-seq Library preparation following manufacture's protocol (Vazyme, Nanjing, China). Sequencing was performed on the NextSeq2000 instrument (Illumina, Cambridge, United Kingdom) using P2 flowcell with v3 chemistry, resulting in average of 45M reads per library with 1x72bp paired-read setup. The sequencing reads for all samples were quantified against the hg38 transcriptome (obtained from Ensembl (https://doi.org/10.1093/nar/gkz890)) using Salmon (1.5.2) (https://doi.org/10.1038/nmeth.4197). Reads not aligned to the transcriptome were discarded at this point. Differential gene expression analysis was performed using DESeq2 (1.32.0) (https://doi.org/10.1186/s13059-014-0550-8) in R (4.1.1) (R Core Team (2021). R: A language and environment for statistical computing. R Foundation for Statistical Computing, Vienna, Austria.). Raw transcript counts were summed per gene and used in the standard DESeq2 differential gene expression analysis workflow, using a negative binomial test over gene counts in each of the combinations of conditions. Batch information was also included in the contrast formula. Similarly to the MACE-seq, enrichment analysis was performed for the RNA seq by using the Enrichr tool.

Adhesion assay

Human microvascular endothelial cells (HMECs) after CRISPR/Cas9-knockout for NTC or POR were cultured in IBIDI-slides (8-well). These cells were stimulated or not with TNF-α (10 ng/ml, 1 hour). Afterwards, THP-1 cells (200.000 /mL) were added and left undisturbed for 15 minutes. Afterwards, the non-adherent cells were removed by washing the well and the leftover adherent cells were imaged using the LSM system and quantified using FIJI.

Ultrasonography of the carotid artery

The diameter of the left common carotid artery (LCCA) was assessed with ultrasonography using a Vevo 3100 device (**Figure 13)**. Body temperature and heart rate were kept at 37°C and 450-500 BPM respectively. Anesthesia was induced with 4 % Isoflurane and 1 L/min O_2 and maintained throughout the procedure with 1.5-2 % Isoflurane and 1 L/min O_2. Electrocardiogram was used as reference for quantification. The Vevo cardiovascular package was used in both B-mode and M-mode. Structures of the neck were first identified in B-mode

short axis view (transducer placed at 0° with the nod to the left, **Figure 13**, left panel). Doppler mode was used to better visualize carotids. Once the LCCA was positioned in the center of the view, the transducer was turned 90° counter clockwise, i.e. long-axis view. The position of the LCCA was adjusted, and the M-mode was selected to assess the diameter of the LCCA (**Figure 13**, right panel). Pictures and recording were taken from the distal LCCA (towards bifurcation) with the marker set outside the carotid's walls. All data analysis was done using the Vevo LAB desktop software using the Vascular Package for carotid artery. LCCA diameter measurements were obtained from M-mode images.

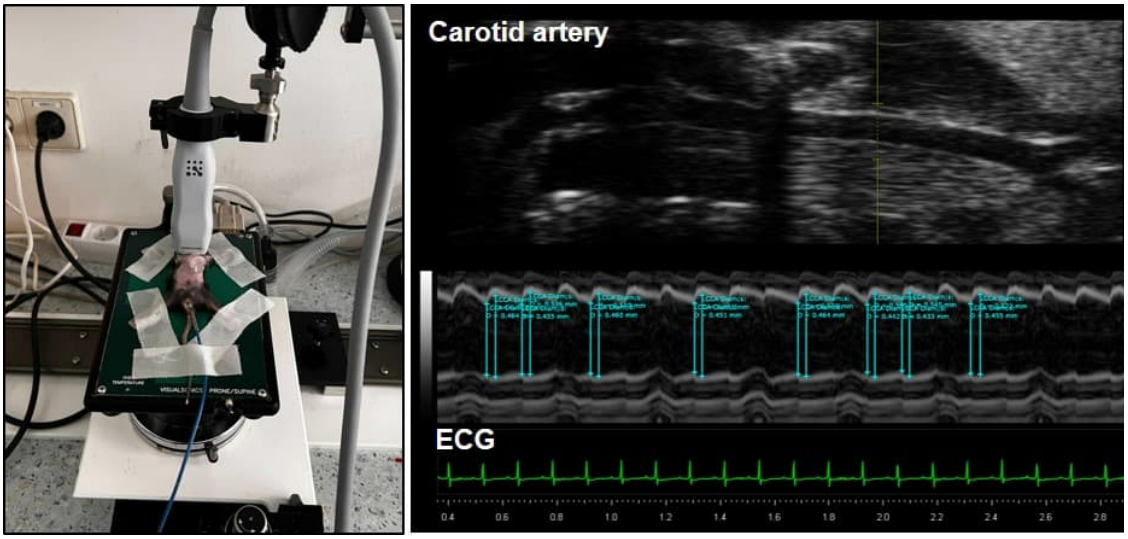

Figure 13: Diameter of the carotid artery as measured by ultrasonography (VEVO 3100 imaging system)
Right panel: Positioning of the mouse and transducer at 0° to locate the carotid artery in B-Mode. Left panel: representative ultrassonographic image of the carotid artery and ECG. Blue arrows denote the diameter of the vessel during systole and diastole using ECG as reference.

Blood pressure (BP) measurements

Tail cuff measurements

Tail cuff measurements were performed using a six-channel setup (Visitech BP2000) and analysed using its corresponding software (Visitech BP2000 Analysis Software). Five rounds of measurement (one a day) were performed before the actual recordings in order to acclimatize the animals with the tail-cuff procedures. The tail cuff plate was warmed to 37°C. The mice were put on top of plate and the tails were placed in the cuff and secured using tape. Five

preliminary measurements in each session were performed aclimatize the mice. Afterwards, ten measurements rounds were performed in each session. Blood pressure values (systolic and diastolic in mmHg) and heart rate (BPM, bites per minute) were taken as an average of 4 days of recording before and after tamoxifen (food). Blood pressure was measured at the very same time each day.

Telemetry

Blood pressure measurements were also performed in a continuous manner through telemetry using the Data Science International (DSI) telemetry system and PA-C10 transmitters. The implantation of the telemetric transmitters was performed by another fellow member of the laboratory as described in her thesis [98].

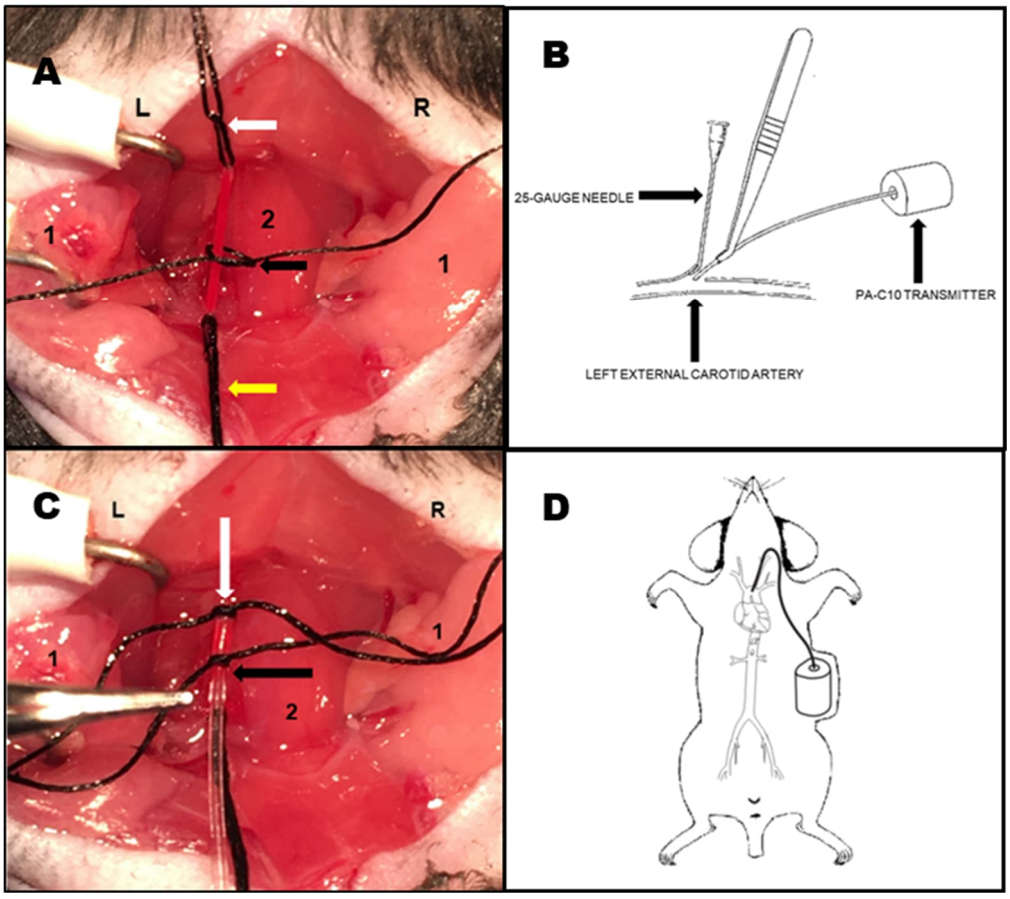

Figure 14: Representative images of the surgery and scheme to implant telemetric transmitters as provide by Ratiu [98]
(A) Silk suture threads tied loosely (white arrow) and tensioned (yellow arrow) around the left external carotid artery (black arrow). (B) and (C): scheme and photo of PA-C10 transmitter insertion into left external carotid artery. (D) Scheme showing the transmitter housed in the body under a subcutaneous pouch on the left side of the animal. Schemes are from the surgical protocol for PA-C10 transmitter implantation by Data Science International). L: left side; R: right side; 1 (left and right): submandibular glands; 2: trachea.

After recovery, blood pressure was measured continuously during up to 55 days, using the PhysioTel Digital Telemetry Platform and the Ponemah Software.

Assessment of blood pressure was performed according to two distinct protocols:

(i) Initially, the animals were monitored for 7 days for basal blood pressure and heart rate value recordings, as well as to check for proper functioning and acquisition of the data. Afterwards, in vivo angiotensin II infusion was performed through the implantation of mini-osmotic pumps at a daily infusion rate of 0.7 mg/kg/24h. In order to induce the knockout of the ecPOR$^{-/-}$ animals, intraperitoneal (i.p.) administration

of tamoxifen (333 mg/kg, for three consecutive days) was performed followed by pressure and heart rate monitoring.

(ii) Animals were at first injected with tamoxifen (i.p., 333 mg/kg, for three consecutive days) in order to induce the knockout and blood pressure was measured in order to obtain basal values for each individual group. Afterwards, in vivo angiotensin II infusion was performed through the implant of mini-osmotic pumps with blood pressure and heart rate being continuously recorded. Finally, to analyse the effect of NSAID (Nonsteroidal anti-inflammatory drug) on the blood pressure, mice were injected for five consecutive days with naproxen (i.p. injection, 30 mg/kg).

Statistics

Unless otherwise indicated, data are given as means ± standard error of mean (SEM). Calculations were performed with Prism 8.0 or R (package ggplot2). In case of multiple testing, Bonferroni or Tukey correction was applied. For multiple group comparisons, ANOVA followed by post hoc testing was performed. Individual statistics of unpaired samples was performed by t-test and if not normally distributed, by Mann-Whitney test. Measurements of vascular reactivity were analysed with ANOVA for repeated measurements. A p-value of <0.05 was considered as significant. n indicates the number of individual experiments or animals. In LC- MS/MS measurements, samples which were not within the range of the calibration curve and thus, did not pass quality control, were excluded.

Results

Generation and characterization of the inducible, endothelial cell-specific knockout mice of POR

The cytochrome P450 reductase (POR) is coded by a single gene. To overcome the unspecific nature of CYP450 inhibitors, as well as the compensation effects that comes from knocking out individual CYP450 isoenzymes, POR was knocked out specifically in endothelial cells as a novel approach to switch off the activity of all microsomal CYP450 isoenzymes to study their vascular function.

The tamoxifen-inducible, endothelial cell-specific knockout mouse of POR was obtained by crossing $CPR^{flox/flox}$ mice (CPR: cytochrome P450 reductase) with Cdh5-Cre*ERT2*$^{0/+}$ mice (**Figure 15**) and designated as ecPOR$^{-/-}$. Western blotting of the endothelial and smooth muscle layer fractions from aorta of these mice confirmed the deletion of POR (approximately 76 KDa) only in the endothelium of the ecPOR$^{-/-}$ mice (**Figure 15**).

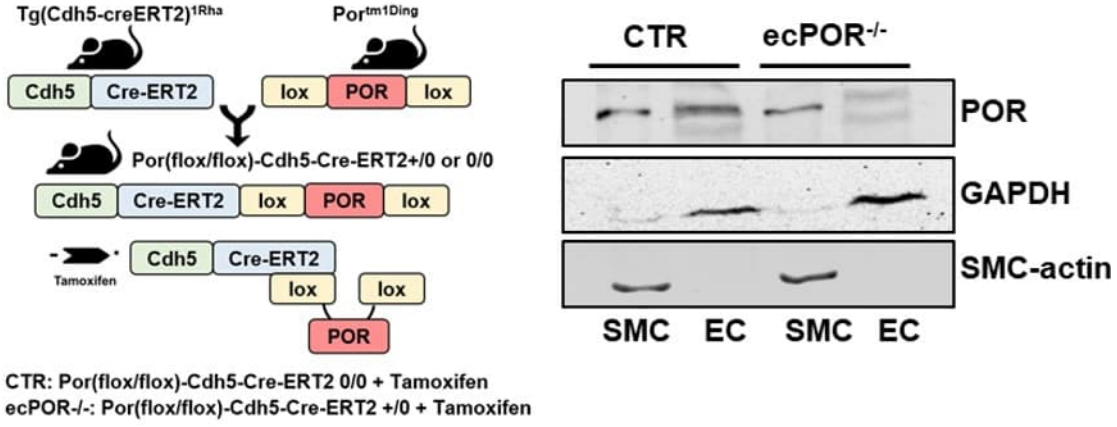

Figure 15: Generation of the tamoxifen-inducible, endothelial cell-specific knockout mouse of POR (ecPOR$^{-/-}$) and validation by western blotting
The ecPOR$^{-/-}$ mouse was generated by cross-breeding $CPR^{flox/flox}$ mice (CPR: cytochrome P450 reductase) with Cdh5-CreERT2$^{0/+}$ mice (left panel). Validation of knockout by western blotting (right panel): POR expression in smooth muscle cell (SMC) and endothelial cell (EC) fractions of aorta isolated from control (CTR) and ecPOR$^{-/-}$ mice.

The impact of the ecPOR$^{-/-}$ on endothelial function was first accessed by organ chamber experiments using aortic and mesenteric rings from ecPOR$^{-/-}$ and CTR mice. There were no differences between the two genotypes in vascular

contraction to phenylephrine in both the aortic and mesenteric vessels (**Figure 16**). However, the acetylcholine-dependent relaxation was attenuated in vessels of ecPOR$^{-/-}$ mice as compared to CTR. The EC50 response was 2.3*10^{-8} and 6.2*10^{-8} in aorta and 5.4*10^{-8} and 5.5*10^{-8} in mesenteric of the CTR and ecPOR$^{-/-}$ mice, respectively (**Figure 17**).

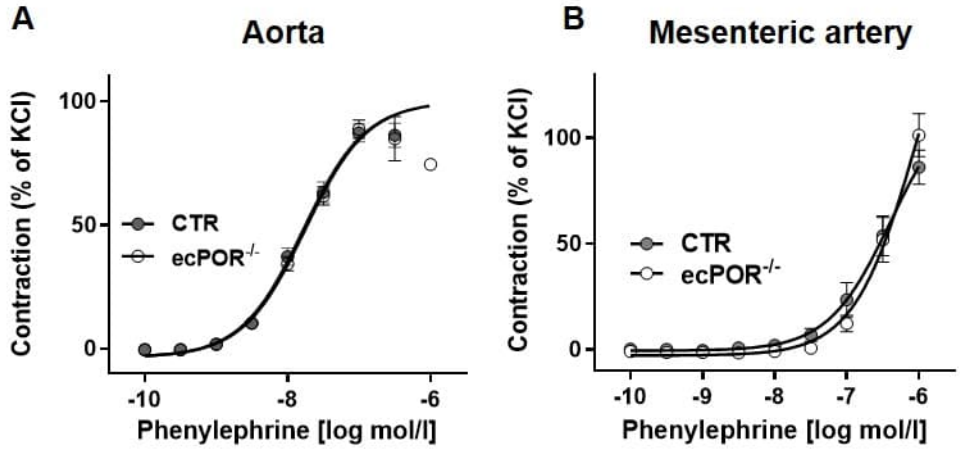

Figure 16: Phenylephrine-dependent vessel contraction
Vessel contraction to increasing concentrations of phenylephrine. (A) Mesenteric vessel and (B) aorta of CTR and ecPOR$^{-/-}$ mice. Constrictor response compared to maximal KCl (80 mmol/L) elicited contraction. n=7 (CTR) & 11 (ecPOR$^{-/-}$). Anova for repeated measurements.

This difference in relaxation was abolished after incubating mesenteric vessels with the eNOS inhibitor L-NAME which shifted the dose response curve to the right and increased the EC50 to 2.7*10^{-7} and 3.3*10^{-7} in the CTR and ecPOR$^{-/-}$ mice, respectively (**Figure 17 B**). No differences were observed when the vessels were exposed to the nitric oxide donor detaNONOate, which resulted in relaxations with EC50 of 5.2*10^{-6} and 8.1*10^{-6} in aorta and 2.5*10^{-6} and 2.1*10^{-6} in mesenteric of the CTR and ecPOR$^{-/-}$, respectively (**Figure 18**).

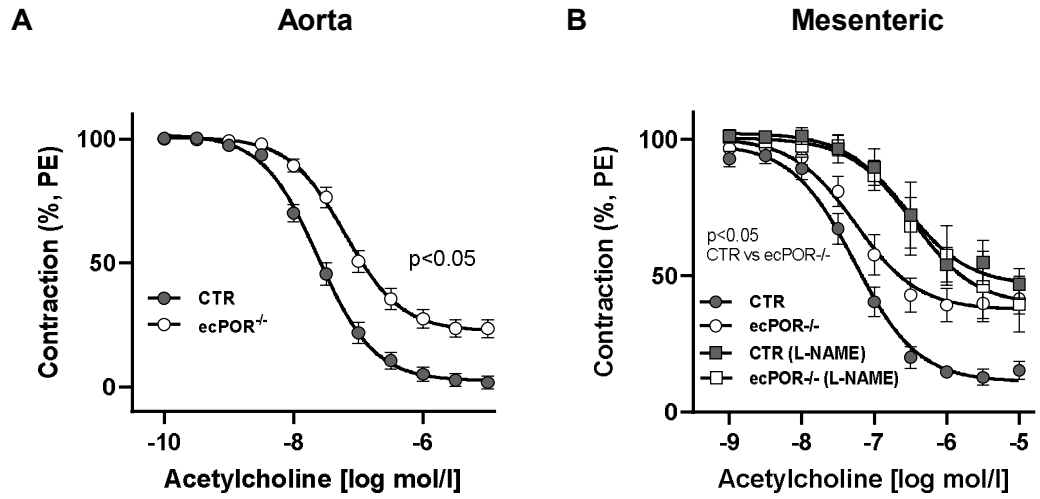

Figure 17: Acetylcholine-dependent vessel relaxation after phenylephrine-induced contraction
Dose response curve to acetylcholine in (A) aorta and (B) mesenteric vessel of CTR and ecPOR$^{-/-}$ mice. Vessels were pre-constricted with phenylephrine to 80% of the maximal contraction with KCl (80 mmol/L). Mesenteric vessels were incubated or not with L-NAME (100 µM) for 30 min prior to the titration. n=7 (CTR) & 11 (ecPOR$^{-/-}$). Anova for repeated measurements.

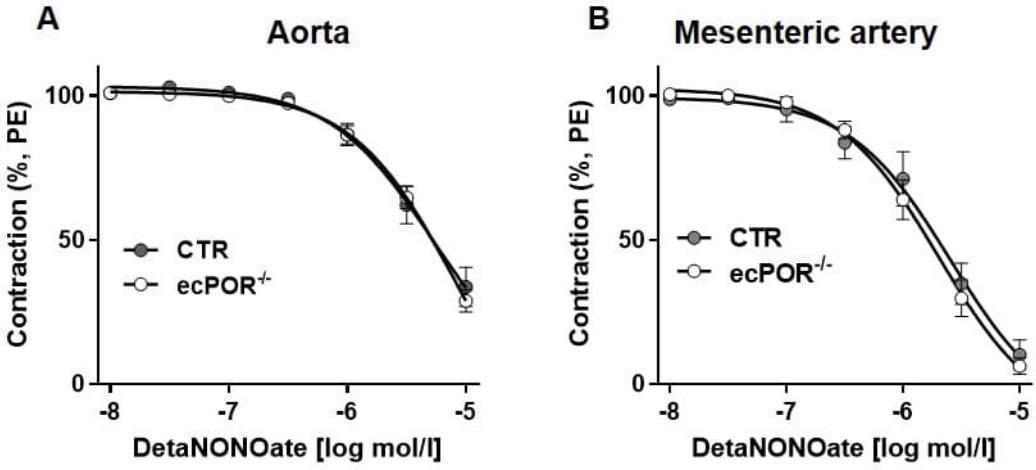

Figure 18 : DetaNONOate-dependent vessel relaxation after phenylephrine-induced contraction
Dose response curve to DetaNONOate in aorta (A) and mesenteric vessel (B) of CTR and ecPOR$^{-/-}$ mice. Vessels were pre-constricted with phenylephrine to a degree of 80% of the maximal contraction with KCl (80 mmol/L). n=7 (CTR) & 11 (ecPOR$^{-/-}$). Anova for repeated measurements.

The gender effect on vascular dysfunction was evaluated by organ bath using aortic rings from CTR and ecPOR$^{-/-}$ female mice. Similarly, to the male counterparts, aortic rings from female ecPOR$^{-/-}$ mice also showed no differences

in the phenylephrine-dependent contractions but an attenuated acetylcholine-dependent relaxation (**Figure 19**).

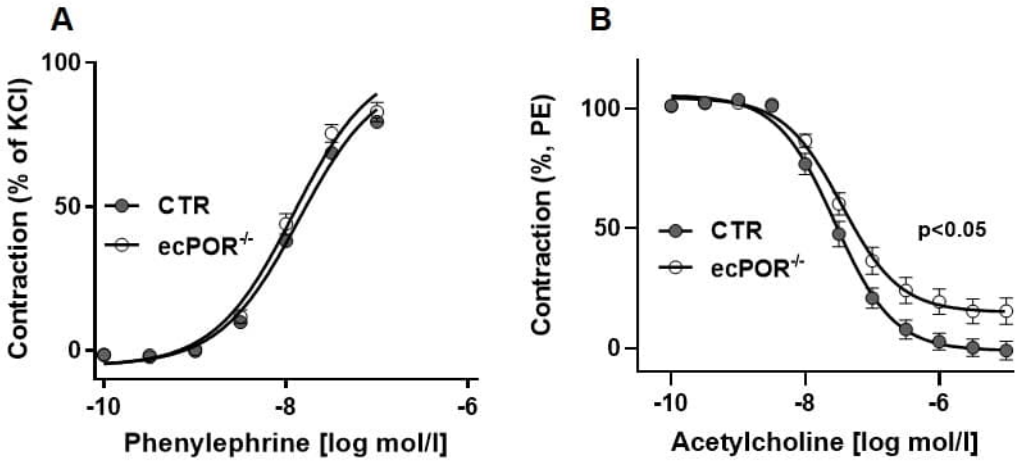

Figure 19: Vascular reactivity of aortic segments of female mice
Phenylephrine-induced constriction (A) and acetylcholine-induced relaxation (B) in aortic segments of CTR and ecPOR$^{-/-}$ female mice. n= 6. Anova for repeated measurements.

ecPOR$^{-/-}$ mice have reduced NO bioavailability

Nitric oxide (NO) is the primary endothelium-derived vasodilator of the mouse aorta. As the acetylcholine-induced vessel relaxation was attenuated in ecPOR$^{-/-}$ mice aortae as compared to CTR, nitrite as footprint for NO, was measured using the NOA setup. The plasma of the ecPOR$^{-/-}$ showed a significant reduction in nitrite (15 %) when compared to the CTR littermate (237 nmol/L ± 77 for CTR and 182 nmol/L ± 34 for ecPOR$^{-/-}$ mice) (**Figure 20**).

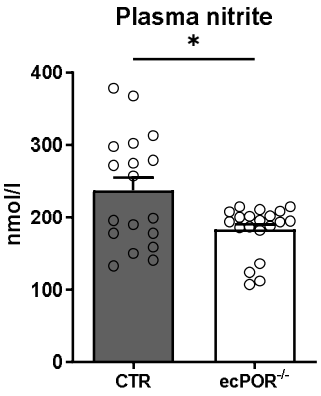

Figure 20: ecPOR$^{-/-}$ have lower plasma levels of nitrite
Nitrite levels in plasma from control (CTR) and ecPOR$^{-/-}$ mice (Mann-Whitney-test).

Endothelial knockout of POR attenuates eNOS activity

Since NO was reduced in plasma of ecPOR$^{-/-}$ as compared to CTR, the activity of eNOS was measured in aortic rings. eNOS activity was first measured by quantifying the formation of cyclic GMP by RIA. A23187 (calcium ionophore)-stimulated cGMP-accumulation was only increased in aortic rings from CTR mice (**Figure 21A**). Next, eNOS activity was measured by the conversion of heavy arginine into heavy citruline. Basal and acetylcholine (10^{-7} mol/L) stimulated, eNOS-dependent aortic conversion of L-arginine to L-citrulline was reduced in response to the knockout of POR in endothelial cells ($1.3*10^{-3}$ AUC ± $0.4*10^{-3}$ for CTR and $0.8*10^{-3}$ AUC ± $0.3*10^{-3}$ for ecPOR$^{-/-}$ at basal conditions; $2.3*10^{-3}$ AUC ± $0.9*10^{-3}$ for CTR and $1.4*10^{-3}$ AUC ± $0.6*10^{-3}$ for ecPOR$^{-/-}$ after incubation with acetylcholine (10^{-7} mol/L))(**Figure 21B**). Collectively, these data indicate that endothelial knockout of POR attenuates eNOS activation.

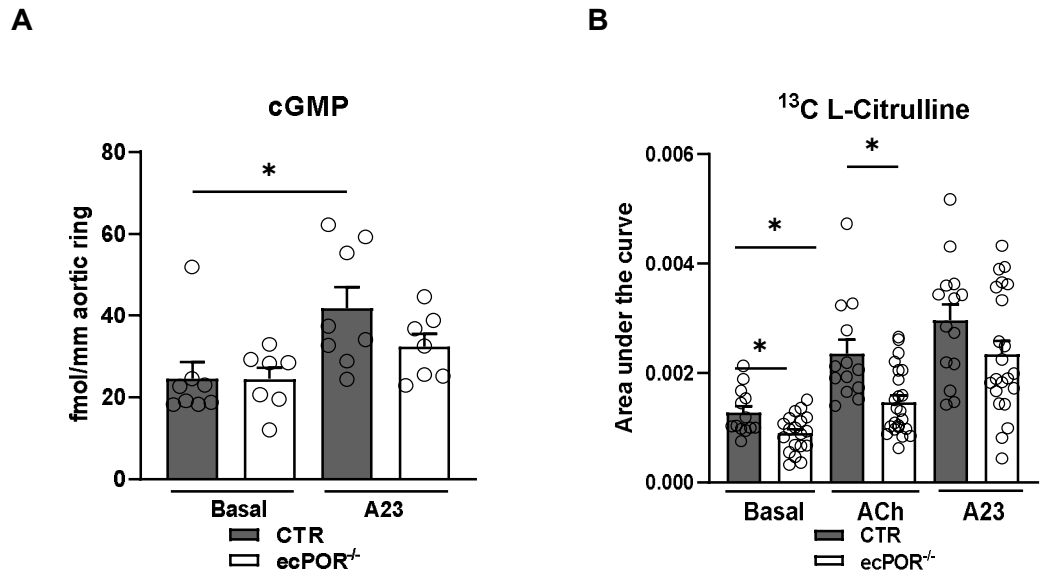

Figure 21 : Endothelial knockout of POR attenuates vascular eNOS activity
(A) Levels of cGMP in aortic rings treated with solvent (Basal) or A23187 (A23; 1 µmol/L, 5 minutes) as measured by RIA; One-way Anova with Bonferroni correction. (B) Conversion of ^{13}C L-arginine to ^{13}C L-citrulline by aortic rings (LC/MS/MS, data shown are area under the curve); One-way Anova with Tukey's post-test. *p<0.05.

Phosphorylation at serine 1177 of eNOS is attenuated in the ecPOR$^{-/-}$ mice

Given that NO levels and eNOS activity were reduced in vessels of ecPOR$^{-/-}$ mice as compared to CTR, vascular eNOS expression was evaluated. The eNOS mRNA as well as the protein in aortic tissue were not different between ecPOR$^{-/-}$ and CTR mice (**Figure 22**). However, the phosphorylation at serine position 1177 which is a known marker to facilitae eNOS activity, was significantly reduced in the endothelium of ecPOR$^{-/-}$ mice when compared to the CTR (**Figure 22**).

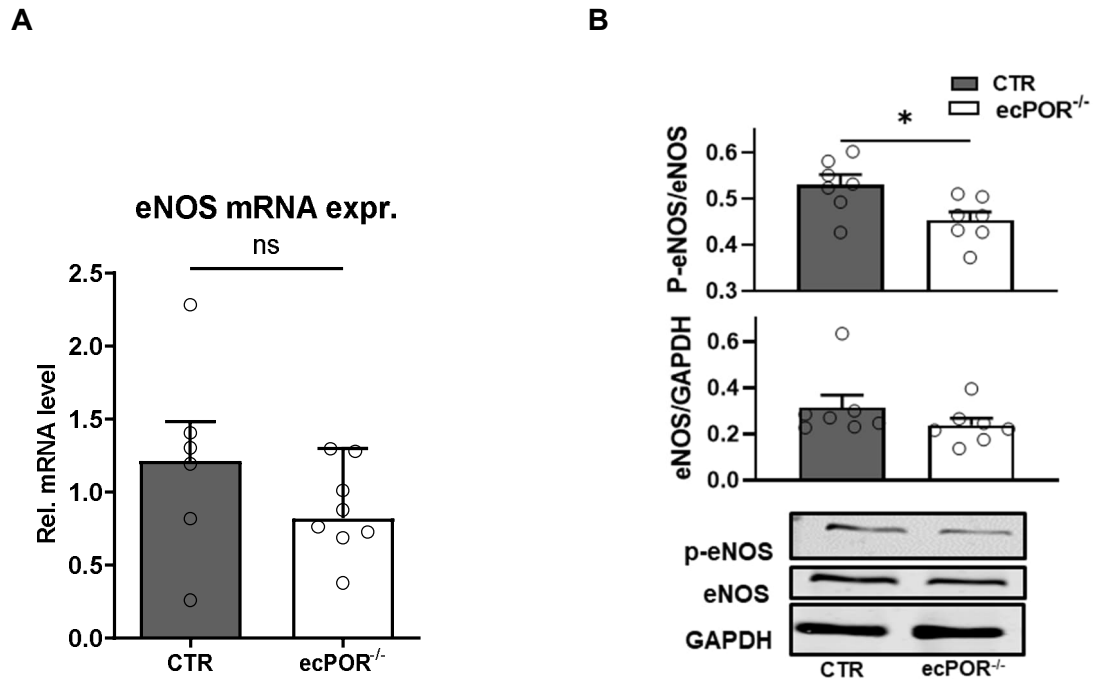

Figure 22: eNOS expression and phosphorylation in aortic rings of CTR and ecPOR$^{-/-}$ mice
(A) eNOS mRNA in aorta from CTR and ecPOR$^{-/-}$ mice (Mann-Whitney-test). (B) Representative blots and densitometry of eNOS and pSer1177-eNOS from endothelium of isolated aortic rings from CTR and ecPOR$^{-/-}$ mice; n= 7 mice per group (paired-t-test).

AKT phosphorylation is reduced in the ecPOR$^{-/-}$ mice

As phosphorylation at Ser1177 of eNOS was significantly reduced in aortae of ecPOR$^{-/-}$ mice compared with CTR, the phosphorylation of AKT was analysed by western blotting from endothelial cells enriched from aortic tissue. Insulin stimulation (0.1 µmol/L, 15 min) increased pAKT in endothelial cells and this effect was significantly attenuated in aortae from ecPOR$^{-/-}$ mice (**Figure 23**).

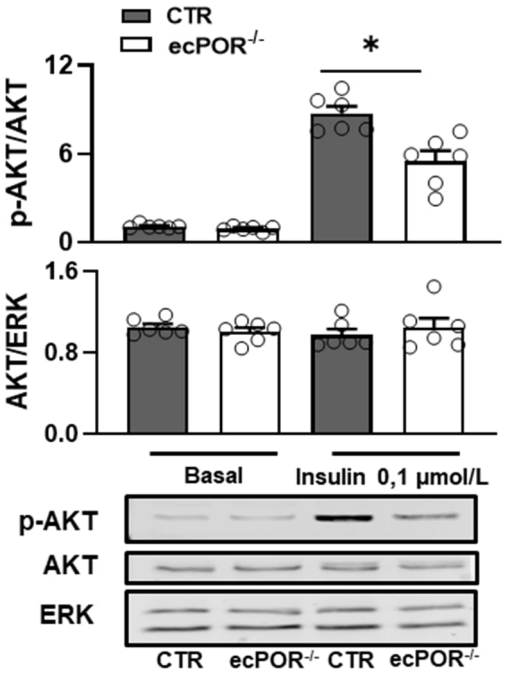

Figure 23: AKT Phosphorylation in aortic endothelial cells of ecPOR$^{-/-}$ and CTR mice
Representative blots and densitometry of p-AKT, AKT and ERK from endothelial cells freshly isolated from aortic rings from CTR and ecPOR$^{-/-}$ mice previously incubated or not with insulin (0,1 µmol/L; 15 min); n= 6 mice per group; One way Anova with Bonferroni correction.

Endothelial knockout of POR in HUVEC lowers vascular EET content

As POR is essential for the function of microsomal CYP450, the role of POR in the metabolism of vasoactive oxylipins was assessed. These lipids were first measured in HUVEC with and without pre-incubation with the CYP inhibitor SKF525a in the presence of arachidonic acid as substrate. The CRISPR/Cas9 POR$^{-/-}$ cells showed lower levels of most lipids determined, being 11,12 EET, 14,15 EET and 9 HODE significantly lower in POR$^{-/-}$ as compared to the non-targeted control (NTC) cells (**Figure 24**). Whereas the CYP450 inhibitor induced a marked reduction of several lipids in the control cells, it had only a weak, non-significant effect on the oxylipins measured in the POR$^{-/-}$ HUVEC. Therefore, POR is indeed essential for the endothelial metabolism of the arachidonic acid-derived oxylipins.

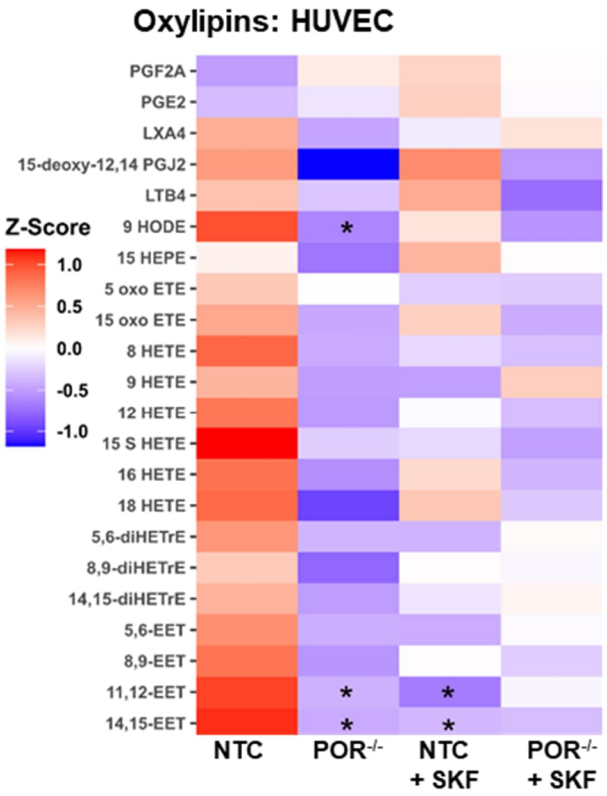

Figure 24: POR deletion in endothelial cells attenuates EET levels
Heatmap of PUFA metabolites in cultured human endothelial cells (HUVEC) transduced with lenti viruses containing non-targeted control (NTC) gRNAs or gRNAs targeting POR (POR-/-). Values represent Z-Score from pg/mL measurements; n=6, One-way Anova.

EETs are reduced in aorta and lung tissue of ecPOR$^{-/-}$ mice

Encouraged by the results observed in the HUVEC, and due to the well-defined function of EETs as being vasoprotective molecules, the effect of endothelium-specific deletion of POR on EETs levels was analysed in the vessels. To measure the total intracellular EETs (free and membrane-bound) samples were subjected to alkaline hydrolysis with potassium hydroxide also because the levels of free EETs in aorta are below the detection level of mass spectrometry. This treatment releases the membrane bound-EET that usually occupy the R2 side chains of phospholipids. The ecPOR$^{-/-}$ mice showed a reduction of approximately 30% across the EETs when compared to CTR littermates and this value reached significance for 5,6 EET, 11,12 EET and 14,15 EETs. In a similar fashion, the EET content of lung, a tissue rich in endothelial cells, was similarly reduced in the ecPOR$^{-/-}$ mice, being significant for 5,6 EET, 8,9 EET and 14,15 EET (**Figure 25**).

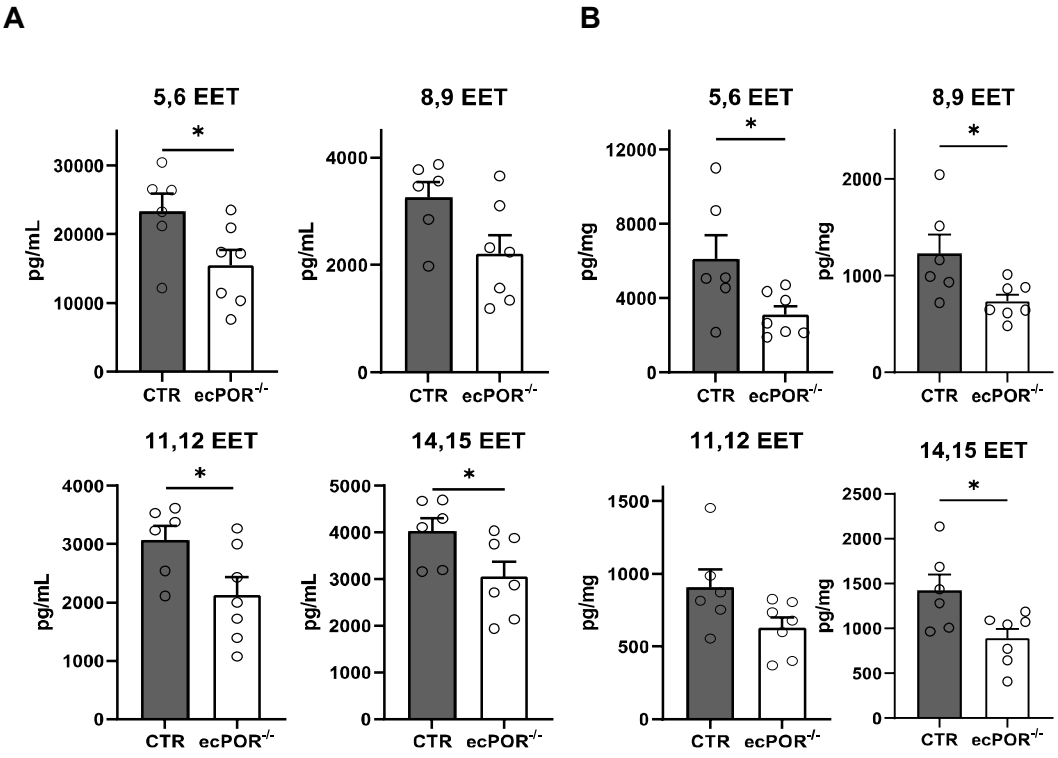

Figure 25: EET levels in murine aortic and lung tissues are reduced after endothelial deletion of POR EET levels from aorta
(A) and lungs (B) of CTR and ecPOR$^{-/-}$ mice; Mann-Whitney-test, *p<0.05.

MACE-Seq annotates for increased eicosanoid production

MACE sequencing was performed to explore potential changes in gene expression in the aorta after endothelium deletion of POR. MACE is an alternative to classic mRNA Seq. It differs by sequencing only one single molecule or “tag” per transcript. Different to other Tag-Seq methods, in MACE-Seq, each molecule is barcoded with a unique sequence. The advantage is that longer transcripts are not overrepresented, while low copy number transcripts are identified with high degree of confidence [99]. The significantly altered genes in aorta of ecPOR$^{-/-}$ mice suggest an overall change in fatty acid metabolism in this line as compared to CTR (**Figure 26**). Eicosanoid- related genes, also annotated as prostanoid, were mostly upregulated in the ecPOR$^{-/-}$ mice. Examples include genes such as Syk (Spleen Associated Tyrosine Kinase), Hpgd (15-Hydroxyprostaglandin Dehydrogenase), Ggt5 (Gamma-Glutamyltransferase 5) and PTGIS (Prostaglandin I2 Synthase). In contrast, cholesterol biosynthesis was significantly decreased in ecPOR$^{-/-}$ as compared to CTR as shown by pathway

enrichment analysis. Interestingly, prostanoid-related genes such as Alox12, (12-lipoxygenase) was downregulated.

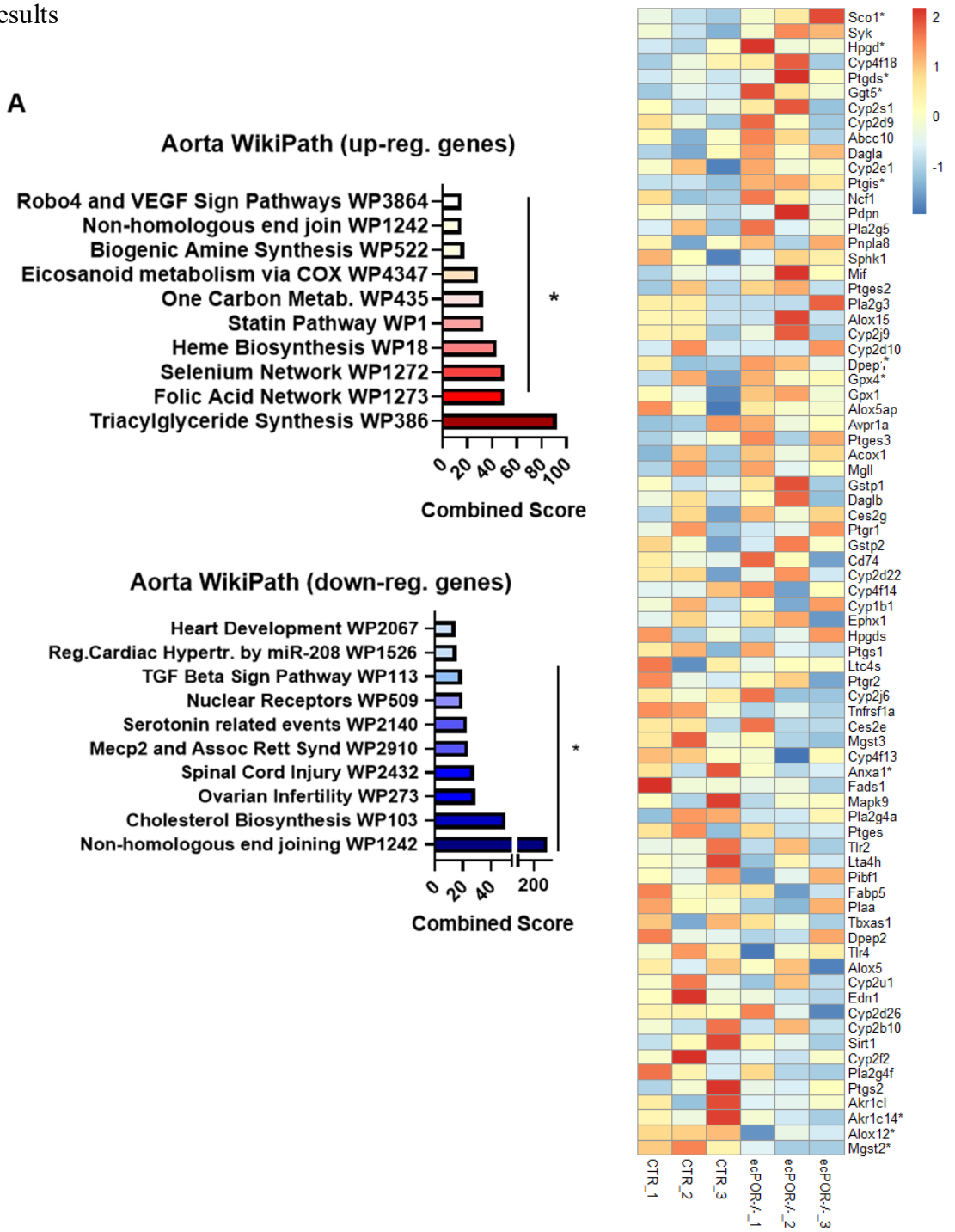

Figure 26 Deletion of POR alters genes of lipid metabolism
(A) Pathway analysis (WikiPath Mouse dataset) for the top 500 up- and down-regulated genes (identified by MACE) in aortae from ecPOR$^{-/-}$ as compared to CTR. Bars represent the combined score from the top ten analyzed pathways (EnrichR online-tool). (B) Heatmap of genes assigned to “eicosanoid metabolic process” (GO: 000669). B-C: n=3, being each a pool of 3 different animals. *p<0.05.

Arachidonic acid is shunted from vasodilating EETs to vasoconstricting COX-derived prostanoids in ecPOR$^{-/-}$ mice

To further explore the changes in lipid metabolism observed at gene expression, prostaglandins and other oxylipids were measured in the lung, aorta and plasma of CTR and ecPOR$^{-/-}$ mice. In addition, cholesterol and its derivatives were also measured from the aorta of these animals. The measurements of cholesterol and its metabolites from aorta, however, showed no differences between the CTR and ecPOR$^{-/-}$ mice (Error! Reference source n ot found.**)**.

The level of the prostanoids PGE2, TXB2 and PGF2α were significantly increased in the lungs of ecPOR$^{-/-}$ mice and a similar increase in vasoconstrictor oxylipids was also observed in the aorta (**Figure 28**). In keeping with the down-regulation of the 12-lipoxygenase gene, the aortic level of 12-HETE was reduced in ecPOR$^{-/-}$ as compared to CTR mice. To understand whether such local differences also impact on whole body oxylipid level, the murine plasma was analysed. Although the differences in oxylipids were more subtle and did mostly not reach the significance level, similar trends were observed as in the lung and in the aorta particularly for the cyclooxygenase product 11-HETE, 15-deoxy-12,14-PGJ2, and thromboxane B2. Altogether, these imply that the loss of endothelial POR leads into a functional shunt of arachidonic acid from the CYP450 pathway towards vasoconstrictor prostaglandins metabolized by COX enzymes.

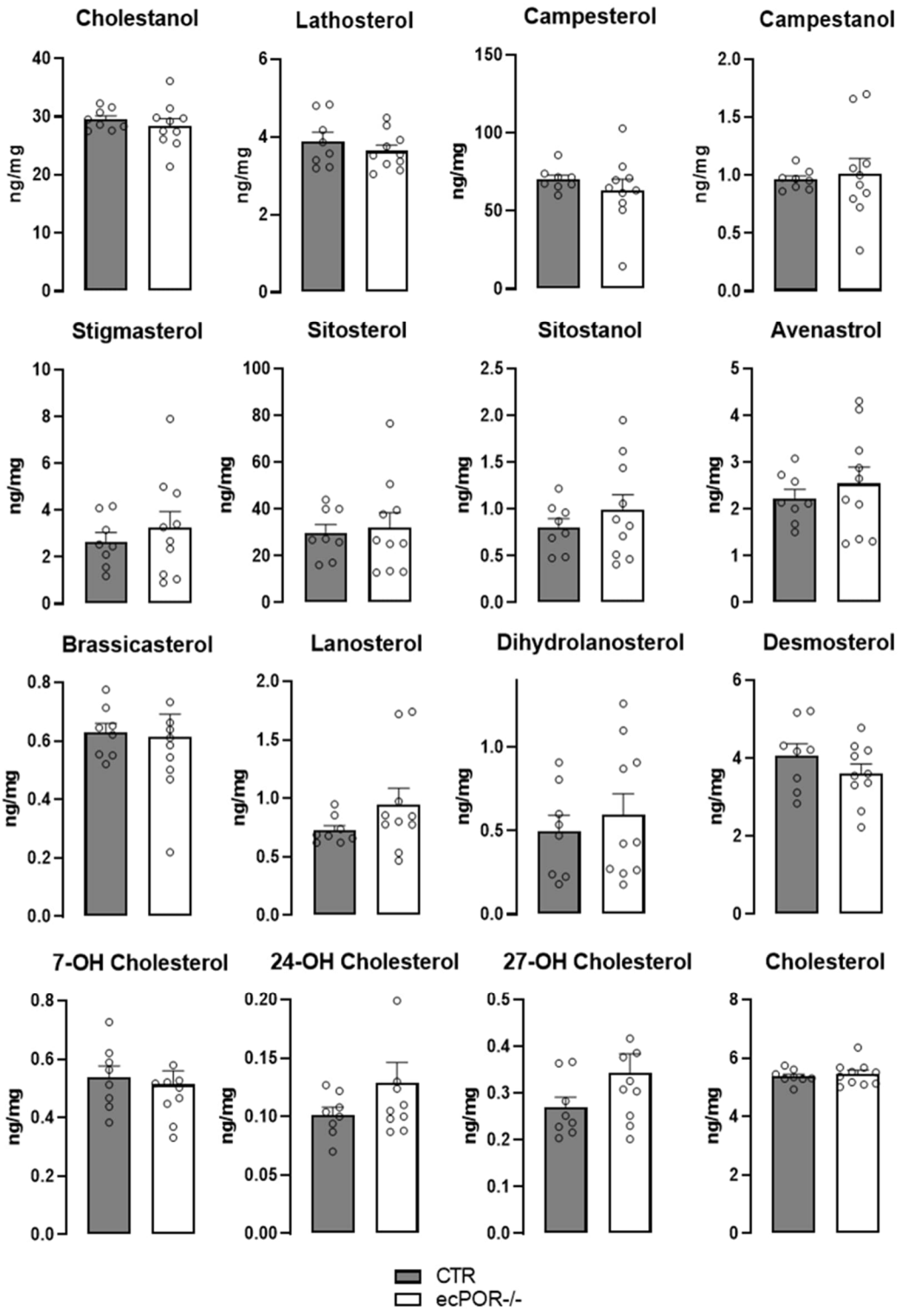

Figure 27: Cholesterol and its derivatives are unchanged in aortae of ecPOR$^{-/-}$ mice as compared CTR.
Measurements of cholesterol and its metabolites by GC/MS from aorta of CTR and ecPOR$^{-/-}$ mice. N= 8 (CTR) and 10 (ecPOR$^{-/-}$).

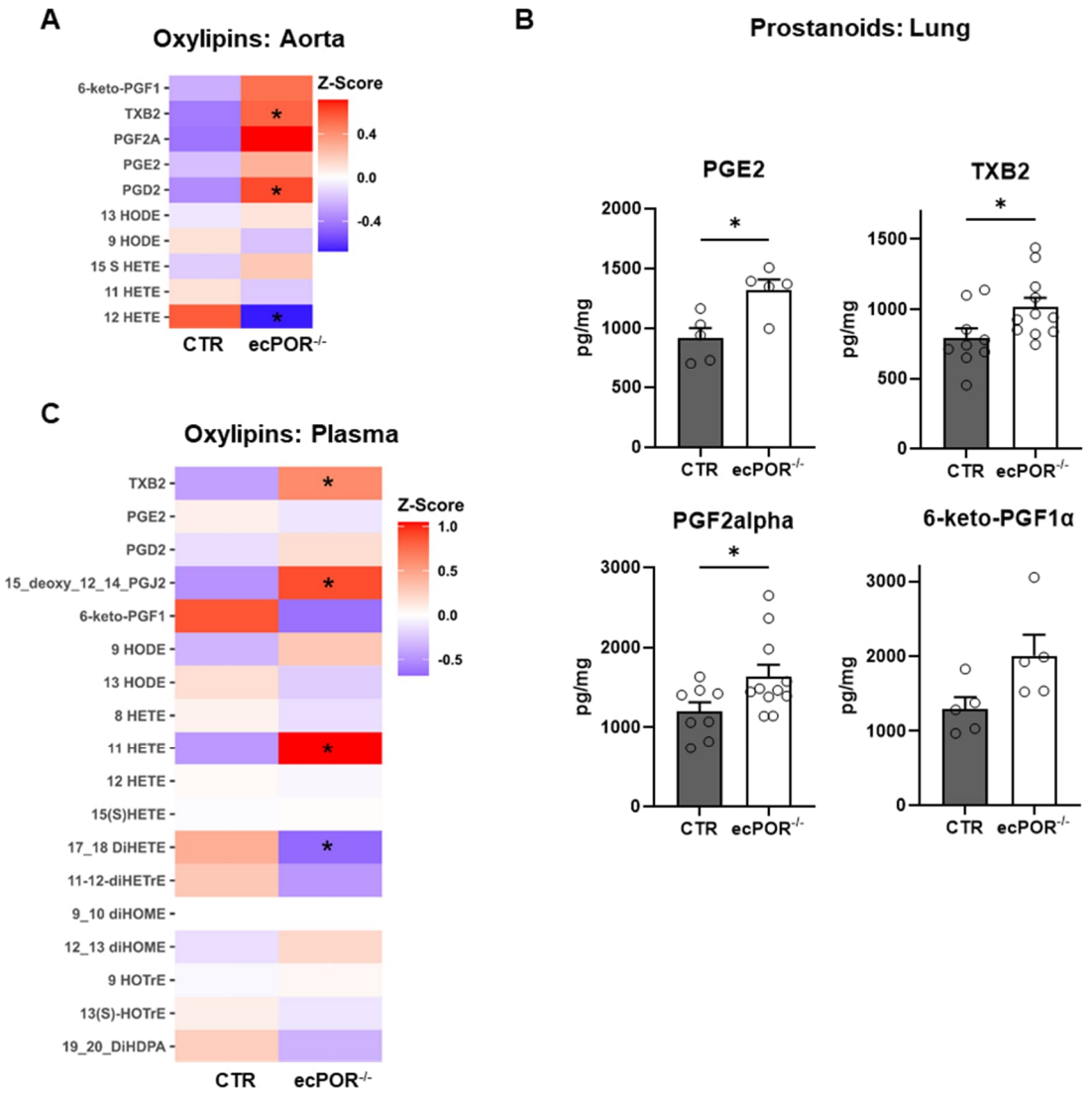

Figure 28 Endothelial knockout of POR alters prostanoid production. (A) Heatmap of oxylipin profiling from aorta of CTR and ecPOR$^{-/-}$ mice. (B) Prostaglandins and thromboxane levels in lungs from CTR and ecPOR$^{-/-}$ mice. (C) Heatmap of oxylipin profiling from plasma of CTR and ecPOR$^{-/-}$ mice. Z-score (A) and (C) from mean values in both CTR and ecPOR$^{-/-}$ mice. Mann-Whitney-test. *p<0.05 CTR versus ecPOR$^{-/-}$.

Endothelial deletion of POR does not result in inflammation

Keeping up with the increase of prostanoids, which are known pro-inflammatory molecules and the fact that EETs have been described to have anti-inflammatory effects linked to NF-kappaB activation [100], it was analysed if the deletion of POR in the endothelium had a pro-inflammatory effect. Gene expression of NF-kB dependent cytokines and chemokines in aorta of ecPOR$^{-/-}$ mice, as estimated by qPCR, were not altered when compared to CTR (**Figure 29A**). Only TNF-α showed a marginal increased but did not reach significance. Additionally, when

THP1 cells were seeded over NTC and $POR^{-/-}$ HMEC, with or without TNFα, no difference was observed between the genotypes (**Figure 29B**). Collectively, knockout of POR in EC essentially activated only COX-related inflammatory pathways with no changes in NF-kB. Thus, the endothelial dysfunction elicited by the knockout of POR cannot be attributed to inflammation.

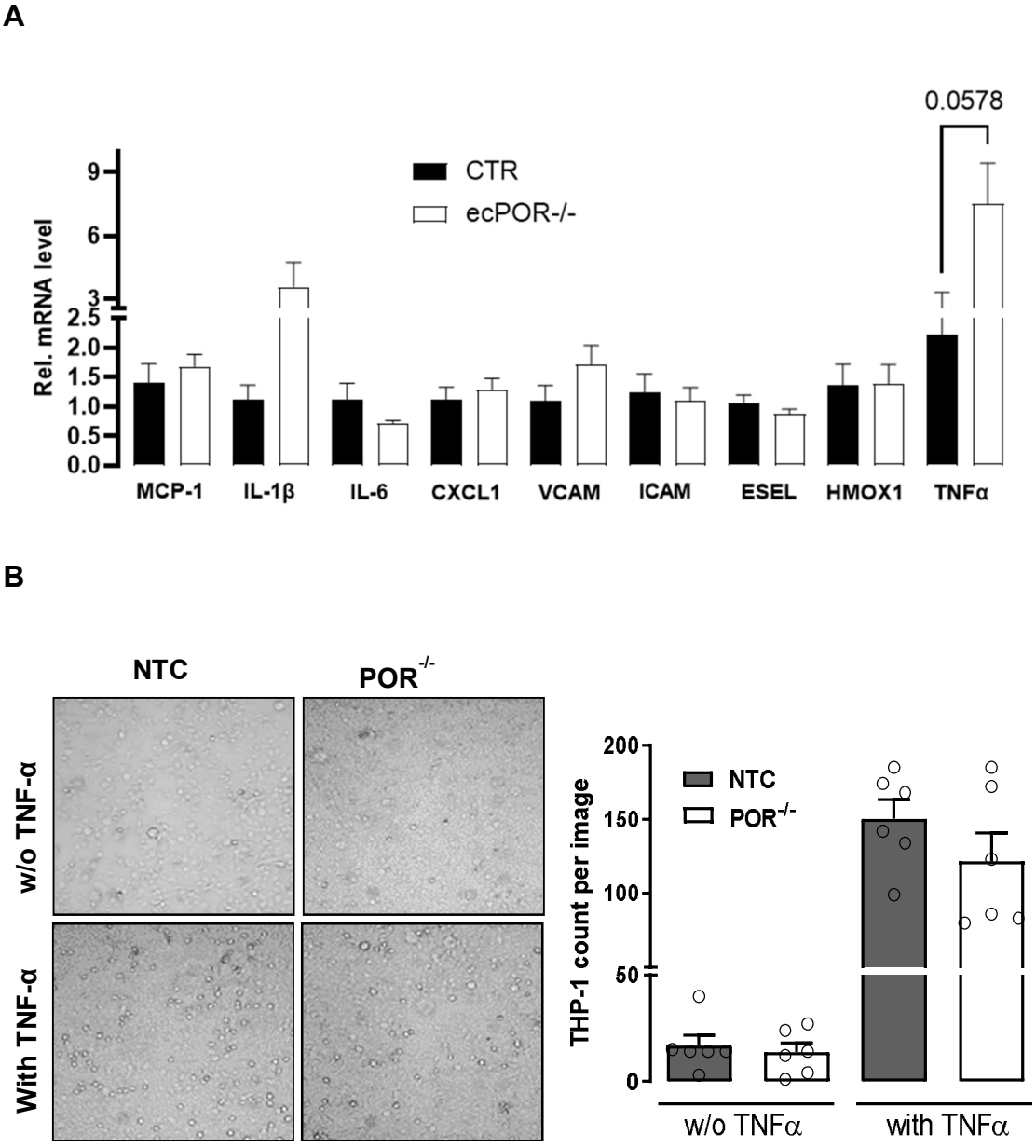

Figure 29 Knockout of POR in the endothelium does not promote inflammation
(A) qPCR for the inflammation markers: MCP-1, Il-1β, IL-6, CXCL1, VCAM, ICAM, E-SELECTIN, HMOX-1 and TNFα in thoracic aorta from CTR and ecPOR$^{-/-}$ animals under basal conditions. (B) Adhesion of THP-1 cells to POR deficient HMEC, with or without TNFα (10 ng/ml, 1 hour); One-way-Anova with Bonferroni correction.

Endothelial knockout of POR increases murine vasoconstrictor tone *in vivo*

Given that the vasorelaxants EETs were reduced and the vasoconstrictor prostanoids were increased in ecPOR$^{-/-}$ as compared to CTR, the diameter of the carotid artery was measured by ultrasound (Vevo 3100) as an *in vivo* measure of vascular tone. In fact, the change towards prostanoids in absence of endothelial

POR reduced the diameter of the carotid artery during both systole and diastole, confirming an increased vascular tone in ecPOR$^{-/-}$ as compared to CTR (**Figure 30**).

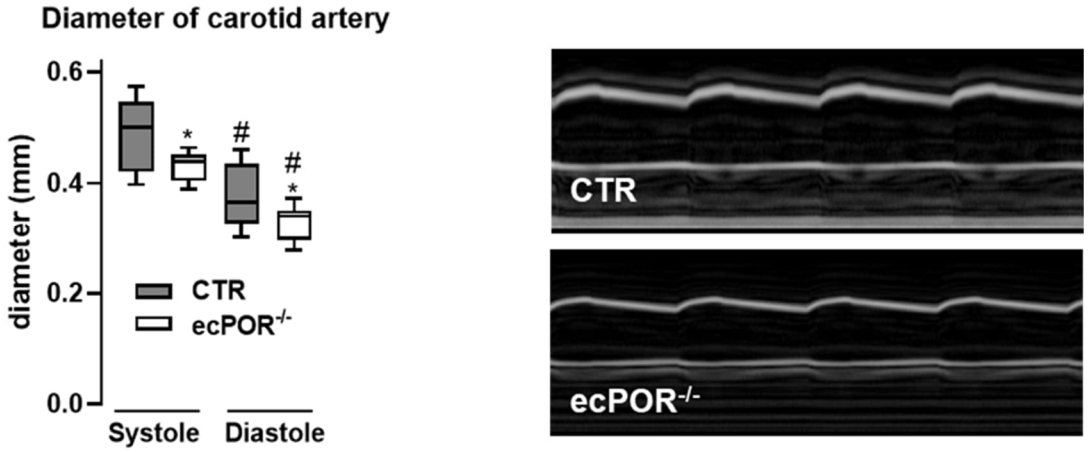

Figure 30: ecPOR$^{-/-}$ mice have increased vascular tone
Diameter of carotid arteries during systole and diastole as measured by ultrasound using Vevo 3100. Right panel: representative ultrasonographic images of carotids, n≥5. *p<0.05 comparing CTR and ecPOR$^{-/-}$, #p<0.05 comparing systole versus diastole, One-way-Anova with Bonferroni correction.

Endothelial Loss of endothelial POR potentiates AngII-mediated changes in blood pressure

Endothelial dysfunction on the base of abnormal endothelium-dependent relaxation has been implicated in the pathogenesis of several cardiovascular diseases including hypertension [101]. Based on the findings that ecPOR$^{-/-}$ mice showed endothelial dysfunction, reduced eNOS activity, lower EETs and increased prostanoids as compared to CTR mice, it was logical to infer that ecPOR$^{-/-}$ mice are hypertensive. To investigate whether the deletion of POR impacts on blood pressure, blood pressure (BP) from CTR and ecPOR$^{-/-}$ mice was recorded using two different technics: through the tail-cuff plethysmography method and the continuous telemetry method.

Tail-cuff: Systolic blood pressure, diastolic blood pressure and heart rate were measured before (basal) and after implantation of angiotensin II pumps in mice previously fed with tamoxifen. No changes were observed in systolic (111 mmHg ± 5.0 for CTR and 113 mmHg ± 5.6) and diastolic blood pressure (50.4 mmHg ± 4.4 for CTR and 49.1 mmHg ± 1.8) nor in heart rate (650 beats per minute (BPM)

± 21.8 for CTR and 639 BPM ± 71.3) at basal condition (**Figure 31**). However, angiotensin II- elicited hypertension was enhanced in the ecPOR$^{-/-}$ mice with a significant increase in systolic blood pressure when compared to the CTR littermates (135 mmHg ± 14.7 for CTR and 152 mmHg ± 7.1). Furthermore, the SBP to heart rate ratio which is a parameter for peripheral resistance was also significantly higher in the knockout animals (0.21 mmHg/BPM ± 0.02 for CTR and 0.25 mmHg/BPM ± 0.03) **Figure 31**.

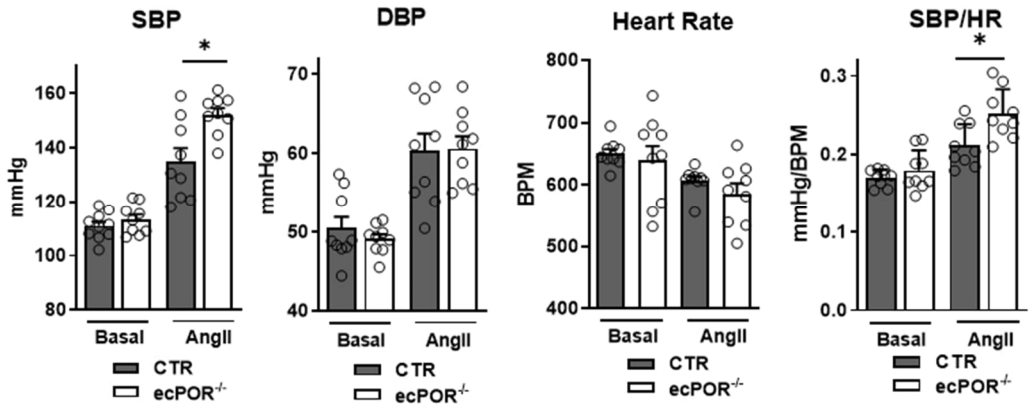

Figure 31: Blood pressure measurements by tail-cuff plethysmography
Animals received tamoxifen prior to the tail-cuff procedure. Basal blood pressure was determined over 10 days and the last 4 days were averaged for the plot. Afterwards, angiotensin II (0.7 mg/kg/day) osmotic mini pumps were implanted on the mice and the tail-cuff measurements were repeated. The data shown represent the average of the measurements from 5 days. SPB: systolic blood pressure, DBP: diastolic blood pressure, SBP/HR: ratio of systolic blood pressure to heart rate as an estimative of peripheral resistance.

Telemetry: blood pressure was monitored continuously and the original traces for continuous blood pressure measurements are shown in (**Figure 32**). A steady basal systolic blood pressure of 120 mmHg, diastolic blood pressure of 90 mmHg and heart rate of 505 BPM was observed in both groups of animals (Error! R eference source not found.). Ang II (0.7 mg/kg/day) *in vivo* treatment raised the systolic and the diastolic BP in the CTR and ecPOR$^{-/-}$ groups to an average of 135 mmHg for SBP and 105 mmHg for DBP, with a heart rate of 500 BPM for both groups. The acute induction of the knockout of POR through tamoxifen injection further increased the Ang II mediated hypertension in the ecPOR$^{-/-}$, as observed by the higher systolic BP as compared to the CTR animals (144 mmHg ± 7.7 for CTR and 158 mmHg ± 6.9 for ecPOR$^{-/-}$). Similarly, diastolic blood

pressure was also significantly higher in the ecPOR$^{-/-}$ (106 mmHg ± 7.8 for CTR and 122 mmHg ± 5.7), as compared to CTR. However, there were no changes in the heart rate which showed an average of 483 BPM in both groups.

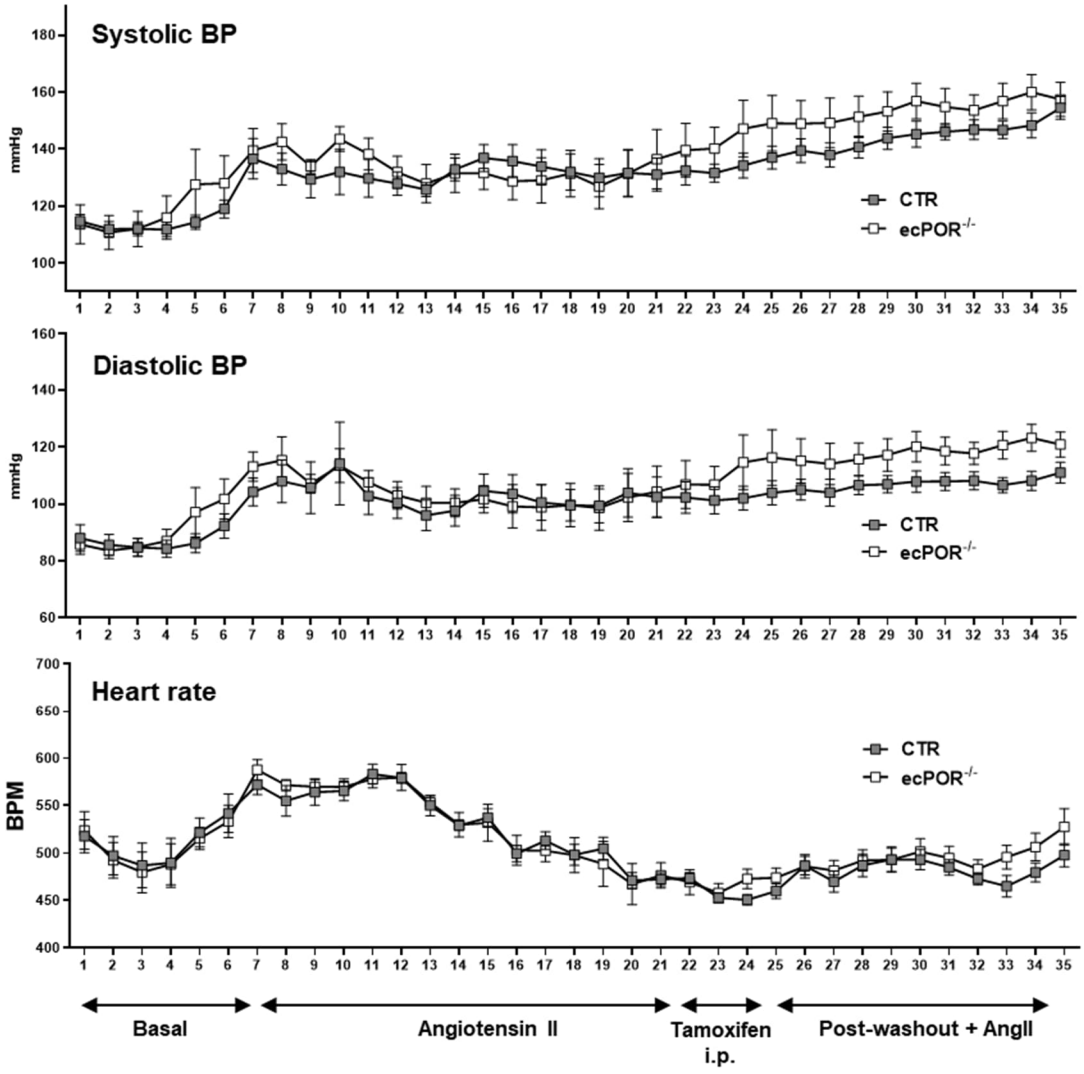

Figure 32: Continuous tracings from telemetric measurements of CTR and ecPOR$^{-/-}$ mice
Systolic and diastolic BP and heart rate were recorded continuously under the following conditions: basal – angiotensin II infusion (0.7 mg/kg/day by minipump) – induction of knockout through intraperitoneal injections of tamoxifen – post-washout tamoxifen period with angiotensin II pumps as indicated.

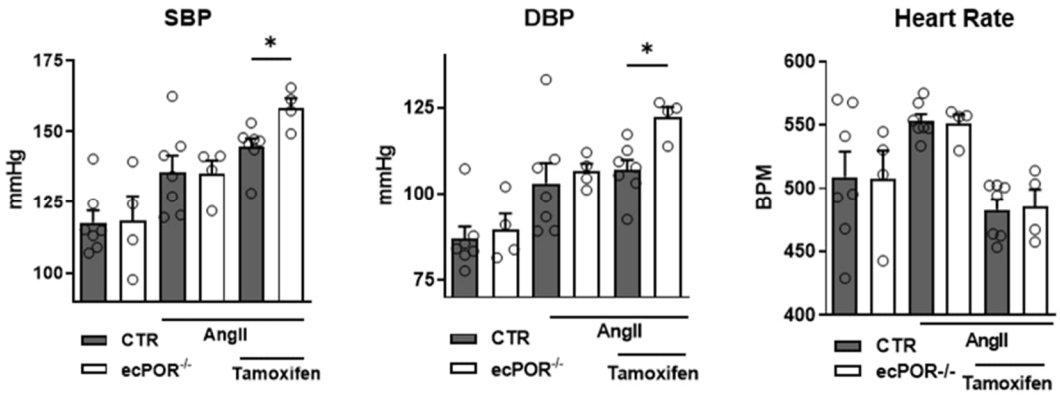

Figure 33: Loss of endothelial POR potentiates angiotensin II induced hypertension
Systolic blood pressure (SBP) and diastolic blood pressure (DBP) and heart rate were recorded continuously with the following steps: basal – angiotensin II infusion (0.7 mg/kg/day by minipump) – induction of knockout through intraperitoneal injections of tamoxifen – post-washout tamoxifen period with angiotensin II pumps.

Cox-inhibition blocks the hypertensive effect of the endothelial knockout of POR

ecPOR$^{-/-}$ mice show higher blood pressure upon AngII treatment when compared to the control mice as measured by tail cuff and telemetry techniques. As the lipidomic measurements showed increased basal production of thromboxane and prostaglandins, it was hypothesized that these lipids underlined the BP effects in the ecPOR$^{-/-}$ mice. To test this, another set of telemetry experiments was performed after induction of the knockout with tamoxifen and treatment with Ang II. Once hypertensive in response to AngII infusion, the mice received five i.p. injections (30 mg) of Naproxen, a non-selective COX inhibitor. Naproxen exclusively reduced the SBP of ecPOR$^{-/-}$ mice from 153.5 ± 4.3 to 135 ± 6.1 SEM mmHg. Systolic blood pressure of CTR mice (130 ± 4.2 mmHg) and Naproxen-treated ecPOR$^{-/-}$ was thus similar (**Figure 34**). The diastolic BP followed the same tendency; however, it did not reach significance but the ratio of SBP/HR confirmed the rescue in peripheral resistance in ecPOR$^{-/-}$ upon Naproxen treatment. Thus, the increased production of prostanoids rather than sole reduced EET production in ecPOR$^{-/-}$ mice elevates blood pressure.

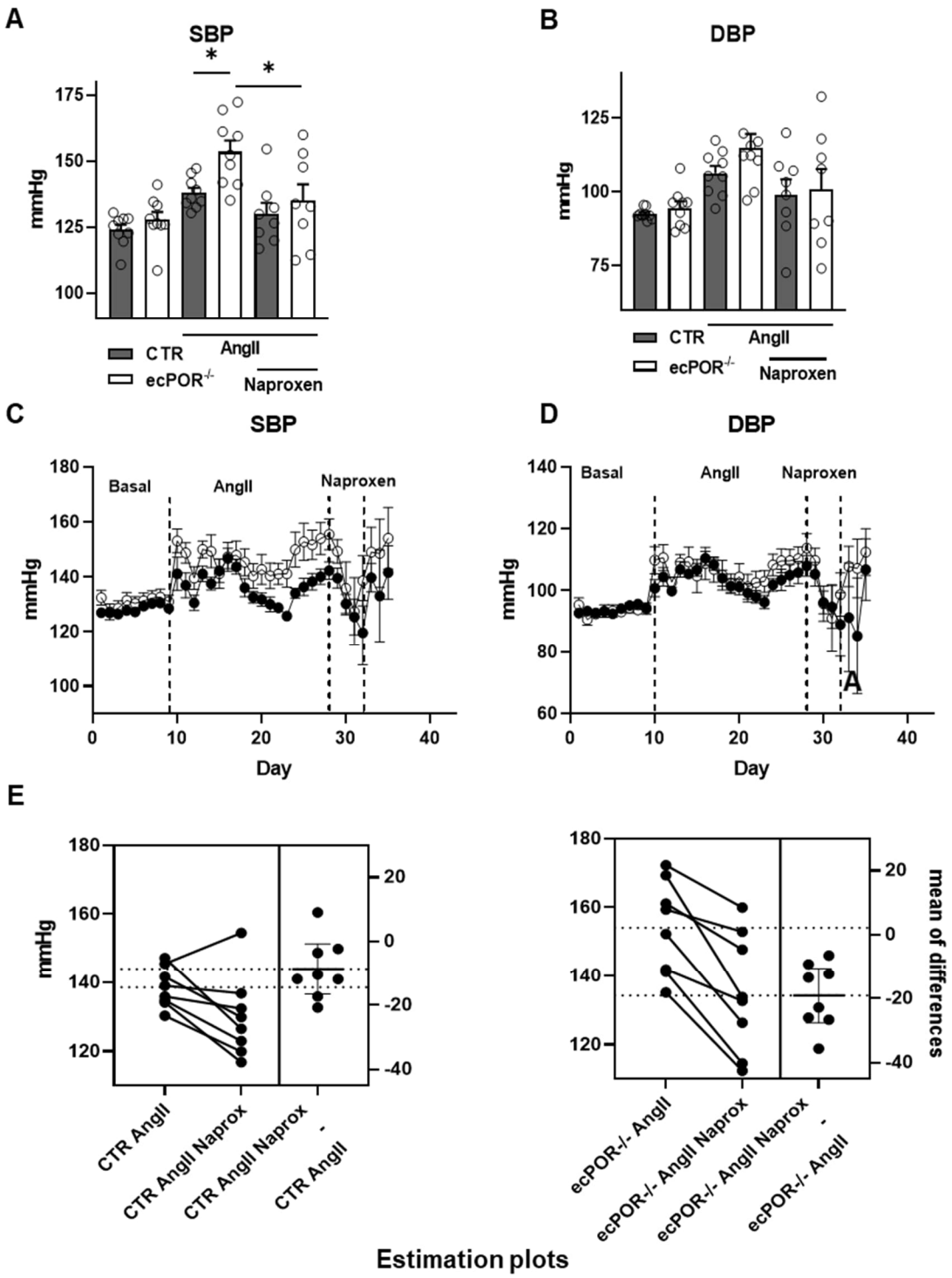

Figure 34: Loss of endothelial POR potentiates AngII-induced hypertension *in vivo* through cyclooxygenase products.
(A-B): Mice were pre-treated with tamoxifen to induce the knockout of POR and blood pressure was measured from day 20 to 24, after tamoxifen, by telemetry. Subsequently, AngII-infusing minipumps were implanted and finally Naproxen (30 mg/kg/day, i.p., 5 days) was injected. n≥8, One-way-Anova with Tukey's post-test. SPB: systolic blood pressure, DBP: diastolic blood pressure. (A and B) Traces of the daily recordings on SBP (C) and DBP (D) of the mice before and after Angiotensin II (0.7 mg/kg/day) and after Naproxen treatment. (E)

Estimation plots of animal-paired systolic blood pressure measurements before and after naproxen treatment.

Reduced EETs and increased prostanoids in ecPOR$^{-/-}$ mice suggest a crosstalk at receptor level to maintain vascular tone

Since the endothelial-specific deletion of POR increases aortic levels of thromboxane and PGD2, the constrictive response of the aorta to U46619 (a thromboxane receptor agonist) was accessed. Aortic vessels from ecPOR$^{-/-}$ mice showed a significantly higher sensitivity to the constrictor U46619 (EC50: approx. −7.8 log mol/L) as compared to vessels from CTR mice (EC50: −7.6 log mol/L) (**Figure 35**) his suggests that the TP receptor is primed or the downstream signalling cascade is sensitized or induced in ecPOR$^{-/-}$ mice. Interestingly, after U46619-mediated contraction, high concentrations of EETs were able to relax the vessels. This may suggest that EETs either compete with U46619 on the TP receptor or interfere with TP receptor signalling (**Figure 35**) o differentiate between these two modes of action, the response of vessels to a second prostanoid constrictor, PGE2, was studied. PGE2 acts through a different receptor but via an analogous signalling pathway. Similarly to the thromboxane agonist, vessel constriction in response to PGE2 was sensitized by the deletion of POR (**Figure 35**). As in the case of U46619, EETs also induced the relaxation of PGE2-preconstricted vessels (**Figure 35**).

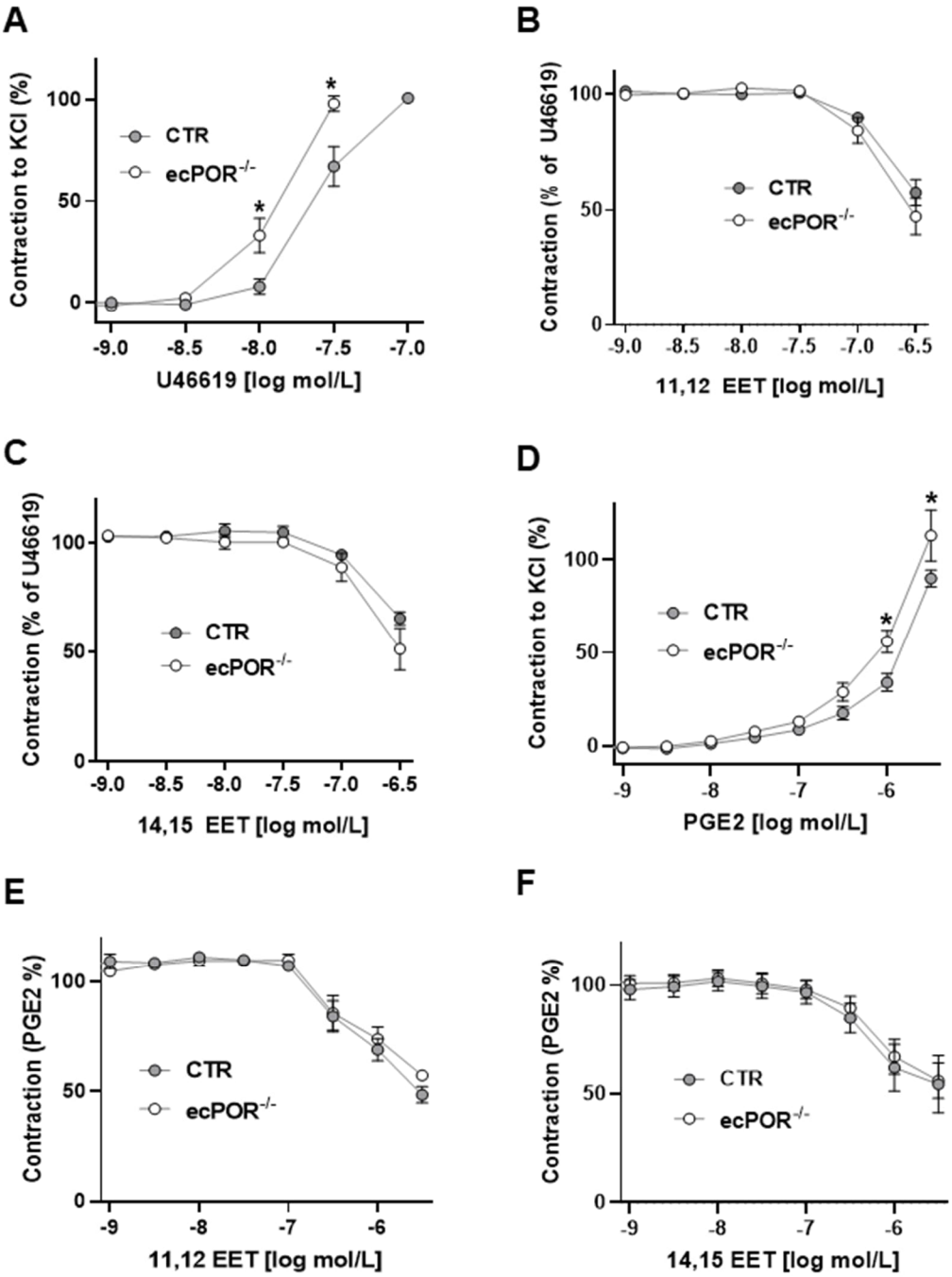

Figure 35: Knockout of POR in the endothelium leads to increased constriction to the thromboxane receptor agonist U46619 and PGE2 in aorta.

Vasoconstriction of aorta of CTR and ecPOR$^{-/-}$ mice towards U46619 (A) and PGE2 (D) *p<0.05, Two-way ANOVA with Bonferroni post-test. n>11 aortic rings. (B,E) Vasodilation CTR and ecPOR$^{-/-}$ mice towards 11,12-EET after pre-constriction with U46619 (B) and PGE2 (E) Two-way ANOVA with Bonferroni post-test. n≥7 aortic rings. Vasodilation of CTR and ecPOR$^{-/-}$ mice towards 14,15-EET after pre-constriction with U46619 (C) and PGE2 (F). Two-way ANOVA with Bonferroni post-test (C) n=4 and (D) n=5 aortic rings.

Discussion

Importance of endothelial CYP450s for the control of vascular tone

The CYP450 family of isoenzymes traces back to ancestral genes of more than 3.5 billion years ago [102] with more than 50 different CYP450 isoenzymes are expressed in a given species [103]. Most studies on CYP450 focus on their pharmacological importance regarding drug clearance and toxicology, due to their abundance and versatility in metabolizing various xenobiotics into harmless or harmful and excretable metabolites [104]. However, CYP450 enzymes have a primary role in metabolizing a multitude of endogenous compounds. One important CYP450 substrate is arachidonic acid which is present in phospholipids of cellular membranes. Along with cyclooxygenases and lipoxygenases, CYP450s metabolize arachidonic acid into several bioactive lipids, many of which are important for the cardiovascular system. These include the bioactive epoxides epoxyeicosatrienoic acids (EETS) as well as some of the hydroxyeicosatetraenoic acids (HETE) [105,106].

Despite more than 35 years of research, the knowledge on the vascular signaling by EETs and their regulation of vascular tone is still not completely understood. This is partly due to the large number of CYP450 family members and the lack of specific CYP450 inhibitors. Nonetheless, sufficient evidences exist to support that EETs modulate cardiovascular function. Most studies have focused on targeting individual CYP isoforms overexpressing CYP450 individually such as CYP2J2 or CYP2C8 [107,108]. Other approaches have aimed to increase the amount of EETs by inhibition of the EET-degrading soluble epoxide hydrolase (sEH).

POR is a key enzyme for the activity of all the different microsomal CYP enzymes since it acts as the essential electron donor necessary for their activity [109]. In order to overcome some of the issues that arise from individual CYP knockout, the strategy here was to switch off the function of the whole CYP450-system by deleting POR. As the constitutive knockout of POR is embryonically lethal, a tamoxifen-inducible endothelial specific knockout mouse was designed. Knocking out POR specifically in endothelial cells has the following advantages: i. the tissue-targeted knockout helps addressing the specific function of these active lipids in the endothelial context; ii. it prevents the compensational effects resulting from knocking out individual CYPs, iii. the *in vivo* approach overcomes

a common problem with CYP research in cultured cells, where cell-cycle-induced dedifferentiation leads to rapid changes in CYP expression [110]. Furthermore, by shutting down the POR/CYP450 system in a CYP-untargeted way the unknown function of CYP450 enzymes (CYP20A1, for example) [26] can be studied.

eNOS activity is impaired after knockout of POR from the endothelium

It was observed that the endothelial-specific deletion of POR led to vascular dysfunction of both mouse aorta and mesenteric vessel. Inhibition of nitric oxide synthases with L-NAME led to loss of the observed dilating difference between the two groups. The loss of effect with L-NAME suggests that the difference in endothelium-dependent dilator response is NO mediated. The endothelium dilator response of aorta is exclusively mediated by NO. Standing as a footprint for NO, nitrite was measured by using the NOA system. This assay is considered the gold standard in the measurement of nitric oxide and is widely used [111]. The nitrite levels were shown to be lower in the plasma of ecPOR$^{-/-}$ mice when compared to the control littermates.

Decreased NO bioavailability is commonly accompanied by endothelial cell dysfunction [112,113]. In fact, numerous therapies assess the possibility of reversing endothelial dysfunction by targeting systems that ultimately enhance the release or maintenance of nitric oxide in the endothelium. Some of these include inhibitors/angiotensin receptors blockers, which increase NO by modifying rennin-angiotensin-aldosterone system [114], the use of anti-oxidants such as vitamin E [115] as well as substances that target the coupling state of eNOS [116].

In mammals, plasma nitrite levels have been shown to be a good parameter to evaluate endothelial nitric oxide synthase activity, going as far as being considered a prognostic marker for cardiovascular diseases. The lower plasma NO in the ecPOR$^{-/-}$ also correlated to lower measured eNOS activity. As NO diffuses from endothelial cells to the vascular smooth muscle cell membranes it activates the enzyme soluble guanylate cyclase (sGC). This enzyme catalyzes the conversion of guanosine triphosphate into cyclic guanosine monophosphate (cGMP) [117]. Therefore, cGMP levels can be used as parameter to estimate eNOS function. Contrarily to the control animals, the calcium ionophore A23187

was unable to increase the levels of cGMP in the aorta of the ecPOR$^{-/-}$ mice. The reduction in eNOS activity was also assessed through a second assay based on the conversion of heavy arginine to heavy citruline by aortic rings. There it was confirmed that the ecPOR$^{-/-}$ mice indeed showed reduced eNOS activity.

It is known that eNOS undergoes phosphorylation at multiple sites including tyrosine, threonine, and serine residues and that this controls its activity. Phosphorylation at residue serine-1177 (Ser1177) [88] and tyrosine-83 [118] is known to facilitate eNOS function, while other sites such as threonine-495 [119,120] and tyrosine-657 [121] have been linked to inhibition of eNOS activity. Western blotting of phosphorylated-Ser1177-eNOS from endothelium fraction isolated from aortic rings revealed lower levels of phospho-Ser1177-eNOS in the ecPOR$^{-/-}$ when compared to the control animals. This provides evidence and correlates well to the lower eNOS activity observed in the previous assays. Furthermore, analysis of AKT, the primary phosphokinase responsible for phosphorylating Ser1177-eNOS, showed that it was less phosphorylated in the endothelium of ecPOR$^{-/-}$ mouse. Lower levels of AKT phosphorylation have been previously associated to hypertension [122]. AKT activation and cell survival has also been shown to be regulated by protein localization through a cholesterol-sensitive manner, where cholesterol drives membrane partition [123].

As with AKT, cholesterol is also important for the phosphorylation and activity of eNOS. eNOS is also known to partition into cholesterol-rich lipid rafts where it is more active [124]. Cholesterol is synthetized by a cascade of enzymatic reactions known as the mevalonate pathway, one of which includes both POR and cholesterol producing Sterol-14α-demethylase or CYP51. Measurements of total cholesterol from aortic tissue as well as several of its metabolites showed similar amounts between control and ecPOR$^{-/-}$ mice with no changes. However, as measurements from the mouse tissue were carried from aortic rings and not only the endothelium lining, it's likely that the due to higher mass content of the smooth muscle layer when compared to the endothelium the lipids derived from the smooth muscle layer out shadows those of the endothelium in the overall measurements.

POR is important for the fate of arachidonic acid metabolism and its vasoactive metabolites

Yet, the endothelial function maintained by POR cannot solely rely on eNOS function. Reduction in NO is usually insufficient to induce hypertension. Peripheral resistance is controlled at the arteriole level. At this site, the mechanisms of NO scavenging leads, through reactive oxygen species or hemoglobin, lead to great reduction in NO levels [125]. In fact, even a complete eNOS knockout only induces moderate hypertension [126] and therefore it is conceivable that the difference on eNOS activity has an impact on aortic endothelium-dependent relaxation, but not on blood pressure.

The microcirculation is rich in local mediators and has profound self-regulation through local metabolites. EDHF, or endothelium derived hyperdilating factors, are known to act predominantly in the resistance microvasculature modulating vasomotor tone [127]. As small resistance vessels contribute to regulate vascular resistance, EDHF is central in the pathogenesis of hypertension. Of the several EDHF secreted by the endothelium, the CYP-derived epoxyeicosatrienoic acids stand out as altered availability of these has been linked to diseases such as diabetes [128].

Indeed, upon knockout of POR in the endothelium of mice, a significant reduction in the four different EETs were observed in various tissues. This was further strengthened by the similar reduction observed in CRISPR $POR^{-/-}$ HUVEC cells. The exact mechanism in which EETs elicit vasodilation is until unknown. Earlier studies attributed the dilation through activation of large-conductance Ca^{2+}-activated K^+ channel (BK_{Ca}) [129,130]. Recent investigations show that EET-mediated BKCa activation can be blocked by the G protein inhibitor guanosine 5′-O-(2-thio)diphosphate suggesting that the actions of EETs are in part mediated via G protein-coupled receptor (GPCR) signaling [131]. A functional screening for G protein-coupled receptor targets of 14,15-EET showed that the binding affinity towards these receptor is considered to be low, with the top five receptors were of the prostaglandin receptor subtypes (FP, EP2, EP4, DP) [132].

It is to note that the effects of EETs in larger vessels such as aortas have, for the most part, been dismissed. Herein, our findings shows that these lipid mediators are present in aorta, and as expected, the deletion of POR lead to vascular

dysfunction accompanied by a reduction in these lipids. The benefits that these lipids may play in keeping the function in larger vessels hang on their mechanism. It has been recently shown that EETs antagonize the action of vasoconstrictor lipids by acting as antagonists of TXA2 [84,133]. The results here not only reproduces the antagonistic properties between EETs and TXA2, but also show that it is not limited towards TBXA2 but to PGE2 as well [84]. Furthermore, the contractility of the vessels of the ecPOR$^{-/-}$ mice themselves were more sensitive towards these prostanoids.

Remarkably, the decrease in EETs seen in the lipidomic measurements was also accompanied by an increase in several different prostanoids. TXB2, or Thromboxane B2, was consistently increased across all measured samples: aorta, lung and plasma. This arachidonic acid metabolite is a stable product of degradation of thromboxane A2 (TXA2). TXA2 is highly produced in platelets being involved in the process of anaphylaxis in which it induces arterial contraction and platelet aggregation by stimulating TP-α receptors. Surprisingly, PGD2 or prostaglandin D2 was another COX-derived metabolite that was significantly increase in the aorta. Normally, PGD2 is associated with the pathogenesis of asthma [134]. The clinical importance of PGD2 for this study remains unclear.

The MACE sequencing results also showed an increase in genes associated to the metabolism of arachidonic acid derived PUFAS including the several prostanoid forming enzymes: HPGD, PTGIS and PTGDS was observed. This was also accompanied by a downregulation of genes from the annexin A family (1, 3, 5 and 6) which are known inhibitors of PLA2 activity [135], and, thus, suppressers of arachidonic acid release from the plasma membrane.

These changes at the gene level comes with no surprise as, as endothelial cells are highly metabolically active, which accounts for their great adaptability [136]. An increase in PGE2 production has already been shown to impact on a process that inhibits the ALOX5 pathway in favor of eicosanoids [137]. It seems plausible that shuttling AA into more PGE2 production could possibly lead to the observed downregulation of ALOX12 expression.

Altogether, these findings illustrate the interdependency of both CYPs:COX system and EET:Prostanoids which not only share the same substrate (arachidonic acid) but also cross-talk at the receptor level. It also highlights that not only different arachidonic acid-derived oxylipins are important for endothelial function but their balance dictate the physiological response of vessel tonus.

The crosstalk between the enzymes that catabolize arachidonic acid has not yet been widely explored in endothelial cells, in *in vivo* models due to the lack of endothelial knockout mice specific for each enzyme of AA metabolism. In a newly developed ecCOX1$^{-/-}$ (cyclooxygenase endothelial-specific knockout mouse), the production of EET throughout the aorta was not significantly altered, but 15-HETE was reduced along with lower PGE2 and thromboxane [138]. On the other hand, lipoxygenase inhibition increases CYP-dependent EET level [139]. COX inhibition has been shown to displace arachidonic acid into the lipoxygenase pool, which is the basis for COX inhibitor-induced respiratory disease exacerbation [140]. That such crosstalk occurs for the CYP system has also been documented: A knockout of Cyp22c44 increased production of PGE2 which increases metastasis in a murine breast cancer model [141]. Research on 5/6-nephrectomy mice (5/6-Nx), a model for chronic renal failure, attempted to check the therapy potential of increased EETs through sEH inhibition in a way to ameliorate progression of the disease. Inhibition of sEH with cis-4-[4-(3-adamantan-1-yl-ureido)-cyclohexyloxy]-benzoic acid (cAUCB) did increase EET levels, but this was also linked to an increase in lipoxygenase-products, which at the end aggravated the progression of the renal disease [142]. Furthermore, a previous study by Inceoglu and collaborators [143] showed a converse effect where increased EET pools through soluble epoxide hydrolase inhibition led to transcriptional down-regulation of COX-2 induction, the isoform responsible for PGE2 and PGF2α, with no further changes to COX-1.

Prostanoids are often highlighted regarding their inflammatory and platelet aggregating functions [144,145]. However, the mRNA levels pro-inflammatory genes, the THP-1 adhesion assay and the RNA sequencing of both aorta and HUVEC control and knockout of POR did not point to any pro-inflammatory effect in the knockout. In parallel, the involvement of prostanoids in control of vessel

tone has attracted much attention of the scientific field. In order to access vascular reactivity of these molecules, organ bath experiments with ecPOR$^{-/-}$ aortas showed that these were more primed for thromboxane dependent constriction when using the thromboxane mimetic U46619 and, on conversely, showed decrease dilating response to 12-HETE. This is a LOX or CYP450 dependent lipid [106] and was also shown to be decreased in both plasma and aorta of the ecPOR$^{-/-}$ mice and is conceptualized to act as a competitive inhibitor to thromboxane receptor in mesenteric arteries [146]. Interestingly, a more recent study showed that in an angiotensin II pro-inflammatory environment, macrophages increase the production of 12-HETE that enhances vascular contractility. They hypothesized that the macrophages-derived 12-HETE lead to production of vascular TP-receptor agonists that mediate the angiotensin II increase in blood pressure [147].

In the present study it was observed that the hypertensive response to AngII was increased in ecPOR$^{-/-}$ mice when compared to their CTR littermates. A lack of basal hypertension, however, was somewhat surprising. The finding may suggest that, in fact, the vasodilatory function of EETs is restricted to larger mammals, such as pigs and humans [12]. Several lines of evidence here shows that this is a consequence of AA diversion to the formation of vasoconstrictor products of COX such as thromboxane A2 and prostaglandin F2α.

Angiotensin II increases intracellular calcium and MAP kinase activation, which stimulate phospholipase A2 activity [148] and thus result in the intracellular release of arachidonic acids from membrane phospholipid stores. Considering that endothelial cells express AT1 receptors, it is conceivable that, as a consequence of insufficient CYP activity, arachidonic acid is preferentially metabolized by COX, which competes with CYP for free arachidonic acid. Such a shunt is a clinically important phenomenon, however, little studied in the vascular system.

Inhibition of COX blocks the hypertensive effect of endothelial knockout of POR

To further understand the potential risks/benefits of controlling prostanoid production we investigated the effect of the non-selective COX inhibitor naproxen, a nonsteroidal anti-inflammatory drug (NSAID), in an angiotensin II

pro-inflammatory model of hypertension. In doses adequate to reduce inflammation and pain, NSAIDs are reported to increase blood pressure in both normotensive and hypertensive individuals [149]. These effects, however were mostly associated to the decrease in vasodilator prostaglandins such as prostacyclin and PGE2 and 4, which compromise renal function and glomerular filtration rate [150,151]. Naproxen, on the other hand, was observed to have the least risk when compared to other common NSAIDs for cardiovascular-related events, and unlike the other inhibitors does not lead to increase systolic blood pressure [152]. This is linked to its COX-1 inhibiting effect with lower thromboxane production, and lesser to a COX-2 prostacyclin inhibition.

The ecPOR$^{-/-}$ mice subjected to angiotensin II treatment showed higher systolic blood pressure when compared to the wild type littermates. With the endothelium being a major regulator of vascular tone, reduced EET generation in the vessels undoubtedly supports the increased hypertension. Importantly, when these animals were treated with naproxen after angiotensin II their blood pressure decreased to similar levels as in the CTR mice. It is well known that the effects of NSAIDS in blood pressure is controversial. A study comparing the differential blood pressure effects of ibuprofen, naproxen, and celecoxib in 444 patients with arthritis reported the relatively small yet lowering BP effects of both celecoxib and naproxen in contrast to the increasing BP effects of ibuprofen [153]. The presents results show that the vascular effect of NSAIDs somehow depend on the metabolic state of the endothelium, regarding the amount and which oxylipins are being actively produced.

Altogether, the current study shows that POR regulates vessel tone and systemic blood pressure through two different mechanisms: i. POR maintains eNOS function, ii. POR balances the metabolic fate of arachidonic acid. In the absence of POR EETs are reduced and the vessel-contracting prostanoids are increased leading to hypertension (**Figure 36**). These conclusions were obtained by using a novel mouse model, the first subtractive approach to study the effect of a total loss of endothelial CYP450 activity and several techniques such as *in vivo* and *ex vivo* vascular studies, lipidomics, telemetry and RNAseq. Thus, the findings presented here add a valuable importance of CYP450 to endothelial-dependent vascular function and affirm the vascular crosstalk of COX and CYP450 enzymes

for proper vascular homeostasis. This work may help understanding how the polymorphisms of the POR/CYP450 system are linked to cardiovascular diseases.

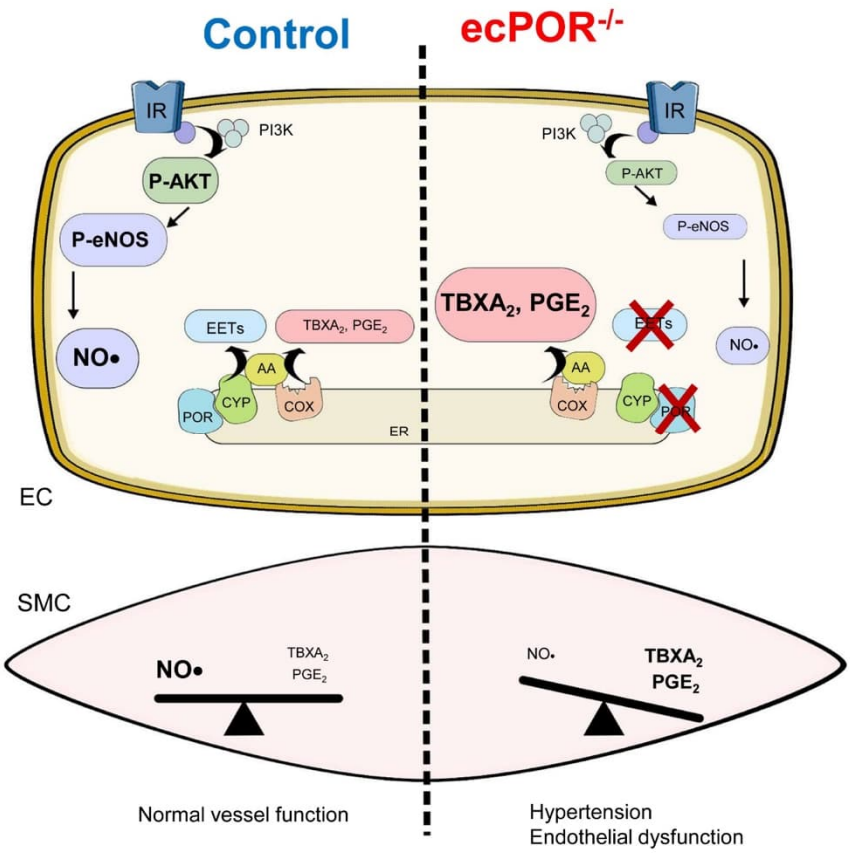

Figure 36 Graphical summary of endothelial knockout of POR
Loss of endothelial POR induces vascular dysfunction in mice through dysfunction of eNOS activity and functional shift of arachidonic acid metabolism to COX-derived prostanoids.

Acknowledgements

I would like to acknowledge and thank the people that directly contributed to this work, as well as those that supported me throughout this gratifying journey.

First, I would like to thank Dr. Flávia Rezende for the support through the PhD and her expertise into the project. Her great ideas helped me push the work forward while the wild ones never allowed it to get boring.

Next I want to thank Prof. Dr. Ralf. Brandes. On one hand for allowing me to work in the institute and the other for the supportive guidance of the project. The philosophy he shares of a single knight, princess and dragon to every story, also impacted this work and shaped up my views of science, along with finding value in scientific explanations that are not overly complicated.

I would also like to thank the members of the Institute for Cardiovascular Research for their support in this project. In specialty Dr. Corina Ratiu who performed the surgeries necessary for the recording of blood pressure in the telemetry experiments and Melina Lopez who performed the echocardiogram of the carotid here presented.

I would like to thank Katalin Palfi, Manuela Spaeth and Tanja Lüneburg for the technical support of this project.

I would also like to thank the support of Carlo Angioni from the Institute for Clinical Pharmacology, Goethe-University, Frankfurt for the mass spectrometry measurements of the Prostaglandin and EET. To Stefan Günther of the Institute for Heart and Lung Research, Max Planck Institute, Bad Nauheim for performing the RNA seq measurements. As well as Dieter Lütjohann of the Institute for Clinical Chemistry and Pharmacology, University of Bonn, Bonn for performing the cholesterol measurements.

Lastly, I would like to thank my parents, family and friends for their support.

Curriculum Vitae

Personal details

Name: Pedro Felipe Malacarne
Address: Oranienstraße 1, 65510 Idstein
Date of birth: 09/06/1990
Place of birth: Vila Velha-ES, Brazil

Education

08/2017 – 01/2023 PhD student at the Institute for Cardiovascular Research, Vascular Research Centre, Goethe University Frankfurt am Main

04/2015 – 03/2017 Master's Degree in Biochemistry and Pharmacology at the Federal University of Espírito Santo (UFES). Associated projects include the characterization of two toxins found in the venom of the Scorpionfish Scorpaena plumieri, Sp-CL, a c-type lectin, and Sp-CTx, a labile multifunctional cytolysin. Research taking course in the Protein Chemistry Laboratory – UFES.

03/2009 – 03/2014 Bachelor in Pharmacy at the Federal University of Espírito Santo (UFES). Throughout my bachelor, I initially aided as an assistance in basic chemistry courses helping the teachers set up the lab and during classes. Later on, I spent 3 years in a part-time scientific initiation in the laboratory of chemistry of proteins (UFES). I have worked in the isolation and characterization of toxins from the venom of the Scorpionfish Scorpaena plumieri.

Professional Experience

04/2014-12/2014 Pharmacist at Raia Drogasil Pharmacy – 44h/week

List of Figures

List of Tables

References

1. Hennigs, J.K.; Matuszcak, C.; Trepel, M.; Körbelin, J. Vascular Endothelial Cells: Heterogeneity and Targeting Approaches. *Cells* **2021**, *10*, doi:10.3390/cells10102712.
2. Vanhoutte, P.M. Endothelium and control of vascular function. State of the Art lecture. *Hypertension (Dallas, Tex. : 1979)* **1989**, *13*, 658–667, doi:10.1161/01.hyp.13.6.658.
3. Virani, S.S.; Alonso, A.; Benjamin, E.J.; Bittencourt, M.S.; Callaway, C.W.; Carson, A.P.; Chamberlain, A.M.; Chang, A.R.; Cheng, S.; Delling, F.N.; et al. Heart Disease and Stroke Statistics-2020 Update: A Report From the American Heart Association. *Circulation* **2020**, *141*, e139-e596, doi:10.1161/CIR.0000000000000757.
4. Alberts, B. *Molecular biology of the cell*, 5th ed.; Garland Science: New York, 2008, ISBN 9780815332183.
5. Eelen, G.; Zeeuw, P. de; Treps, L.; Harjes, U.; Wong, B.W.; Carmeliet, P. Endothelial Cell Metabolism. *Physiol. Rev.* **2018**, *98*, 3–58, doi:10.1152/physrev.00001.2017.
6. Potente, M.; Gerhardt, H.; Carmeliet, P. Basic and therapeutic aspects of angiogenesis. *Cell* **2011**, *146*, 873–887, doi:10.1016/j.cell.2011.08.039.
7. Félétou, M.; Vanhoutte, P.M. EDHF: an update. *Clin Sci (Lond)* **2009**, *117*, 139–155, doi:10.1042/CS20090096.
8. Scotland, R.S.; Madhani, M.; Chauhan, S.; Moncada, S.; Andresen, J.; Nilsson, H.; Hobbs, A.J.; Ahluwalia, A. Investigation of vascular responses in endothelial nitric oxide synthase/cyclooxygenase-1 double-knockout mice: key role for endothelium-derived hyperpolarizing factor in the regulation of blood pressure in vivo. *Circulation* **2005**, *111*, 796–803, doi:10.1161/01.CIR.0000155238.70797.4E.
9. Kang, K.-T. Endothelium-derived Relaxing Factors of Small Resistance Arteries in Hypertension. *Toxicol. Res.* **2014**, *30*, 141–148, doi:10.5487/TR.2014.30.3.141.
10. Brandes, R.P. Endothelial dysfunction and hypertension. *Hypertension (Dallas, Tex. : 1979)* **2014**, *64*, 924–928, doi:10.1161/HYPERTENSIONAHA.114.03575.
11. Ignarro, L.J. Biosynthesis and metabolism of endothelium-derived nitric oxide. *Annu. Rev. Pharmacol. Toxicol.* **1990**, *30*, 535–560, doi:10.1146/annurev.pa.30.040190.002535.
12. Fleming, I. The factor in EDHF: Cytochrome P450 derived lipid mediators and vascular signaling. *Vascular pharmacology* **2016**, *86*, 31–40, doi:10.1016/j.vph.2016.03.001.
13. Richard E. Klabunde. *Cardiovascular Physiology Concepts*, 3rd edition; Wolters Kluwer Health, 2020, ISBN 1975150074.
14. Degtyarenko, K.N.; Archakov, A.I. Molecular evolution of P450 superfamily and P450-containing monooxygenase systems. *FEBS Letters* **1993**, *332*, 1–8, doi:10.1016/0014-5793(93)80470-F.
15. Sono, M.; Roach, M.P.; Coulter, E.D.; Dawson, J.H. Heme-Containing Oxygenases. *Chem. Rev.* **1996**, *96*, 2841–2888, doi:10.1021/cr9500500.
16. Dorner, M.E.; McMunn, R.D.; Bartholow, T.G.; Calhoon, B.E.; Conlon, M.R.; Dulli, J.M.; Fehling, S.C.; Fisher, C.R.; Hodgson, S.W.; Keenan, S.W.; et al. Comparison of intrinsic dynamics of cytochrome p450 proteins using normal mode analysis. *Protein Sci.* **2015**, *24*, 1495–1507, doi:10.1002/pro.2737.

17. Ortiz de Montellano, P.R.; Voss, J.J. de. Substrate Oxidation by Cytochrome P450 Enzymes. *Cytochrome P450*; Springer, Boston, MA, 2005; pp 183–245.
18. Nelson, D.R.; Kamataki, T.; Waxman, D.J.; Guengerich, F.P.; Estabrook, R.W.; Feyereisen, R.; Gonzalez, F.J.; Coon, M.J.; Gunsalus, I.C.; Gotoh, O. The P450 superfamily: update on new sequences, gene mapping, accession numbers, early trivial names of enzymes, and nomenclature. *DNA Cell Biol.* **1993**, *12*, 1–51, doi:10.1089/dna.1993.12.1.
19. Zanger, U.M.; Schwab, M. Cytochrome P450 enzymes in drug metabolism: regulation of gene expression, enzyme activities, and impact of genetic variation. *Pharmacology & Therapeutics* **2013**, *138*, 103–141, doi:10.1016/j.pharmthera.2012.12.007.
20. TOM LYNCH; AMY PRICE. The Effect of Cytochrome P450 Metabolism on Drug Response, Interactions, and Adverse Effects. *afp* **2007**, *76*, 391–396.
21. NISHIMURA, M.; YAGUTI, H.; YOSHITSUGU, H.; NAITO, S.; SATOH, T. Tissue distribution of mRNA expression of human cytochrome P450 isoforms assessed by high-sensitivity real-time reverse transcription PCR. *YAKUGAKU ZASSHI* **2003**, *123*, 369–375, doi:10.1248/yakushi.123.369.
22. Fleming, I. Vascular cytochrome p450 enzymes: physiology and pathophysiology. *Trends in Cardiovascular Medicine* **2008**, *18*, 20–25, doi:10.1016/j.tcm.2007.11.002.
23. Bidstrup, T.B.; Bjørnsdottir, I.; Sidelmann, U.G.; Thomsen, M.S.; Hansen, K.T. CYP2C8 and CYP3A4 are the principal enzymes involved in the human in vitro biotransformation of the insulin secretagogue repaglinide. *Br. J. Clin. Pharmacol.* **2003**, *56*, 305–314, doi:10.1046/j.0306-5251.2003.01862.x.
24. van der Weide, J.; Hinrichs, J.W.J. The influence of cytochrome P450 pharmacogenetics on disposition of common antidepressant and antipsychotic medications. *Clin. Biochem. Rev.* **2006**, *27*, 17–25.
25. Khojasteh, S.C.; Prabhu, S.; Kenny, J.R.; Halladay, J.S.; Lu, A.Y.H. Chemical inhibitors of cytochrome P450 isoforms in human liver microsomes: a re-evaluation of P450 isoform selectivity. *Eur. J. Drug Metab. Pharmacokinet.* **2011**, *36*, 1–16, doi:10.1007/s13318-011-0024-2.
26. Khan, M.; Mohan, I.K.; Kutala, V.K.; Kumbala, D.; Kuppusamy, P. Cardioprotection by sulfaphenazole, a cytochrome p450 inhibitor: mitigation of ischemia-reperfusion injury by scavenging of reactive oxygen species. *J Pharmacol Exp Ther* **2007**, *323*, 813–821, doi:10.1124/jpet.107.129486.
27. Bellien, J.; Iacob, M.; Gutierrez, L.; Isabelle, M.; Lahary, A.; Thuillez, C.; Joannides, R. Crucial role of NO and endothelium-derived hyperpolarizing factor in human sustained conduit artery flow-mediated dilatation. *Hypertension (Dallas, Tex. : 1979)* **2006**, *48*, 1088–1094, doi:10.1161/01.HYP.0000246672.72188.bd.
28. Flück, C.E.; Pandey, A.V. Chapter 3H - P450 Oxidoreductase Deficiency (PORD). In *Genetic steroid disorders*; New, M.I., Ed.; Elsevier: Amsterdam, 2014; pp 125–143, ISBN 978-0-12-416006-4.
29. Gan, L.; Moltke, L.L. von; Trepanier, L.A.; Harmatz, J.S.; Greenblatt, D.J.; Court, M.H. Role of NADPH-cytochrome P450 reductase and cytochrome-b5/NADH-b5 reductase in variability of CYP3A activity in human liver microsomes. *Drug Metab. Dispos.* **2009**, *37*, 90–96, doi:10.1124/dmd.108.023424.

30. Reed, J.R.; Cawley, G.F.; Backes, W.L. Inhibition of cytochrome P450 1A2-mediated metabolism and production of reactive oxygen species by heme oxygenase-1 in rat liver microsomes. *DML* **2011**, *5*, 6–16, doi:10.2174/187231211794455253.
31. Peterson, J.A.; Ebel, R.E.; O'Keeffe, D.H.; Matsubara, T.; Estabrook, R.W. Temperature dependence of cytochrome P-450 reduction. A model for NADPH-cytochrome P-450 reductase:cytochrome P-450 interaction. *The Journal of biological chemistry* **1976**, *251*, 4010–4016.
32. Ellis, J.; Gutierrez, A.; Barsukov, I.L.; Huang, W.-C.; Grossmann, J.G.; Roberts, G.C.K. Domain motion in cytochrome P450 reductase: conformational equilibria revealed by NMR and small-angle x-ray scattering. *Journal of Biological Chemistry* **2009**, *284*, 36628–36637, doi:10.1074/jbc.M109.054304.
33. Barsukov, I.; Modi, S.; Lian, L.Y.; Sze, K.H.; Paine, M.J.; Wolf, C.R.; Roberts, G.C. 1H, 15N and 13C NMR resonance assignment, secondary structure and global fold of the FMN-binding domain of human cytochrome P450 reductase. *J. Biomol. NMR* **1997**, *10*, 63–75, doi:10.1023/a:1018313830207.
34. Hamdane, D.; Xia, C.; Im, S.-C.; Zhang, H.; Kim, J.-J.P.; Waskell, L. Structure and function of an NADPH-cytochrome P450 oxidoreductase in an open conformation capable of reducing cytochrome P450. *Journal of Biological Chemistry* **2009**, *284*, 11374–11384, doi:10.1074/jbc.M807868200.
35. Mukherjee, G.; Nandekar, P.P.; Wade, R.C. An electron transfer competent structural ensemble of membrane-bound cytochrome P450 1A1 and cytochrome P450 oxidoreductase. *Commun. Biol.* **2021**, *4*, 55, doi:10.1038/s42003-020-01568-y.
36. Kalluri, A.S.; Vellarikkal, S.K.; Edelman, E.R.; Nguyen, L.; Subramanian, A.; Ellinor, P.T.; Regev, A.; Kathiresan, S.; Gupta, R.M. Single-Cell Analysis of the Normal Mouse Aorta Reveals Functionally Distinct Endothelial Cell Populations. *Circulation* **2019**, *140*, 147–163, doi:10.1161/CIRCULATIONAHA.118.038362.
37. O'Leary, K.A.; Kasper, C.B. Molecular basis for cell-specific regulation of the NADPH-cytochrome P450 oxidoreductase gene. *Archives of Biochemistry and Biophysics* **2000**, *379*, 97–108, doi:10.1006/abbi.2000.1862.
38. Flück, C.E.; Tajima, T.; Pandey, A.V.; Arlt, W.; Okuhara, K.; Verge, C.F.; Jabs, E.W.; Mendonça, B.B.; Fujieda, K.; Miller, W.L. Mutant P450 oxidoreductase causes disordered steroidogenesis with and without Antley-Bixler syndrome. *Nat Genet* **2004**, *36*, 228–230, doi:10.1038/ng1300.
39. Huang, N.; Agrawal, V.; Giacomini, K.M.; Miller, W.L. Genetics of P450 oxidoreductase: sequence variation in 842 individuals of four ethnicities and activities of 15 missense mutations. *PNAS* **2008**, *105*, 1733–1738, doi:10.1073/pnas.0711621105.
40. Arlt, W.; Walker, E.A.; Draper, N.; Ivison, H.E.; Ride, J.P.; Hammer, F.; Chalder, S.M.; Borucka-Mankiewicz, M.; Hauffa, B.P.; Malunowicz, E.M.; et al. Congenital adrenal hyperplasia caused by mutant P450 oxidoreductase and human androgen synthesis: analytical study. *The Lancet* **2004**, *363*, 2128–2135, doi:10.1016/S0140-6736(04)16503-3.
41. PhenoScanner. PhenoScanner. Available online: (http://www.phenoscanner.medschl.cam.ac.uk/) (accessed on 1 January 2018).

42. Otto, D.M.E.; Henderson, C.J.; Carrie, D.; Davey, M.; Gundersen, T.E.; Blomhoff, R.; Adams, R.H.; Tickle, C.; Wolf, C.R. Identification of novel roles of the cytochrome p450 system in early embryogenesis: effects on vasculogenesis and retinoic Acid homeostasis. *Mol. Cell. Biol.* **2003**, *23*, 6103–6116, doi:10.1128/MCB.23.17.6103-6116.2003.
43. Wu, L.; Gu, J.; Weng, Y.; Kluetzman, K.; Swiatek, P.; Behr, M.; Zhang, Q.-Y.; Zhuo, X.; Xie, Q.; Ding, X. Conditional knockout of the mouse NADPH-cytochrome p450 reductase gene. *Genesis* **2003**, *36*, 177–181, doi:10.1002/gene.10214.
44. Shen, A.L.; O'Leary, K.A.; Kasper, C.B. Association of multiple developmental defects and embryonic lethality with loss of microsomal NADPH-cytochrome P450 oxidoreductase. *Journal of Biological Chemistry* **2002**, *277*, 6536–6541, doi:10.1074/jbc.M111408200.
45. Rosselló, C.A.; Torres, M.; Busquets, X.; Escribá, P.V. Polyunsaturated Fatty Acids. *Encyclopedia of Cancer*; Springer, Berlin, Heidelberg, 2016; pp 3665–3671.
46. Pompéia, C.; Lopes, L.R.; Miyasaka, C.K.; Procópio, J.; Sannomiya, P.; Curi, R. Effect of fatty acids on leukocyte function. *Braz J Med Biol Res* **2000**, *33*, 1255–1268, doi:10.1590/S0100-879X2000001100001.
47. Tallima, H.; El Ridi, R. Arachidonic acid: Physiological roles and potential health benefits - A review. *J. Adv. Res.* **2018**, *11*, 33–41, doi:10.1016/j.jare.2017.11.004.
48. Hanna, V.S.; Hafez, E.A.A. Synopsis of arachidonic acid metabolism: A review. *J. Adv. Res.* **2018**, *11*, 23–32, doi:10.1016/j.jare.2018.03.005.
49. Kuehl, F.A.; Egan, R.W. Prostaglandins, arachidonic acid, and inflammation. *Science* **1980**, *210*, 978–984, doi:10.1126/science.6254151.
50. Wong, A.; Sagar, D.R.; Ortori, C.A.; Kendall, D.A.; Chapman, V.; Barrett, D.A. Simultaneous tissue profiling of eicosanoid and endocannabinoid lipid families in a rat model of osteoarthritis. *J. Lipid Res.* **2014**, *55*, 1902–1913, doi:10.1194/jlr.M048694.
51. Institute for Systems Biology. Cytoscape. Available online: https://cytoscape.org/ (accessed on 1 January 2020).
52. Maayah, Z.H.; El-Kadi, A.O.S. The role of mid-chain hydroxyeicosatetraenoic acids in the pathogenesis of hypertension and cardiac hypertrophy. *Arch Toxicol* **2016**, *90*, 119–136, doi:10.1007/s00204-015-1620-8.
53. Campbell, W.B.; Fleming, I. Epoxyeicosatrienoic acids and endothelium-dependent responses. *Pflugers Arch.* **2010**, *459*, 881–895, doi:10.1007/s00424-010-0804-6.
54. Gross, G.J.; Falck, J.R.; Gross, E.R.; Isbell, M.; Moore, J.; Nithipatikom, K. Cytochrome P450 and arachidonic acid metabolites: role in myocardial ischemia/reperfusion injury revisited. *Cardiovasc Res* **2005**, *68*, 18–25, doi:10.1016/j.cardiores.2005.06.007.
55. Spector, A.A.; Kim, H.-Y. Cytochrome P450 epoxygenase pathway of polyunsaturated fatty acid metabolism. *Biochim. Biophys. Acta* **2015**, *1851*, 356–365, doi:10.1016/j.bbalip.2014.07.020.
56. Cizkova, K.; Konieczna, A.; Erdosova, B.; Lichnovska, R.; Ehrmann, J. Peroxisome proliferator-activated receptors in regulation of cytochromes P450: new way to overcome multidrug resistance? *J. Biomed. Biotechnol.* **2012**, *2012*, 656428, doi:10.1155/2012/656428.

57. Spector, A.A.; Norris, A.W. Action of epoxyeicosatrienoic acids on cellular function. *Am. J. Physiol. Cell Physiol.* **2007**, *292*, C996-1012, doi:10.1152/ajpcell.00402.2006.
58. Yang, L.; Mäki-Petäjä, K.; Cheriyan, J.; McEniery, C.; Wilkinson, I.B. The role of epoxyeicosatrienoic acids in the cardiovascular system. *Br. J. Clin. Pharmacol.* **2015**, *80*, 28–44, doi:10.1111/bcp.12603.
59. Gauthier, K.M.; Edwards, E.M.; Falck, J.R.; Reddy, D.S.; Campbell, W.B. 14,15-epoxyeicosatrienoic acid represents a transferable endothelium-dependent relaxing factor in bovine coronary arteries. *Hypertension (Dallas, Tex. : 1979)* **2005**, *45*, 666–671, doi:10.1161/01.HYP.0000153462.06604.5d.
60. Yang, W.; Tuniki, V.R.; Anjaiah, S.; Falck, J.R.; Hillard, C.J.; Campbell, W.B. Characterization of epoxyeicosatrienoic acid binding site in U937 membranes using a novel radiolabeled agonist, 20-125i-14,15-epoxyeicosa-8(Z)-enoic acid. *J Pharmacol Exp Ther* **2008**, *324*, 1019–1027, doi:10.1124/jpet.107.129577.
61. Pfister, S.L.; Gauthier, K.M.; Campbell, W.B. Vascular Pharmacology of Epoxyeicosatrienoic Acids. *Cardiovascular Pharmacology - Endothelial Control*; Elsevier, 2010; pp 27–59, ISBN 9780123850614.
62. Edwards, G.; Dora, K.A.; Gardener, M.J.; Garland, C.J.; Weston, A.H. K+ is an endothelium-derived hyperpolarizing factor in rat arteries. *Nature* **1998**, *396*, 269–272, doi:10.1038/24388.
63. Campbell, W.B.; Gebremedhin, D.; Pratt, P.F.; Harder, D.R. Identification of epoxyeicosatrienoic acids as endothelium-derived hyperpolarizing factors. *Circulation Research* **1996**, *78*, 415–423, doi:10.1161/01.res.78.3.415.
64. Hercule, H.C.; Schunck, W.-H.; Gross, V.; Seringer, J.; Leung, F.P.; Weldon, S.M.; da Costa Goncalves, A.C.; Huang, Y.; Luft, F.C.; Gollasch, M. Interaction between P450 eicosanoids and nitric oxide in the control of arterial tone in mice. *Arterioscler. Thromb. Vasc. Biol.* **2009**, *29*, 54–60, doi:10.1161/ATVBAHA.108.171298.
65. Michaelis, U.R.; Fleming, I. From endothelium-derived hyperpolarizing factor (EDHF) to angiogenesis: Epoxyeicosatrienoic acids (EETs) and cell signaling. *Pharmacology & Therapeutics* **2006**, *111*, 584–595, doi:10.1016/j.pharmthera.2005.11.003.
66. Archer, S.L.; Gragasin, F.S.; Wu, X.; Wang, S.; McMurtry, S.; Kim, D.H.; Platonov, M.; Koshal, A.; Hashimoto, K.; Campbell, W.B.; et al. Endothelium-derived hyperpolarizing factor in human internal mammary artery is 11,12-epoxyeicosatrienoic acid and causes relaxation by activating smooth muscle BK(Ca) channels. *Circulation* **2003**, *107*, 769–776, doi:10.1161/01.cir.0000047278.28407.c2.
67. Fisslthaler, B.; Popp, R.; Kiss, L.; Potente, M.; Harder, D.R.; Fleming, I.; Busse, R. Cytochrome P450 2C is an EDHF synthase in coronary arteries. *Nature* **1999**, *401*, 493–497, doi:10.1038/46816.
68. an Huang; Sun, D.; Jacobson, A.; Carroll, M.A.; Falck, J.R.; Kaley, G. Epoxyeicosatrienoic acids are released to mediate shear stress-dependent hyperpolarization of arteriolar smooth muscle. *Circulation Research* **2005**, *96*, 376–383, doi:10.1161/01.RES.0000155332.17783.26.
69. Fleming, I. Cytochrome P450 epoxygenases as EDHF synthase(s). *Pharmacol. Res.* **2004**, *49*, 525–533, doi:10.1016/j.phrs.2003.11.016.

70. Imig, J.D. Epoxides and soluble epoxide hydrolase in cardiovascular physiology. *Physiol. Rev.* **2012**, *92*, 101–130, doi:10.1152/physrev.00021.2011.
71. Morisseau, C.; Hammock, B.D. Impact of soluble epoxide hydrolase and epoxyeicosanoids on human health. *Annu. Rev. Pharmacol. Toxicol.* **2013**, *53*, 37–58, doi:10.1146/annurev-pharmtox-011112-140244.
72. Ai, D.; Fu, Y.; Guo, D.; Tanaka, H.; Wang, N.; Tang, C.; Hammock, B.D.; Shyy, J.Y.-J.; Zhu, Y. Angiotensin II up-regulates soluble epoxide hydrolase in vascular endothelium in vitro and in vivo. *Proc. Natl. Acad. Sci. U. S. A.* **2007**, *104*, 9018–9023, doi:10.1073/pnas.0703229104.
73. Chiamvimonvat, N.; Ho, C.-M.; Tsai, H.-J.; Hammock, B.D. The soluble epoxide hydrolase as a pharmaceutical target for hypertension. *J. Cardiovasc. Pharmacol.* **2007**, *50*, 225–237, doi:10.1097/FJC.0b013e3181506445.
74. Imig, J.D. Epoxide hydrolase and epoxygenase metabolites as therapeutic targets for renal diseases. *Am. J. Physiol. Renal Physiol.* **2005**, *289*, F496-503, doi:10.1152/ajprenal.00350.2004.
75. Choi, S.-H.; Langenbach, R.; Bosetti, F. Cyclooxygenase-1 and -2 enzymes differentially regulate the brain upstream NF-kappa B pathway and downstream enzymes involved in prostaglandin biosynthesis. *J. Neurochem.* **2006**, *98*, 801–811, doi:10.1111/j.1471-4159.2006.03926.x.
76. Smyth, E.M.; Grosser, T.; Wang, M.; Yu, Y.; FitzGerald, G.A. Prostanoids in health and disease. *J. Lipid Res.* **2009**, *50 Suppl*, S423-8, doi:10.1194/jlr.R800094-JLR200.
77. FitzGerald, G.A.; Loll, P. COX in a crystal ball: current status and future promise of prostaglandin research. *J. Clin. Invest.* **2001**, *107*, 1335–1337, doi:10.1172/JCI13037.
78. Antman, E.M.; DeMets, D.; Loscalzo, J. Cyclooxygenase inhibition and cardiovascular risk. *Circulation* **2005**, *112*, 759–770, doi:10.1161/CIRCULATIONAHA.105.568451.
79. Al-Saeed, A. Gastrointestinal and Cardiovascular Risk of Nonsteroidal Anti-inflammatory Drugs. *Oman Med. J.* **2011**, *26*, 385–391, doi:10.5001/omj.2011.101.
80. Tsuboi, K.; Sugimoto, Y.; Ichikawa, A. Prostanoid receptor subtypes. *Prostaglandins Other Lipid Mediat.* **2002**, *68-69*, 535–556, doi:10.1016/s0090-6980(02)00054-0.
81. Shen, R.F.; Tai, H.H. Thromboxanes: synthase and receptors. *Journal of biomedical science* **1998**, *5*, 153–172, doi:10.1007/BF02253465.
82. Cao, X.; Peterson, J.R.; Wang, G.; Anrather, J.; Young, C.N.; Guruju, M.R.; Burmeister, M.A.; Iadecola, C.; Davisson, R.L. Angiotensin II-dependent hypertension requires cyclooxygenase 1-derived prostaglandin E2 and EP1 receptor signaling in the subfornical organ of the brain. *Hypertension (Dallas, Tex. : 1979)* **2012**, *59*, 869–876, doi:10.1161/HYPERTENSIONAHA.111.182071.
83. Yang, T.; Du, Y. Distinct roles of central and peripheral prostaglandin E2 and EP subtypes in blood pressure regulation. *Am. J. Hypertens.* **2012**, *25*, 1042–1049, doi:10.1038/ajh.2012.67.
84. Malacarne, P.F.; Bezzenberger, J.; Lopez, M.; Warwick, T.; Müller, N.; Brandes, R.P.; Rezende, F. Epoxyeicosatrienoic Acid and Prostanoid

Crosstalk at the Receptor and Intracellular Signaling Levels to Maintain Vascular Tone. *Int. J. Mol. Sci.* **2022**, *23*, doi:10.3390/ijms23115939.
85. Zhang, J.; Martàsek, P.; Paschke, R.; Shea, T.; Siler Masters, B.S.; Kim, J.J. Crystal structure of the FAD/NADPH-binding domain of rat neuronal nitric-oxide synthase. Comparisons with NADPH-cytochrome P450 oxidoreductase. *Journal of Biological Chemistry* **2001**, *276*, 37506–37513, doi:10.1074/jbc.M105503200.
86. Siragusa, M.; Fleming, I. The eNOS signalosome and its link to endothelial dysfunction. *Pflugers Arch.* **2016**, *468*, 1125–1137, doi:10.1007/s00424-016-1839-0.
87. Förstermann, U.; Sessa, W.C. Nitric oxide synthases: regulation and function. *Eur. Heart J.* **2012**, *33*, 829-37, 837a-837d, doi:10.1093/eurheartj/ehr304.
88. Dimmeler, S.; Fleming, I.; Fisslthaler, B.; Hermann, C.; Busse, R.; Zeiher, A.M. Activation of nitric oxide synthase in endothelial cells by Akt-dependent phosphorylation. *Nature* **1999**, *399*, 601–605, doi:10.1038/21224.
89. Butt, E.; Bernhardt, M.; Smolenski, A.; Kotsonis, P.; Fröhlich, L.G.; Sickmann, A.; Meyer, H.E.; Lohmann, S.M.; Schmidt, H.H. Endothelial nitric-oxide synthase (type III) is activated and becomes calcium independent upon phosphorylation by cyclic nucleotide-dependent protein kinases. *Journal of Biological Chemistry* **2000**, *275*, 5179–5187, doi:10.1074/jbc.275.7.5179.
90. Chen, Z.-P.; Mitchelhill, K.I.; Michell, B.J.; Stapleton, D.; Rodriguez-Crespo, I.; Witters, L.A.; Power, D.A.; Ortiz de Montellano, P.R.; Kemp, B.E. AMP-activated protein kinase phosphorylation of endothelial NO synthase. *FEBS Letters* **1999**, *443*, 285–289, doi:10.1016/s0014-5793(98)01705-0.
91. Michell, B.J.; Chen, Z.; Tiganis, T.; Stapleton, D.; Katsis, F.; Power, D.A.; Sim, A.T.; Kemp, B.E. Coordinated control of endothelial nitric-oxide synthase phosphorylation by protein kinase C and the cAMP-dependent protein kinase. *Journal of Biological Chemistry* **2001**, *276*, 17625–17628, doi:10.1074/jbc.C100122200.
92. Ozkor, M.A.; Quyyumi, A.A. Endothelium-derived hyperpolarizing factor and vascular function. *Cardiology Research and Practice* **2011**, *2011*, 156146, doi:10.4061/2011/156146.
93. Hink, U.; Münzel, T. COX-2, another important player in the nitric oxide-endothelin cross-talk: good news for COX-2 inhibitors? *Circulation Research* **2006**, *98*, 1344–1346, doi:10.1161/01.RES.0000228471.38761.93.
94. Wang, Y.; Nakayama, M.; Pitulescu, M.E.; Schmidt, T.S.; Bochenek, M.L.; Sakakibara, A.; Adams, S.; Davy, A.; Deutsch, U.; Lüthi, U.; et al. Ephrin-B2 controls VEGF-induced angiogenesis and lymphangiogenesis. *Nature* **2010**, *465*, 483–486, doi:10.1038/nature09002.
95. Jespersen, B.; Tykocki, N.R.; Watts, S.W.; Cobbett, P.J. Measurement of smooth muscle function in the isolated tissue bath-applications to pharmacology research. *J. Vis. Exp.* **2015**, 52324, doi:10.3791/52324.
96. Rezende, F.; Prior, K.-K.; Löwe, O.; Wittig, I.; Strecker, V.; Moll, F.; Helfinger, V.; Schnütgen, F.; Kurrle, N.; Wempe, F.; et al. Cytochrome P450 enzymes but not NADPH oxidases are the source of the NADPH-dependent lucigenin chemiluminescence in membrane assays. *Free Radic. Biol. Med.* **2017**, *102*, 57–66, doi:10.1016/j.freeradbiomed.2016.11.019.
97. Šošić-Jurjević, B.; Lütjohann, D.; Renko, K.; Filipović, B.; Radulović, N.; Ajdžanović, V.; Trifunović, S.; Nestorović, N.; Živanović, J.; Manojlović

Stojanoski, M.; et al. The isoflavones genistein and daidzein increase hepatic concentration of thyroid hormones and affect cholesterol metabolism in middle-aged male rats. *The Journal of steroid biochemistry and molecular biology* **2019**, *190*, 1–10, doi:10.1016/j.jsbmb.2019.03.009.

98. Raţiu, C. *The Contribution of Monoamine Oxidase (MAO) and Cytochrome P450 Reductase (POR) to Angiotensin II-mediated Hypertension;* Johann Wolfgang Goethe-Universität Frankfurt am Main, 2021.
99. Zawada, A.M.; Rogacev, K.S.; Müller, S.; Rotter, B.; Winter, P.; Fliser, D.; Heine, G.H. Massive analysis of cDNA Ends (MACE) and miRNA expression profiling identifies proatherogenic pathways in chronic kidney disease. *Epigenetics* **2014**, *9*, 161–172, doi:10.4161/epi.26931.
100. Deng, Y.; Edin, M.L.; Theken, K.N.; Schuck, R.N.; Flake, G.P.; Kannon, M.A.; DeGraff, L.M.; Lih, F.B.; Foley, J.; Bradbury, J.A.; et al. Endothelial CYP epoxygenase overexpression and soluble epoxide hydrolase disruption attenuate acute vascular inflammatory responses in mice. *FASEB J.* **2011**, *25*, 703–713, doi:10.1096/fj.10-171488.
101. Schulz, E.; Gori, T.; Münzel, T. Oxidative stress and endothelial dysfunction in hypertension. *Hypertens Res* **2011**, *34*, 665–673, doi:10.1038/hr.2011.39.
102. Gopisankar, M.G. CYP2D6 pharmacogenomics. *Egyptian Journal of Medical Human Genetics* **2017**, *18*, 309–313, doi:10.1016/j.ejmhg.2017.03.001.
103. Roman, R.J. P-450 metabolites of arachidonic acid in the control of cardiovascular function. *Physiol. Rev.* **2002**, *82*, 131–185, doi:10.1152/physrev.00021.2001.
104. McDonnell, A.M.; Dang, C.H. Basic review of the cytochrome p450 system. *J. Adv. Pract. Oncol.* **2013**, *4*, 263–268, doi:10.6004/jadpro.2013.4.4.7.
105. Pascale, J.V.; Lucchesi, P.A.; Garcia, V. Unraveling the Role of 12- and 20- HETE in Cardiac Pathophysiology: G-Protein-Coupled Receptors, Pharmacological Inhibitors, and Transgenic Approaches. *J. Cardiovasc. Pharmacol.* **2021**, *77*, 707–717, doi:10.1097/FJC.0000000000001013.
106. Powell, W.S.; Rokach, J. Biosynthesis, biological effects, and receptors of hydroxyeicosatetraenoic acids (HETEs) and oxoeicosatetraenoic acids (oxo-ETEs) derived from arachidonic acid. *Biochim. Biophys. Acta* **2015**, *1851*, 340–355, doi:10.1016/j.bbalip.2014.10.008.
107. Yang, B.; Graham, L.; Dikalov, S.; Mason, R.P.; Falck, J.R.; Liao, J.K.; Zeldin, D.C. Overexpression of cytochrome P450 CYP2J2 protects against hypoxia-reoxygenation injury in cultured bovine aortic endothelial cells. *Mol. Pharmacol.* **2001**, *60*, 310–320, doi:10.1124/mol.60.2.310.
108. Fleming, I.; Michaelis, U.R.; Bredenkötter, D.; Fisslthaler, B.; Dehghani, F.; Brandes, R.P.; Busse, R. Endothelium-derived hyperpolarizing factor synthase (Cytochrome P450 2C9) is a functionally significant source of reactive oxygen species in coronary arteries. *Circulation Research* **2001**, *88*, 44–51, doi:10.1161/01.res.88.1.44.
109. Xia, C.; Hamdane, D.; Shen, A.L.; Choi, V.; Kasper, C.B.; Pearl, N.M.; Zhang, H.; Im, S.-C.; Waskell, L.; Kim, J.-J.P. Conformational changes of NADPH-cytochrome P450 oxidoreductase are essential for catalysis and cofactor binding. *Journal of Biological Chemistry* **2011**, *286*, 16246–16260, doi:10.1074/jbc.M111.230532.

110. Michaelis, U.R.; Fleming, I. From endothelium-derived hyperpolarizing factor (EDHF) to angiogenesis: Epoxyeicosatrienoic acids (EETs) and cell signaling. *Pharmacology & Therapeutics* **2006**, *111*, 584–595, doi:10.1016/j.pharmthera.2005.11.003.
111. Piknova, B.; Park, J.W.; Cassel, K.S.; Gilliard, C.N.; Schechter, A.N. Measuring Nitrite and Nitrate, Metabolites in the Nitric Oxide Pathway, in Biological Materials using the Chemiluminescence Method. *J. Vis. Exp.* **2016**, doi:10.3791/54879.
112. Clapp, B.R.; Hingorani, A.D.; Kharbanda, R.K.; Mohamed-Ali, V.; Stephens, J.W.; Vallance, P.; MacAllister, R.J. Inflammation-induced endothelial dysfunction involves reduced nitric oxide bioavailability and increased oxidant stress. *Cardiovasc Res* **2004**, *64*, 172–178, doi:10.1016/j.cardiores.2004.06.020.
113. Ogita, H.; Liao, J. Endothelial function and oxidative stress. *Endothelium* **2004**, *11*, 123–132, doi:10.1080/10623320490482664.
114. Zhuo, J.L.; Mendelsohn, F.A.O.; Ohishi, M. Perindopril alters vascular angiotensin-converting enzyme, AT(1) receptor, and nitric oxide synthase expression in patients with coronary heart disease. *Hypertension (Dallas, Tex. : 1979)* **2002**, *39*, 634–638, doi:10.1161/hy0202.103417.
115. Micheletta, F.; Natoli, S.; Misuraca, M.; Sbarigia, E.; Diczfalusy, U.; Iuliano, L. Vitamin E supplementation in patients with carotid atherosclerosis: reversal of altered oxidative stress status in plasma but not in plaque. *Arterioscler. Thromb. Vasc. Biol.* **2004**, *24*, 136–140, doi:10.1161/01.ATV.0000104028.07929.72.
116. Wallace, J.L.; Ignarro, L.J.; Fiorucci, S. Potential cardioprotective actions of no-releasing aspirin. *Nat. Rev. Drug Discov.* **2002**, *1*, 375–382, doi:10.1038/nrd794.
117. Denninger, J.W.; Marletta, M.A. Guanylate cyclase and the ·NO/cGMP signaling pathway. *Biochimica et Biophysica Acta (BBA) - Bioenergetics* **1999**, *1411*, 334–350, doi:10.1016/S0005-2728(99)00024-9.
118. Fulton, D.; Church, J.E.; Ruan, L.; Li, C.; Sood, S.G.; Kemp, B.E.; Jennings, I.G.; Venema, R.C. Src kinase activates endothelial nitric-oxide synthase by phosphorylating Tyr-83. *Journal of Biological Chemistry* **2005**, *280*, 35943–35952, doi:10.1074/jbc.M504606200.
119. Lin, M.I.; Fulton, D.; Babbitt, R.; Fleming, I.; Busse, R.; Pritchard, K.A.; Sessa, W.C. Phosphorylation of threonine 497 in endothelial nitric-oxide synthase coordinates the coupling of L-arginine metabolism to efficient nitric oxide production. *Journal of Biological Chemistry* **2003**, *278*, 44719–44726, doi:10.1074/jbc.M302836200.
120. Fleming, I.; Fisslthaler, B.; Dimmeler, S.; Kemp, B.E.; Busse, R. Phosphorylation of Thr(495) regulates Ca(2+)/calmodulin-dependent endothelial nitric oxide synthase activity. *Circulation Research* **2001**, *88*, E68-75, doi:10.1161/hh1101.092677.
121. Fisslthaler, B.; Loot, A.E.; Mohamed, A.; Busse, R.; Fleming, I. Inhibition of endothelial nitric oxide synthase activity by proline-rich tyrosine kinase 2 in response to fluid shear stress and insulin. *Circulation Research* **2008**, *102*, 1520–1528, doi:10.1161/CIRCRESAHA.108.172072.
122. Iaccarino, G.; Ciccarelli, M.; Sorriento, D.; Cipolletta, E.; Cerullo, V.; Iovino, G.L.; Paudice, A.; Elia, A.; Santulli, G.; Campanile, A.; et al. AKT participates

in endothelial dysfunction in hypertension. *Circulation* **2004**, *109*, 2587–2593, doi:10.1161/01.CIR.0000129768.35536.FA.
123. Zhuang, L.; Lin, J.; Lu, M.L.; Solomon, K.R.; Freeman, M.R. Cholesterol-rich lipid rafts mediate akt-regulated survival in prostate cancer cells. *Cancer Res.* **2002**, *62*, 2227–2231.
124. Tran, J.; Magenau, A.; Rodriguez, M.; Rentero, C.; Royo, T.; Enrich, C.; Thomas, S.R.; Grewal, T.; Gaus, K. Activation of Endothelial Nitric Oxide (eNOS) Occurs through Different Membrane Domains in Endothelial Cells. *PLoS One* **2016**, *11*, e0151556, doi:10.1371/journal.pone.0151556.
125. Buerk, D.G.; Barbee, K.A.; Jaron, D. Nitric oxide signaling in the microcirculation. *Crit. Rev. Biomed. Eng.* **2011**, *39*, 397–433, doi:10.1615/critrevbiomedeng.v39.i5.40.
126. Huang, P.L.; Huang, Z.; Mashimo, H.; Bloch, K.D.; Moskowitz, M.A.; Bevan, J.A.; Fishman, M.C. Hypertension in mice lacking the gene for endothelial nitric oxide synthase. *Nature* **1995**, *377*, 239–242, doi:10.1038/377239a0.
127. Oyama, J.; Node, K. Endothelium-derived hyperpolarizing factor and hypertension. *Hypertens Res* **2013**, *36*, 852–853, doi:10.1038/hr.2013.97.
128. Duflot, T.; Moreau-Grangé, L.; Roche, C.; Iacob, M.; Wils, J.; Rémy-Jouet, I.; Cailleux, A.-F.; Leuillier, M.; Renet, S.; Li, D.; et al. Altered bioavailability of epoxyeicosatrienoic acids is associated with conduit artery endothelial dysfunction in type 2 diabetic patients. *Cardiovasc Diabetol* **2019**, *18*, 35, doi:10.1186/s12933-019-0843-z.
129. Benoit, C.; Renaudon, B.; Salvail, D.; Rousseau, E. EETs relax airway smooth muscle via an EpDHF effect: BK(Ca) channel activation and hyperpolarization. *Am. J. Physiol. Lung Cell. Mol. Physiol.* **2001**, *280*, L965-73, doi:10.1152/ajplung.2001.280.5.L965.
130. Zhang, Y.; Oltman, C.L.; Lu, T.; Lee, H.C.; Dellsperger, K.C.; VanRollins, M. EET homologs potently dilate coronary microvessels and activate BK(Ca) channels. *Am. J. Physiol. Heart Circ. Physiol.* **2001**, *280*, H2430-40, doi:10.1152/ajpheart.2001.280.6.H2430.
131. Li, P.L.; Campbell, W.B. Epoxyeicosatrienoic acids activate K+ channels in coronary smooth muscle through a guanine nucleotide binding protein. *Circulation Research* **1997**, *80*, 877–884, doi:10.1161/01.res.80.6.877.
132. Liu, X.; Qian, Z.-Y.; Xie, F.; Fan, W.; Nelson, J.W.; Xiao, X.; Kaul, S.; Barnes, A.P.; Alkayed, N.J. Functional screening for G protein-coupled receptor targets of 14,15-epoxyeicosatrienoic acid. *Prostaglandins Other Lipid Mediat.* **2017**, *132*, 31–40, doi:10.1016/j.prostaglandins.2016.09.002.
133. Behm, D.J.; Ogbonna, A.; Wu, C.; Burns-Kurtis, C.L.; Douglas, S.A. Epoxyeicosatrienoic acids function as selective, endogenous antagonists of native thromboxane receptors: identification of a novel mechanism of vasodilation. *J Pharmacol Exp Ther* **2009**, *328*, 231–239, doi:10.1124/jpet.108.145102.
134. Suto, W.; Ando, Y.; Hirabayashi, T.; Takenoya, F.; Shioda, S.; Kamei, J.; Sakai, H.; Chiba, Y. Prostaglandin D_2 Induces Ca2+ Sensitization of Contraction without Affecting Cytosolic Ca2+ Level in Bronchial Smooth Muscle. *Int. J. Mol. Sci.* **2018**, *19*, 3036, doi:10.3390/ijms19103036.
135. Raynal, P.; Pollard, H.B. Annexins: the problem of assessing the biological role for a gene family of multifunctional calcium- and phospholipid-binding

proteins. *Biochimica et Biophysica Acta (BBA) - Reviews on Biomembranes* **1994**, *1197*, 63–93, doi:10.1016/0304-4157(94)90019-1.
136. Zecchin, A.; Kalucka, J.; Dubois, C.; Carmeliet, P. How Endothelial Cells Adapt Their Metabolism to Form Vessels in Tumors. *Front. Immunol.* **2017**, *8*, 1750, doi:10.3389/fimmu.2017.01750.
137. Levy, B.D.; Clish, C.B.; Schmidt, B.; Gronert, K.; Serhan, C.N. Lipid mediator class switching during acute inflammation: signals in resolution. *Nat. Immunol.* **2001**, *2*, 612–619, doi:10.1038/89759.
138. Mitchell, J.A.; Shala, F.; Pires, M.E.L.; Loy, R.Y.; Ravendren, A.; Benson, J.; Urquhart, P.; Nicolaou, A.; Herschman, H.R.; Kirkby, N.S. Endothelial cyclooxygenase-1 paradoxically drives local vasoconstriction and atherogenesis despite underpinning prostacyclin generation. *Sci. Adv.* **2021**, *7*, doi:10.1126/sciadv.abf6054.
139. Revermann, M.; Mieth, A.; Popescu, L.; Paulke, A.; Wurglics, M.; Pellowska, M.; Fischer, A.S.; Steri, R.; Maier, T.J.; Schermuly, R.T.; et al. A pirinixic acid derivative (LP105) inhibits murine 5-lipoxygenase activity and attenuates vascular remodelling in a murine model of aortic aneurysm. *Br. J. Pharmacol.* **2011**, *163*, 1721–1732, doi:10.1111/j.1476-5381.2011.01321.x.
140. Woo, S.-D.; Luu, Q.Q.; Park, H.-S. NSAID-Exacerbated Respiratory Disease (NERD): From Pathogenesis to Improved Care. *Front. Pharmacol.* **2020**, *11*, 1147, doi:10.3389/fphar.2020.01147.
141. Kesavan, R.; Frömel, T.; Zukunft, S.; Laban, H.; Geyer, A.; Naeem, Z.; Heidler, J.; Wittig, I.; Elwakeel, E.; Brüne, B.; et al. Cyp2c44 regulates prostaglandin synthesis, lymphangiogenesis, and metastasis in a mouse model of breast cancer. *PNAS* **2020**, *117*, 5923–5930, doi:10.1073/pnas.1921381117.
142. Jung, O.; Jansen, F.; Mieth, A.; Barbosa-Sicard, E.; Pliquett, R.U.; Babelova, A.; Morisseau, C.; Hwang, S.H.; Tsai, C.; Hammock, B.D.; et al. Inhibition of the soluble epoxide hydrolase promotes albuminuria in mice with progressive renal disease. *PLoS One* **2010**, *5*, e11979, doi:10.1371/journal.pone.0011979.
143. Inceoglu, B.; Schmelzer, K.R.; Morisseau, C.; Jinks, S.L.; Hammock, B.D. Soluble epoxide hydrolase inhibition reveals novel biological functions of epoxyeicosatrienoic acids (EETs). *Prostaglandins Other Lipid Mediat.* **2007**, *82*, 42–49, doi:10.1016/j.prostaglandins.2006.05.004.
144. Murata, T.; Ushikubi, F.; Matsuoka, T.; Hirata, M.; Yamasaki, A.; Sugimoto, Y.; Ichikawa, A.; Aze, Y.; Tanaka, T.; Yoshida, N.; et al. Altered pain perception and inflammatory response in mice lacking prostacyclin receptor. *Nature* **1997**, *388*, 678–682, doi:10.1038/41780.
145. Ricciotti, E.; FitzGerald, G.A. Prostaglandins and inflammation. *Arterioscler. Thromb. Vasc. Biol.* **2011**, *31*, 986–1000, doi:10.1161/ATVBAHA.110.207449.
146. Siangjong, L.; Gauthier, K.M.; Pfister, S.L.; Smyth, E.M.; Campbell, W.B. Endothelial 12(S)-HETE vasorelaxation is mediated by thromboxane receptor inhibition in mouse mesenteric arteries. *Am. J. Physiol. Heart Circ. Physiol.* **2013**, *304*, H382-92, doi:10.1152/ajpheart.00690.2012.
147. Kriska, T.; Herrnreiter, A.; Pfister, S.L.; Adebesin, A.; Falck, J.R.; Campbell, W.B. Macrophage 12(S)-HETE Enhances Angiotensin II-Induced Contraction by a BLT2 (Leukotriene B4 Type-2 Receptor) and TP (Thromboxane Receptor)-Mediated Mechanism in Murine Arteries.

Hypertension (Dallas, Tex. : 1979) **2022**, *79*, 104–114, doi:10.1161/HYPERTENSIONAHA.121.17824.
148. Hunyady, L.; Catt, K.J. Pleiotropic AT1 receptor signaling pathways mediating physiological and pathogenic actions of angiotensin II. *Mol. Endocrinol.* **2006**, *20*, 953–970, doi:10.1210/me.2004-0536.
149. Johnson, A.G. NSAIDs and increased blood pressure. What is the clinical significance? *Drug Saf.* **1997**, *17*, 277–289, doi:10.2165/00002018-199717050-00001.
150. Yu, Y.; Stubbe, J.; Ibrahim, S.; Song, W.; Smyth, E.M.; Symth, E.M.; Funk, C.D.; FitzGerald, G.A. Cyclooxygenase-2-dependent prostacyclin formation and blood pressure homeostasis: targeted exchange of cyclooxygenase isoforms in mice. *Circulation Research* **2010**, *106*, 337–345, doi:10.1161/CIRCRESAHA.109.204529.
151. Kim, G.-H. Renal effects of prostaglandins and cyclooxygenase-2 inhibitors. *Electrolyte Blood Press.* **2008**, *6*, 35–41, doi:10.5049/EBP.2008.6.1.35.
152. Angiolillo, D.J.; Weisman, S.M. Clinical Pharmacology and Cardiovascular Safety of Naproxen. *Am. J. Cardiovasc. Drugs* **2017**, *17*, 97–107, doi:10.1007/s40256-016-0200-5.
153. Ruschitzka, F.; Borer, J.S.; Krum, H.; Flammer, A.J.; Yeomans, N.D.; Libby, P.; Lüscher, T.F.; Solomon, D.H.; Husni, M.E.; Graham, D.Y.; et al. Differential blood pressure effects of ibuprofen, naproxen, and celecoxib in patients with arthritis: the PRECISION-ABPM (Prospective Randomized Evaluation of Celecoxib Integrated Safety Versus Ibuprofen or Naproxen Ambulatory Blood Pressure Measurement) Trial. *Eur. Heart J.* **2017**, *38*, 3282–3292, doi:10.1093/eurheartj/ehx508.

Schriftliche Erklärung

Ich erkläre ehrenwörtlich, dass ich die dem Fachbereich Medizin der Johann Wolfgang Goethe-Universität Frankfurt am Main zur Prüfung eingereichte Thesis mit dem Titel

"Loss of endothelial cytochrome P450 reductase induces vascular dysfunction in mice"

in dem Institut für Physiologie I (Kardiovaskuläre Physiologie) unter Betreuung und Anleitung von Prof. Dr. Ralf Brandes ohne sonstige Hilfe selbst durchgeführt und bei der Abfassung der Arbeit keine anderen als die in der Thesis angeführten Hilfsmittel benutzt habe. Darüber hinaus versichere ich, nicht die Hilfe einer kommerziellen Promotionsvermittlung in Anspruch genommen zu haben.

Ich habe bisher an keiner in- oder ausländischen Universität ein Gesuch um Zulassung zu einem PhD-Verfahren eingereicht. Die vorliegende Arbeit wurde bisher nicht als Thesis oder Dissertation eingereicht.

Die Grundsätze der Johann Wolfgang Goethe-Universität Frankfurt am Main zur Sicherung guter wissenschaftlicher Praxis in ihrer gültigen Form liegen mir vor und wurden bei der wissenschaftlichen Arbeit eingehalten.

_____ _____

(Ort, Datum) (Unterschrift)